K-JOINTS OF DOUBLE CHORD SQUARE HOLLOW SECTIONS

K-JOINTS OF DOUBLE CHORD SQUARE HOLLOW SECTIONS

by

MAGDI ANTOINE CHIDIAC

A Thesis

Submitted to the School of Graduate Studies

in Partial Fulfilment of the Requirements

for the Degree

Doctor of Philosophy

McMaster University

January 1980

To My Dear Wife

ANDREE

DOCTOR OF PHILOSOPHY (1979)
(Civil Engineering)

McMASTER UNIVERSITY
Hamilton, Ontario

TITLE: K-Joints of Double Chord Square Hollow Sections

AUTHOR: Magdi Antoine Chidiac, B.Sc. (Cairo University) Egypt
M.Eng. (McMaster University) Canada

SUPERVISOR: Dr. R.M. Korol

NUMBER OF PAGES: xvi, 177

ACKNOWLEDGEMENTS

I would like to express my sincere appreciation to my research supervisor, Dr. R.M. Korol, for his guidance, interest and encouragement during the course of this study. It has been a privelege and a pleasure to work under his supervision.

I am greatly indebted to the other members of my supervisory committee, Dr. G.A. Oravas, Dr. H. Robinson and Dr. M.B. Ives, for their valuable comments and suggestions.

This investigation was made possible through the financial assistance of McMaster University, the Natural Sciences and Engineering Research Council of Canada and the Ministry of Colleges and Universities, for which I am very grateful.

The research programme was jointly sponsored by C.I.D.E.C.T. (Comite International pour le Developpement et l'Etude de la Construction Tubulaire) and C.S.I.C.C. (Canadian Steel Industries Construction Council) and is gratefully acknowledged.

The provision of the hollow structural sections for the test programme by the Steel Company of Canada and the combined efforts of CANRON, Frankel Steel and Hepburn Steel to fabricate the joints is much appreciated.

The author is very grateful to Dave Perrett, Willy Berkemeier, Ross McAndrew and Dave Pfohl for their cooperation and assistance during the testing programme undertaken at the Applied Dynamic Laboratory.

The speed and accuracy in typing by Miss Pat Dillon of the Engineering Word Processing Centre is much appreciated.

I would like to thank my dear mother who dedicated herself to my education, and also for her encouragement to pursue graduate studies.

This work is dedicated to my lovely wife, Andree, in recognition of the sacrifices which she has made during the period of this investigation.

ABSTRACT

Trusses and Vierendeel girders are usually built from a single chord HSS "Hollow Structural Sections", but the largest HSS size as produced in Canada may limit its use for longer span applications. Therefore, the possibility of using double chord sections to enable the use of HSS for longer span trusses without the need for manufacturing new larger sections, presented itself.

A new concept utilizing double chord square hollow sections in welded K-joints of Warren trusses is described. The experimental results of 29 tests are reported, including four connection types - standard, channel, bolted and back-to-back. The latter type comprised gapped, overlapped and gapped with connecting stiffener plates.

The results indicate that the standard type is an excellent joint in both strength and stiffness. The channel type is generally susceptible to twisting. It was found adequate only when a significant increase in chord thickness ($\simeq 50\%$) was employed. The bolted connection appears to hold promise when on-site assembly of large trusses is necessary. Its performance was further improved by connecting the chords with small tie bars. The back-to-back type needed to be reinforced or fully overlapped to develop full branch member strength.

The double chord system of connection reveals itself to be much superior in strength to an equivalent single chord joint.

The effects of eccentricity, branch member to chord angle, and

chord preloading were investigated. Interaction formulae are presented for the standard and channel type joints and their use illustrated with examples. Satisfactory agreement between predicted and experimental ultimate strengths were obtained for joints which suffered from a chord failure at the connection.

Results of four T-type connections using the double chord concept are also reported and were recently published in the ASCE (8).

TABLE OF CONTENTS

TABLE OF CONTENTS (continued)

TABLE OF CONTENTS (continued)

LIST OF FIGURES

LIST OF FIGURES (continued)

LIST OF FIGURES (continued)

LIST OF TABLES

NOMENCLATURE

A	cross section area
b, b_o	section width (Figure 7.1)
b_a, b_{va}	partitioned widths for axial and shear forces (Figure 7.1)
CHS	Circular Hollow Section
$2C$	the clearance between branch members for Standard Joint
d	depth of branch for T-Connection
e	eccentricity
E	Young's Modulus
E_{st}	Strain hardening modulus
F_y	yield stress
f_a, f_v	axial and shear stresses
g	gap distance between weld
g^*	gap distance between toes of branch members equals $2C$
HSS	Hollow Structural Sections
h	total width of the chord equals $2b_o$
K_f, K_w	ultimate to plastic moment ratio of flange and web
K_t	ultimate to plastic moment ratio of section
L_w	branch member length or weld length between chord members for T-connections
L_{wc}	Compression branch member length
L_{wt}	tension branch member length
$2L_c$	Total chord length

NOMENCLATURE (continued)

M, M_y, M_p	bending, yield and plastic moment
N	Axial force in chord (compression positive)
P	axial force for K-Type joint
P_{max}	Maximum applied load a T-Type joint
P_y	yield force
$P_w = P_{web}$	branch forces
$(P_w)_y$, $(P_w)_{ult}$	branch yield and branch ultimate forces
RHS	Rectangular Hollow Section
SHS	Square Hollow Section
t	thickness
t_b	branch thickness for T-connection
t_o	chord thickness
t_s	stiffening plate thickness
T.L.	Total length
T, T_p	torsional and plastic torsional moments
V, V_p	shear and plastic shear forces
z	plastic section modulus
z_f, z_w	plastic section moduli of part of flanges and webs respectively
z_t	torsional modulus
$\Delta = \delta$	displacements
Δ_c, Δ_t	L.V.D.T. displacements (Figure 3.2)
Δ_o	chord displacement along line of diagonals

NOMENCLATURE (continued)

ε, ε_{st}, ε_u	normal, plastic limit and ultimate strains
ε_{max}	maximum principal strain
γ_{max}	maximum shear strain
σ, σ_y, σ_u	normal, yield and ultimate stresses
σ_a, σ_{vt}	axial and shear stresses due to torsion
σ_y^c	yield stress in chord
σ_{ex}, σ_{in}	incremental exterior and interior fibre strains
λ	branch width-thickness ratio
λ^*	branch to chord width ratio

CHAPTER 1

INTRODUCTION

1.1 General

Hollow Structural Sections (HSS) have played an increasingly important role in steel structural applications during the last twenty years, particularly in Europe, Japan and Canada. However, the high residual stresses caused by the manufacturing of these members necessitated limiting their use to single structural components such as canopy columns for shopping plazas and service stations, highway bridge railings, handrails and bus shelters.

To permit wider application much research had to be done to improve the quality of HSS and to provide sufficient data for more sophisticated design. Today, HSS is fully accepted by the engineering fraternity. In fact tubular members fill a special niche in architectural demands of form and simplicity, as for example their use in Ontario Place and the CN Tower Pedestrian Overpass in Toronto, Ontario.

Presently, there has been a major limitation in their use for long span trusses in buildings, bridges and overpasses. Single chords in trusses have been used extensively in which the web members are fastened to the top of the chord member. Since two branch members must be mated to the chord at a joint, a gap is normally produced.

Otherwise, an overlap joint must be detailed to relieve the joint of some eccentricity that accompanies the gap.

Nevertheless, gap joints are most economical [1,2] and are generally used in design. Another constraint in using single chord HSS is the practical aspect of connecting the branches to the chord. When welded connections are used the web members should be 25 to 50 mm narrower in width than the chord so that fillet welds can be used. If the web and chord members are of the same width, a difficult butt weld has to be made, which means a higher cost for fabrication. In heavily loaded trusses, unreinforced gap joints cannot withstand the full compressive or tensile strength of the individual web members and are thus, generally uneconomical. Lap joints require additional fabrication costs, however, they are generally 100% efficient in transferring forces through the connection.

In Canada, the largest size of square hollow section (SHS) that is produced has a cross section 304.8 x 304.8 x 12.7 mm which imposes a major restriction on the maximum unsupported span. For example, roof trusses with normal span to depth ratios of 8 to 10 and subject to normal snow and dead loads cannot be expected to span more than 30-40 meters. However longer spans would give greater interior design flexibility within buildings and improve the competitiveness of HSS.

Such appears to be the potential for the double chord HSS truss utilizing K joints (Warren configuration). The concept, then, is to use two square or rectangular chord members - either sandwiching the branch members (also square or rectangular) or placing the chords back to back

and detailing the connections as for the single chord case.

There appears to be a number of advantages to using such a joint configuration. It provides for ease and economical fabrication and has the potential for efficient joint design. The web member forces will be shown to be transferred directly to the webs of the double chords, whereas the connecting flange of the chord plate must transfer these forces in the case of the single chord. Consequently the double chord will be shown to provide a much stronger joint. For the same chord properties, the double chord using a single fillet weld connection behaves better than an overlapped butt-welded single chord joint. In addition, the double chord will require less, if any lateral bracing due to its inherent lateral rigidity.

However, before double chord truss systems can be employed in general use, research must be undertaken on the behaviour of the joints through which the member forces must be transferred. The work to be described herewith, therefore, focusses on the connections, rather than on the members themselves.

1.2 Literature Review

Up to the present time no research on double chord HSS joints has been reported in the literature. However, a considerable amount of work has been published on single chord HSS connections using circular and square HSS for chord members. The following presentation will deal only with connections having square HSS for chord members, and in which the web members of K, T or N configurations are either circular (CHS) or

rectangular (RHS).

Research in England on HSS welded joints began at Sheffield University in the early 1960's. The experimental work was performed on isolated N-type joints utilizing RHS chord members and CHS or RHS web members in which the tension member was positioned at 45^{o} to the chord member.

Blockley [3], conducted static tests on 60 mild steel joints using CHS web members with a varying gap or overlap and covering a wide range of member sizes. He found that the ultimate strength of gap joints was significantly less than when the web members were lapped, particularly when the chord thickness was relatively thin, in which case large local deformations occurred at loads below the working load of the specimen. Local deformations encountered in lap joints, on the other hand, were much lower. An elastic analysis was developed based on the elastic theory of thin plates using a finite difference technique.

Shinouda [4] investigated stiffened joints with a series of 61 tests on CHS to RHS weld gap joints. He concluded that gap joints are practical and do not necessitate end profiling. However, excessive deformations and stresses can occur in the gap area when the ratio of the thickness of the chord to the height of the chord is less than 0.07. Using an adequate stiffening plate reduces greatly the local deformations, thus providing a more uniform stress distribution in the web members. Shinouda also adopted the elastic small deflection theory of plates and the finite difference technique to predict joint behaviour under working load.

Babiker [5] studied the cyclic loading effect on 55 mild steel joints with CHS web members and found that although a joint may be considered sufficiently strong for static purposes, its life under fatigue conditions could be so low that it would be unacceptable for normal applications. Summarizing his results, he stated that gap joints are most unsafe, joints with partial overlapping show some improvement while joints with 100% overlap are fully satisfactory. He concluded also that no increase in the fatigue endurance limit can be gained by using a gusset plate or a stiffening plate.

Mee [6] undertook research on the static strength of RHS to RHS joints with 57 tests on specimens having a varying weld gap or lap and with different chord preloadings. He confirmed Blockley's findings that the joint strength and stiffness increased as the weld gap decreased or lap increased. The behaviour of the joints was again found to depend mainly upon the joint geometry, while the ultimate strength increased with increasing λ^* or t_o (λ^* is branch to chord width ratio while t_o is chord thickness). When λ^* approached unity the increase of strength due to an overlap was found to be insignificant compared with the increased cost of welding and cutting the branch members. Mee carried out a theoretical analysis of the elastic load deformation characteristics of the connecting chord face of a gap joint by treating it as a laterally loaded plate and analysing it by means of the "theory of thin plates" using a finite difference technique.

Eastwood and Wood [7] summarized the work done at Sheffield University by proposing a set of tentative design rules for hot-rolled

CHS or RHS branch members mating onto an RHS chord. These recommendations received particular acceptance in Canada, and are used by STELCO [1] and the CISC [9].

A further research project at Sheffield University was undertaken by Chandrakeerthy [10], who tested 47 RHS to RHS 45° N-joint specimens from cold-formed sections, with test specimens covering gap and lap joints. The aim was to study the influence of typical joint parameters, identified from tests on hot-rolled sections to cold-formed RHS joints. Initial steps were also taken to set up an elasto-plastic finite element program for their analysis.

At Nottingham University, full size trusses, for which the joint design was based upon certain isolated joint tests at Sheffield, were tested by Dasgupta [11]. These trusses, 11 in all, were of 6 meters span and 0.84 m deep. CHS to RHS N-joints were used with a small weld gaps and varying eccentricities. Failure loads of truss joint were found to be up to 30% lower than the equivalent isolated joint failure loads. The actual joint flexibility was calculated by a finite element analysis. It was found that the secondary moments increase considerably with the increase in axial flexibility, and that the latter increases at a faster rate when λ^* is small (λ^* = 1/2 to 2/3).

To complement the research done at Sheffield and Nottingham Universities, further testing was undertaken by Davie and Gidings [20] at the British Steel Corporation "Corby" to investigate larger sections. All of the 30 specimens were N-type joints except for one which was of the Warren type. In general, it was found that the results were in

reasonable agreement with the Sheffield and Nottingham tests. It was found that the 45° Warren joint failed at 18% less load than the 45°N joint equivalent but no general conclusions could be made. Subsequently, a series of ultimate strength curves were empirically derived for both CHS to RHS and RHS to RHS isolated N joints [20].

Meanwhile, in the Netherlands a very extensive experimental research program was undertaken at the TNO Institute and Delft University of technology. About 450 isolated joint specimens of which many are with RHS members have been tested, the final results having been published by Wardenier [13] in 1978. The bulk of the experiments were with Pratt and Warren truss joints with the aim of studying 12 different parameters. The results were published in a series of reports by Wardenier et al., leading to the draft version of the Dutch regulations for Tubular construction. Although the size of the gap appeared to have some influence upon the ultimate joint strength depending on the b_o/t_o and λ^*_{av}, this parameter is not included in the empirical equation that was developed, since the results were deemed to be "inconclusive" [13, 31] as to its effect.

Eight Pratt trusses with RHS chords and spans of between 14 and 16 meters were fabricated in England and then tested at Pisa University, Italy [14]. In association with these trusses, some of the joints being investigated were reproduced as isolated joint specimens for testing at Corby [15] to give further correlation, if possible, between the behaviour of the isolated joint and similar connections in complete trusses. Many of the isolated joint tests failed by local buckling of

the chord but this did not occur in any of the truss tests. The latter also showed no appreciable difference between the strength of joints for the compression chord as compared with the tension chord [16].

From the results of the Pisa [14], Corby [15] and Dutch [13] tests, another set of equations was developed by Coutie et al. [17] and Haleem [18] to express the mean ultimate static strength of RHS or CHS to RHS gap and lap joints. The equations for the gap joint included as parameters b_o, t_o, the angle of inclination and the chord preloading. The lap joint strength was independent of the bracing angles but dependent on the strut area; meaning that for the same width the strength of CHS bracing member is less than that for the RHS bracing members.

In West Germany, research on rectangular hollow sections joints has been done recently at Karlsruhe University of Technology and the Mannesmann Research Institute, in Düsseldorf. A total of 43 joints were tested, and included CHS or RHS to RHS Warren braced specimens. These are reported by Mang [19]. He found that different behavioural characteristics were obtained for Warren joints when compared to the "Corby Curves" presented by Davie and Giddings [20] for N joints.

In 1974, six large size RHS to RHS Warren joints were tested at Mannesman by Hohl [21] of which three were gapped and three were lapped. All were fabricated from mild steel. Hohl's test results were much higher than these predicted by the "Corby Curves" of Davie and Giddings [20].

In a sequel to these tests a further six RHS to RHS Warren joints

were tested [22] using higher yield steels for three tests, and mild steel web members with higher yield steel chord members for the other three specimens. For these joints, all of which were lapped, it was found that using a steel with a higher yield stress for the chord member, produced a 15 to 30% higher joint strength, yet, little additional joint strength was obtained by using higher yield steel bracing members in addition.

The analysis of a joint in the post-elastic range has been approached by using the Yield-Line method. Jubb and Redwood [23] first applied the simple yield line theory to T joints between RHS members. Patel [24] and Wardenier [25] did similar analyses and found good agreement between the joint yield load and the theory.

Davies and Roper [26, 27, 28] applied the yield line method to gapped joints of Pratt truss with RHS bracing members of the same size framing into an RHS chord member. They tested this yield line model with a comparison of the results of experiments by Mee [6] and Davie and Giddings [20]. Acceptable correlations were obtained, providing allowances were made for the fillet welds around the bracing members except for large λ values. In this case, Davies and Roper [27] recognized that other failure modes needed to be considered.

Mouty [29, 30] extended the yield line pattern of Davies and Roper to cover Warren and unsymmetrical gapped joints, and applied the yield line theory to RHS lapped joints as well. The effect of axial load upon the plastic moment of resistance on the yield line pattern was also considered.

Packer [31] conducted a theoretical analysis for statically loaded joints. This analysis was based upon a set of joint failure modes which enable the yield and ultimate strengths of such joints to be assessed. The push-pull yield line mechanisms which were proposed for modelling the deformations of RHS to RHS gap joints gave satisfactory predictions for both the yield load and ultimate load capacities of gapped joints which failed in this manner. Strut buckling mechanisms were proposed and gave good agreement between the predicted and actual strut buckling loads of both the gap and lapped joints. Simple approaches for calculating the utlimate strength of gap or lapped joints which failed by chord shearing or chord local buckling failure modes were also prepared. Packer concluded that the reduction in ultimate strength when preloading the chord depends on the joint failure mechanism and can often be severe. He found also, that the ultimate strength of all joints is directly dependent upon the yield strength of the members, but the strength of some gap joints was also dependent upon the ultimate stress of the chord members. Joints that failed by compression web member had strength capacities independent of the angle of inclination of the bracings to the chord. However, gap joints which failed by the push-pull mode of failure, were found to be dependent on the angle of inclination.

Little work has been done on the interaction effects of stress resultants and their influence on joint strength. Brockenbrough [32] studied an HSS beam-column connection subjected to combined loads. Interaction equations were proposed to predict the ultimate capacity of

the connections neglecting the effects of strain hardening on the joint strength. The test results of 11 specimens showed the theoretical prediction to be rather conservative. The moments obtained experimentally were considerably higher than was predicted.

1.3 Objectives and Scope

Research on double chord HSS joints is being reported for the first time in this work. Although new, the concept is simple, i.e. to arrange the branch members in such a way as to minimize material cost and fabrication whilst maximizing strength and rigidity. Essential to the process of truss design is the capability of the joints to withstand member forces. Hence this work will be devoted to the assessment of various joints deemed to be plausible for double chord K trusses.

Four different types of connection were proposed for study: Standard, Channel, Bolted and Back-to-Back joints. For each connection, the effects of eccentricity, chord preloading and slope angle are investigated. While not a major part of this work, the costs of fabrication for the various types are also discussed.

The following organization of material in this dissertation is presented below. Chapter 2 contains a description of the test specimens and the test set-up. Also included are the basic material properties and the different parameters which are required for the analysis.

The experimental results for the Standard type joints are reported in Chapter 3, while the experimental results for the other three joints are reported in Chapter 4.

Chapter 5 contains a comparison between the four types of joints including the cost of fabrication. Chapter 6 deals with an investigation on the use of double chord HSS in Vierendeel connections, where a comparison with single chord connection is made.

In Chapter 7, the description of the method of analysis to predict the ultimate capacity for the standard and channel joints is given together with a comparison between the theoretical and experimental results. Chapter 8 provides a summary of the investigation, it presents the overall conclusions and some recommendations for future research.

CHAPTER 2

EXPERIMENTAL PROGRAM FOR DOUBLE CHORD K-TYPE JOINT

2.1 Parameters Considered

The double chord joints that were studied were confined to a Warren truss configuration. Four different types of joint were considered for this investigation. In all, a total of 29 joints were tested to determine the effect of: connection type, eccentricity between web and chord members, slope of the web members and chord preloading. In addition, the benefits of reinforcing were assessed for one type of connection.

The joint types that were assessed are presented below.

2.1.1 Connection Types

a) "S" or "STANDARD JOINT". In this case the webs are sandwiched between the chords and are attached to the latter member by fillet welds. This type encounters in-plane eccentricity and/or weld length constraints, as illustrated in Figure 2.1(a).

b) "C" or "CHANNEL JOINT". Only the compression member lies between the chords while the tension branch is represented by two channels located on the exterior of the chord members. By using this type of joint, in-plane eccentricity of forces is eliminated due to the freedom obtained of positioning all branch members in three different planes. This is indicated in Figure 2.1(b).

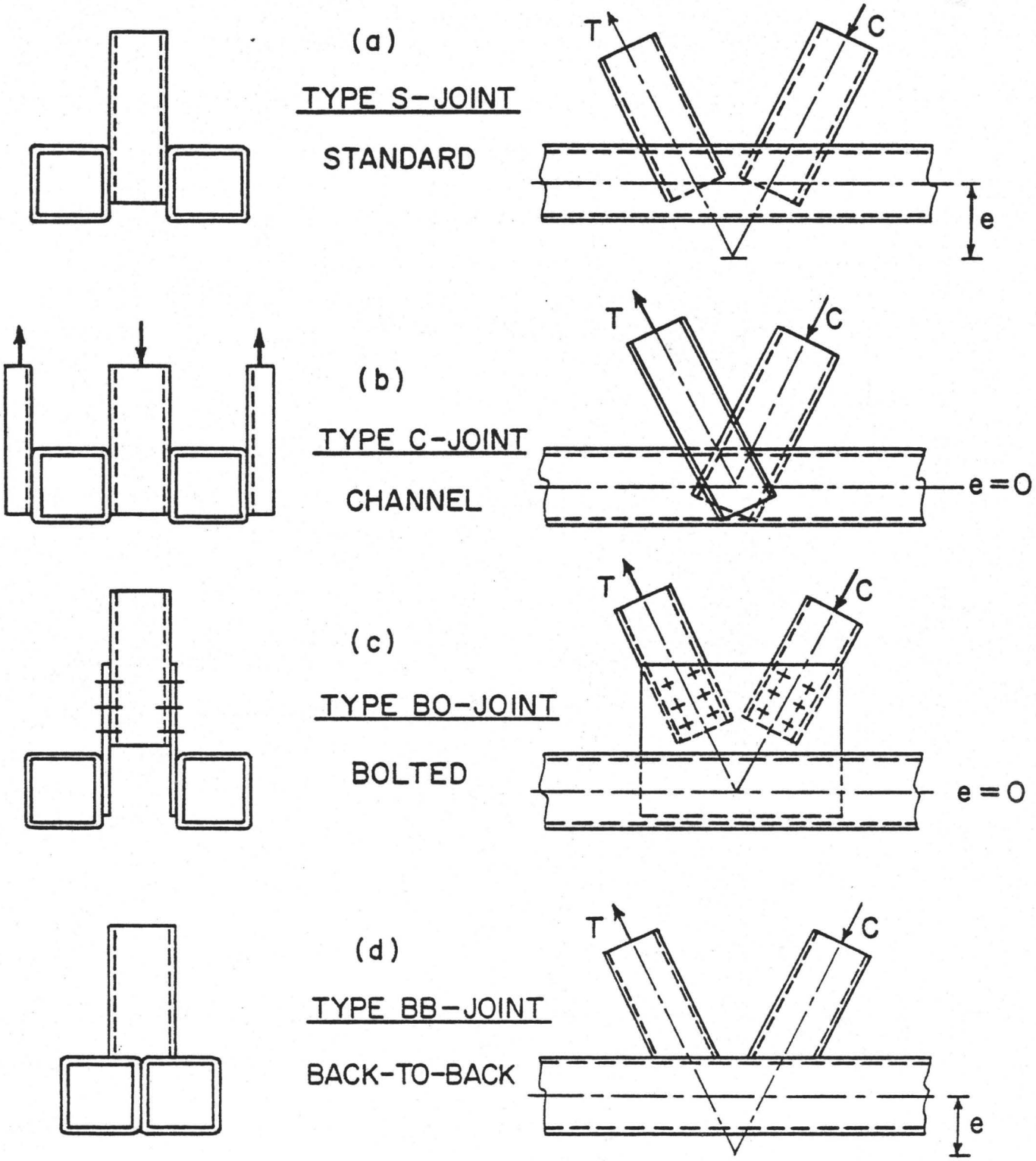

FIGURE 2.1 TYPE OF JOINTS.

c) "BO" or "BOLTED JOINT". This connection is similar to the standard joint in that both branch members are SHS. However, member attachment is with bolts that utilize gusset plates that are welded to the chords. This type is sketched in Figure 2.1(c).

The BO-type reduces the problem of transporting full sized trusses to the site - a major problem for large structural assemblies. Because of the use of gussets, in-plane eccentricity can also be eliminated.

d) "BB" or "BACK-TO-BACK Joint". This connection is different from the other three types, in that the chords contact one another in a "back-to-back" configuration. The branch members are thus welded to their composite top flanges as indicated Figure 2.1(d).

This type of joint reduces the amount of material needed for web member in the final truss, however fabrication costs will normally be higher than for the other types. The Back-to-Back joint may be reinforced by using stiffening plates as will be discussed in section 2.2.4.

Photographs of all four joint types prior to testing in the laboratory are presented in Figure 2.2.

2.1.2 Eccentricity Effect

It is obvious that once an eccentricity exists between the center lines of the web and chord members, the capacity of the joint will be reduced due to the resulting additional moment that must be resisted. A

a) STANDARD

b) CHANNEL

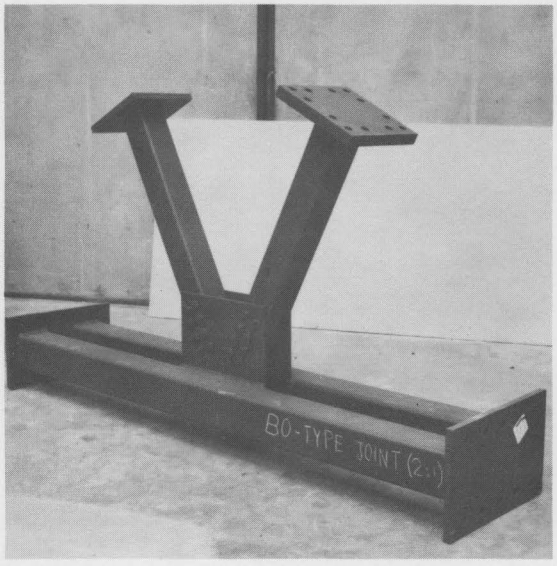

c) BOLTED

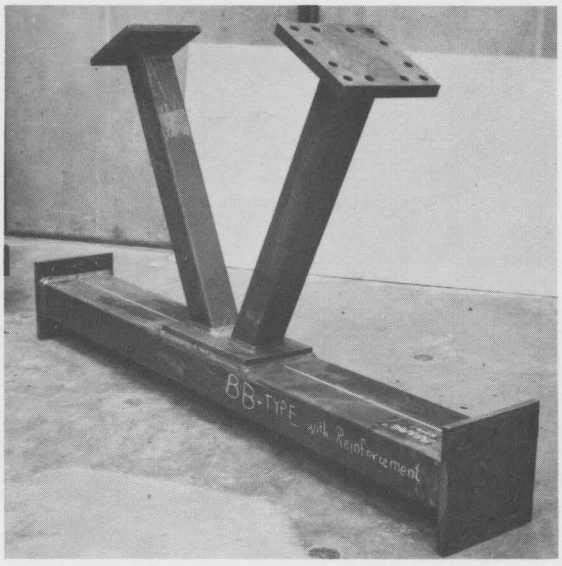

d) BACK-TO-BACK

FIGURE 2.2 — PHOTOGRAPHS OF JOINT TYPES

constant objective in joint design is to decrease the eccentricity or eliminate it completely if possible. Depending upon the arrangement of members, the eccentricity may be positive, zero or negative. Positive and zero eccentricities indicated by the dimension "e" are shown in Figure 2.1.

Only positive eccentricity is obtained when using the S-Type joint. It is obvious from Figure 2.1(a), that even when the two web members are very close to each other, a considerable amount of positive eccentricity still exists. Nonetheless, it is possible to obtain a smaller eccentricity for the standard joint by having an angled cut at the ends of the branch member as in Figure 2.3. The cost of cutting the end of the web member is rewarded by a 40% decrease in the original eccentricity.

When using the channel or Bolted type joints, any of the three eccentricities may be obtained. For the Back-to-Back joint, a gap joint produces a positive eccentricity, a partial overlapping produces a zero eccentricity and a full overlapping will result in a negative eccentricity as illustrated in Figure 2.4.

2.1.3 Slope of the Web Members

The slope angle for the branch members used in trusses varies between 30° and 70° [1]. The choice of the angle depends on the panel point spacing and loading, the depth of the truss and the span.

It is obvious from Figure 2.5 that for a reduced angle with a prescribed gap, a smaller eccentricity is obtained. The chord member at

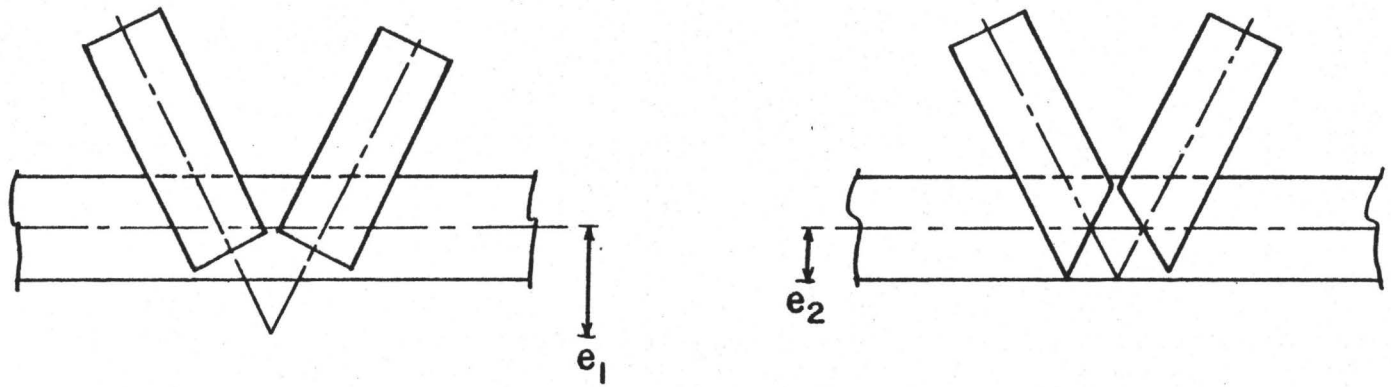

FIGURE 2.3 ECCENTRICITY IN STANDARD TYPE JOINT.

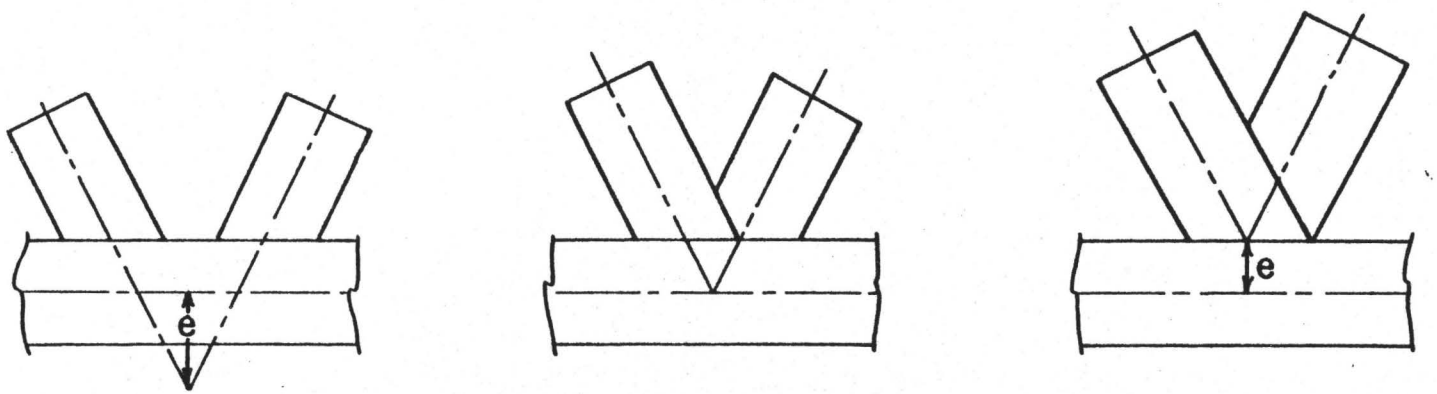

GAP JOINT
+ve e

PARTIAL OVERLAPPING
e=0

FULL OVERLAPPING
−ve e

FIGURE 2.4 ECCENTRICITY IN BACK-TO-BACK JOINT.

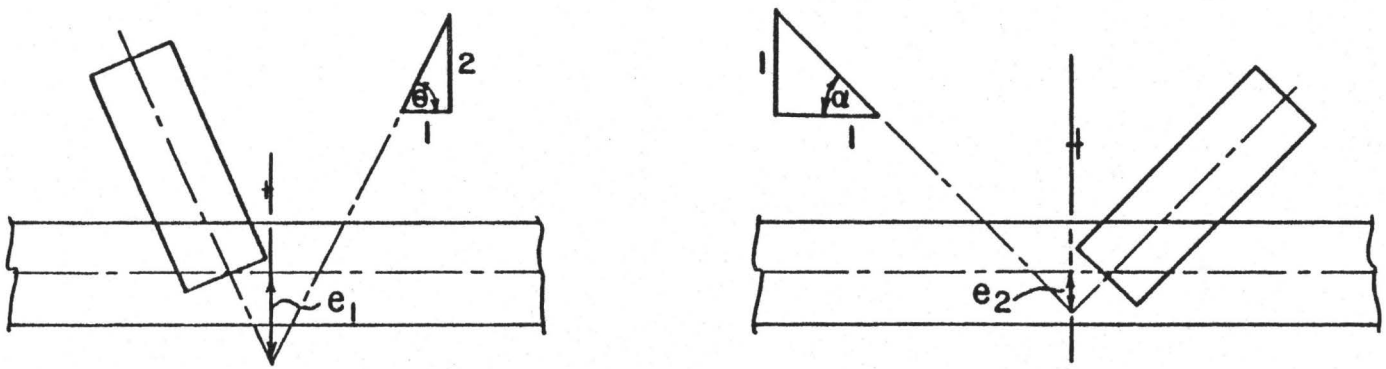

$\theta_1 = 63°43$ $\theta_2 = 45°$

$e_1 > e_2$

FIGURE 2.5 SLOPE ANGLE EFFECT ON ECCENTRICITY.

the joint will be subjected to a larger axial load, smaller shearing force and moment due to eccentricity.

The disadvantage of smaller angles is that the panel point spacing is increased, which causes greater unsupported lengths of members. Greater overall flexibility, susceptibility to buckling and the effects of member loading have to be carefully assessed.

It was decided to test two different slopes 2:1 ($\theta = 63.43^{\circ}$) and 1:1 ($\theta = 45^{\circ}$) with the former being used in the majority of tests where other parameters were to be evaluated. Hence all connections types utilized the 2:1 web member inclination as a baseline for evaluating the effects of the other variables. Both angles were used as a basis for comparison for the standard type joint.

2.1.4 Chord Preloading

Preloading the chord with different levels of load was identified as a means of simulating different combinations of forces in trusses subject to different loading conditions and at various panel points. Since many states of force distribution will exist in an actual truss, it was decided to establish the following preloading system to approximately simulate normal loading conditions.

The chord was preloaded with a certain amount of load in tension or in compression, and this preloading was kept constant through the test. The preloading level ($\mp$23.5%, $\mp$3.5% and +16.5% of nominal yield value of the chord) was calculated such that at failure the average stresses in the chord members, resulting from the web load and the chord

preloading, would be at their working values or at a fraction thereof i.e. at 0.6 F_y, 0.4 F_y or 0.2 F_y.

2.2 Labelling System

To easily identify joint type, eccentricity, preloading etc., a labelling system was devised for each specimen. The letters for joint type described earlier, are the first characters in identification. Subsequent characters are: a numeral to represent slope (i.e. 2 for 2:1 and 1 for 1:1), a letter-numeral to identify eccentricity (P for positive, N for negative and numeral is approximate distance in inches), and a numeral-letter for the chord preloads in addition to the horizontal reaction from diagonals (number indicates 1/10th of percentage of nominal yield value, while C and T indicate compression and tension respectively). In the case of the BB type, the stiffening plate thickness (where applicable) is given as a subscript in sixteenths of an inch. Table 2.1 lists all specimens with appropriate group placement. Note the P_y in the fifth row is the nominal yield strength of the chord member which was 350 MPa (50.8 ksi).

2.3 Specimen Details

A total of 29 specimens were tested. These were divided into 7 groups as is shown in Table 2.1.

Based on the maximum-sized square HSS produced in Canada i.e. 304.8 x 304.8 x 12.7 mm (12 x 12 x 1/2"), half scale tests were considered sufficient to be representative of joint behaviour for large

Group Number	1	2	3	4	5	6	7
Joint Type	S	S	S	C	C	BO	BB
Slope of Web Members	2:1	2:1	1:1	2:1	2:1	2:1	2:1
Eccentricity mm (inches)	+178 (+7)	+108 (4.25)	+ 45 (1.75)	Zero	- 76 (- 3)	Zero	117, 0, -76 (4.6), 0, (-3)
Anticipated Chord Levels at failure, Ratio of P_y	-0.6 + 0.6 -0.4 + 0.4 -0.2	-0.6 -0.4 +0.6	-0.6 +0.6	-0.6 + 0.6 -0.4 + 0.4 -0.2	-0.6	-0.6 -0.4	-0.6
Number of Specimens	6	3	3	5	1	3	8
Labelling System	S2P76C S2P74C S2P72C S2P74T S2P76T S2P76C*	S2P46C S2P44C S2P46T	S1P26C S1P26C* S1P26T	C2P06C C2P04C C2P02C C2P04T C2P06T	C2N36C	B02P06C B02P06C* B02P04C	BB2P56C $BB2P56C_4$ $BB2P56C_8$ $BB2P56C_{12}$ $BB2P56C_{20}$ BB2P06C BB2N36C BB2N36C*

Table 2.1 Specimen Parameters

size trusses. Hence all the double chord members were composed of two HSS 152.4 x 152.4 mm (6 x 6") with web members 127.0 x 127.0 mm (5 x 5").

Twelve specimens were investigated in the Standards series comprising groups 1 to 3. Groups 1 and 2 had the same slope, but with different eccentricities 178 mm (7") and 108 mm (4.25") respectively. Five different cases of preloading were tested in group 1, with three in group 2 and two in group 3. The group 3 specimens had a different slope (1:1), a smaller eccentricity resulted with two different preloads. Dimensions and details of the S-type specimens are given in Table 2.2 and Figure 2.6.

Six channel type specimens were investigated (Groups 4 and 5). Only one slope angle (2:1) was used together with two different eccentricities with a range of preloading. Two thicknesses, 6.37 and 9.53 mm (1/4 and 3/8") were used for the chord members in order to investigate the possibility of obtaining higher capacity with the larger chord thickness. Dimensions and details for the channel type specimens are shown in Table 2.3 and Figure 2.7.

Three specimens of the BO-type (group 6) were tested with zero eccentricity. The effect of preloading was studied on 2 specimens and the benefit of using ties on the bottom side of the chord was evaluated in the third specimen. Specimen details are presented in Table 2.4 and shown in Figure 2.8.

Eight specimens of the BB type were studied and comprised in group 7. Included were a gap joint, a partial overlap joint, two full

Specimen Code Number	Length of Chord Member mm	Length of Web Member - mm			Slope of Web Member	Eccentricity - mm		Web Dimensions at the Joint - mm					Weld Size - mm	
		L_{wo}	L_w	L_{wi}		e	e_w	W_a	W_b	W_c	W_d	c	W_a, W_c, W_d	W_b
S2P76C														
S2P74C														
S2P72C	2337	1219	1219	1219	2:1	178	159	94	127	157	142	12.7	12.7	4.8
S2P74T	(92)	(48)	(48)	(48)		(7)	(6.25)	(3.7)	(5.0)	(6.2)	(5.6)	(0.5)	(1/2)	(3/16)
S2P76T														
S2P46C														
S2P44C	2337	1226	1194	1162	2:1	108	109	32	142	159	142	6.35	14.3	4.8
S2P46T	(92)	(48.25)	(47)	(45.75)		(4.25)	(4.31)	(1.25)	(5.6)	(6.25)	(5.6)	(0.25)	(9/16)	(3/16)
S1P26C														
S1P26C*	2337	1203	1181	1159	2:1	45	51	32	135	203	178	6.35	11.1	4.8
S1P26T	(92)	(47.375)	(46.5)	(45.625)		(1.75)	(2.0)	(1.25)	(5.3)	(8.0)	(7.0)	(0.25)	(7/16)	(3/16)

Notes: Numbers in parentheses are inches

All chords are 152 x 152 x 6.35 HSS (mm)

All webs are 127 x 127 x 6.35 HSS (mm)

Table 2.2 Dimensions for S-Type Specimens

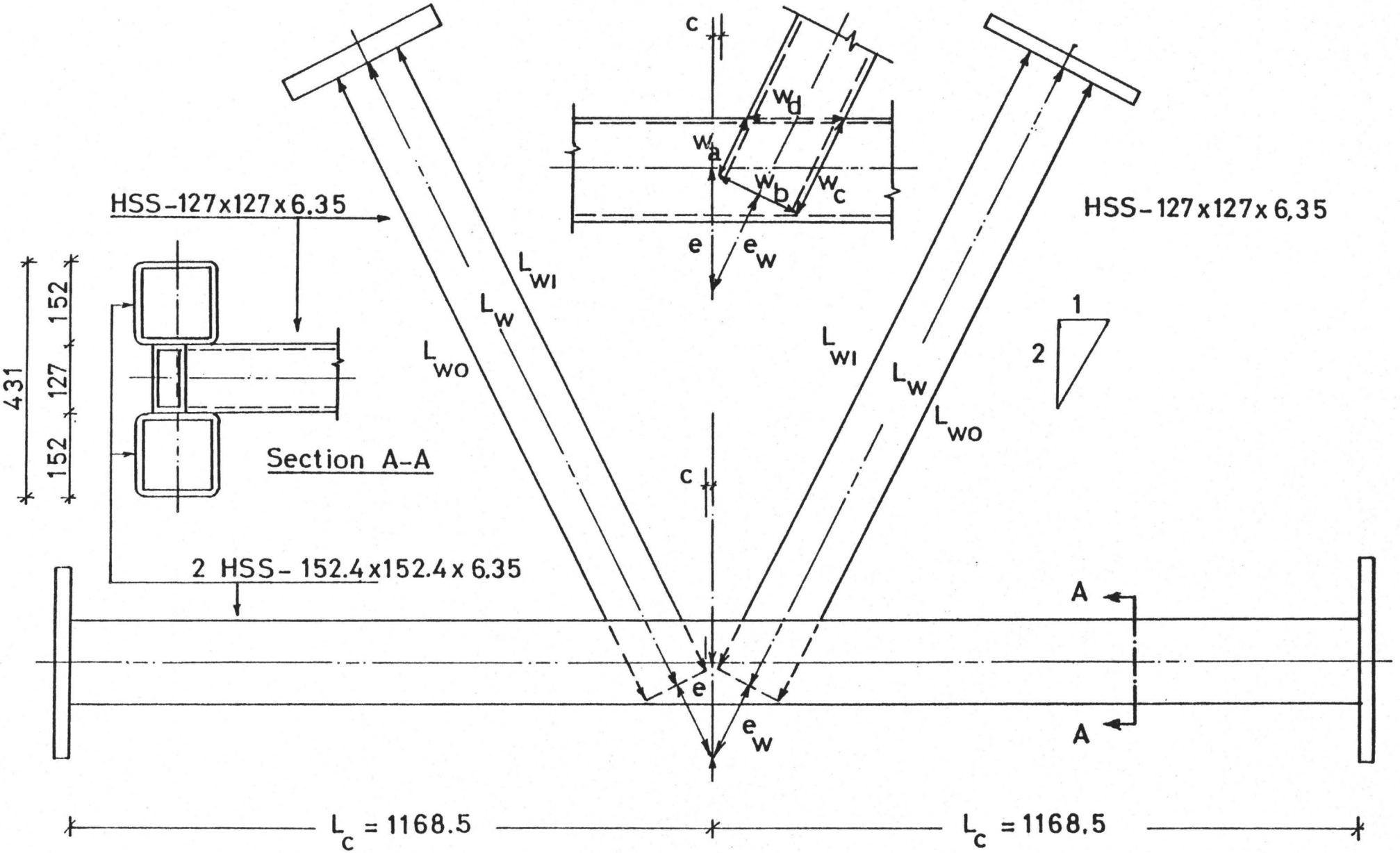

FIGURE 2.6 STANDARD TYPE JOINT (Dimension in mm)

Specimen Code Number	Chord Members (mm)	Length (mm)		Slope of Web Members	Eccentricity (mm)	c (mm)	Weld Size in mm along	
		Compression Web HSS-127x127x6.35 L_{Wc}	Tension Web 2C - 130 x 13 L_{Wt}		e		W_b	W_a, W_c, W_d
C2P06C	2 HSS							
C2P04C	152.4 x 152.4 x 6.35	1219	1524	2:1	0	142	4.8	12.7
C2P02C	152.4 x 152.4 x 6.35 152.4 x 152.4 x 9.53	1219	1524	2:1	0	142	4.8	12.7
C2P04T	2 HSS							
C2P06T	152.4 x 152.4 x 9.53	1219	1524	2:1	0	142	4.8	12.7
C2N36C	2 HSS							
	152.4 x 152.4 x 9.53	1219	1524	2:1	-76	224	4.8	12.7

Table 2.3 Dimensions for C-type Specimens

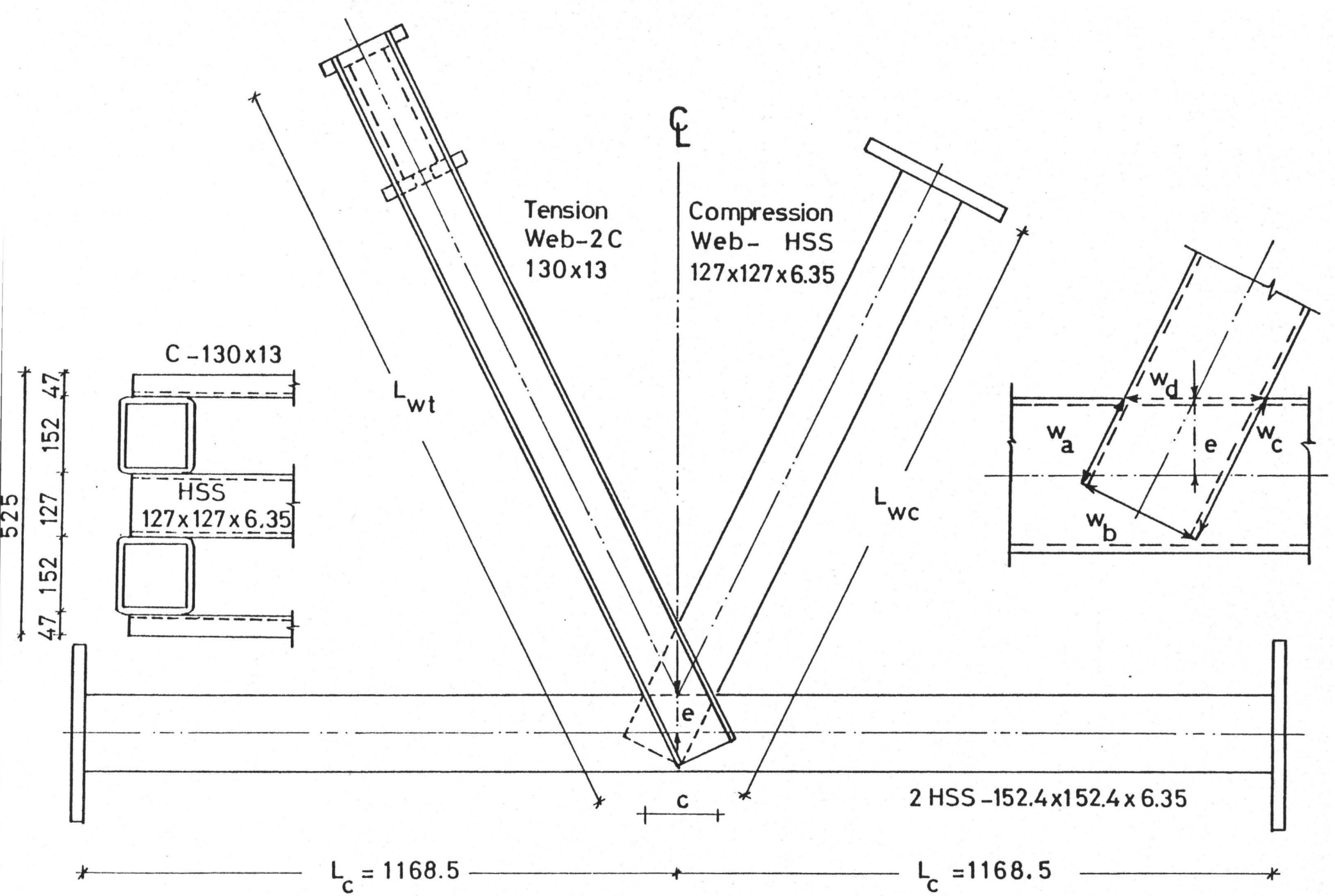

FIGURE 2.7 CHANNEL TYPE JOINT (Dimension in mm)

Specimen Code Number	Length (mm)		Slope of Web Member	Eccentricity (mm)		Gusset Plates mm	Tie Plates mm	Number of 19.05 ϕ bolts (3/4")	Weld Size for Gusset Plate mm
	Chord Member $2L_c$	Web Member $L_{wc} = L_{wt}$		e	e_w				
B02P06C	2337	1029	2:1	0	159	2PL	N/A	32	8
B02P04C	2337					432x457x9.5			
B02P06C*	2337	1029	2:1	0	159	2PL	2	32	8
	2337					432x457x9.5	76x406x9.5		

Notes: All chords are 152 x 152 x 9.53 HSS (mm)

All webs are 127 x 127 x 6.35 HSS (mm)

Table 2.4 Dimension for EC-Type Specimens

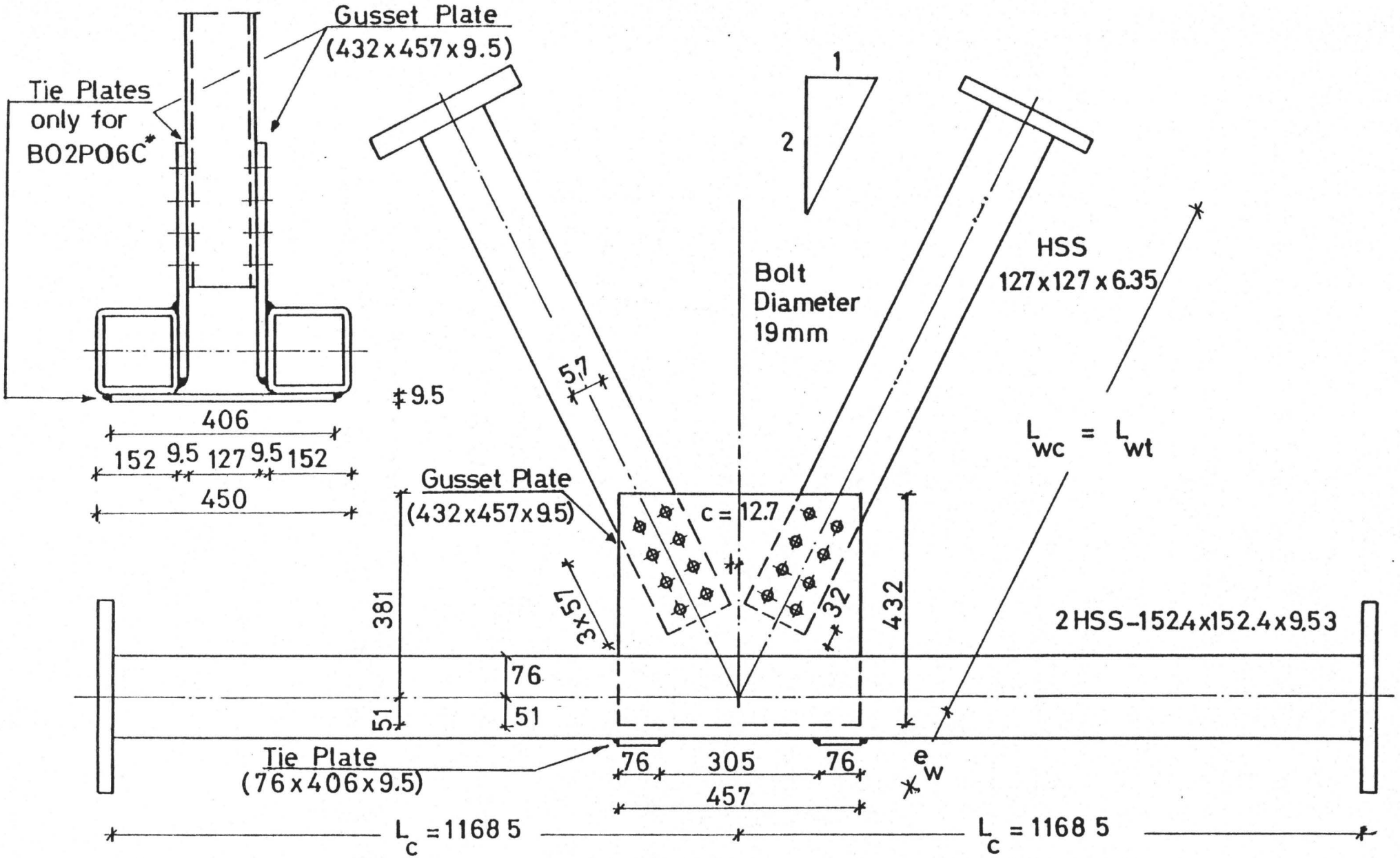

FIGURE 2.8 BOLTED CONNECTION (Dimension in mm)

overlap joints with the remainder having stiffening plates.

For the full overlap joint, two cases were studied:

(i) BB2N36C, where the tension web was welded on top of the compression web (Figure 2.9(a)).

(ii) BB2N36C*, where the compression web was welded to the top of the tension web (Figure 2.9(b)).

For the stiffening plate cases, four thicknesses were investigated. The objective was to determine the optimal thickness for full member strength. Specimen details are shown in Table 2.5 and Figure 2.10.

2.4 Material Properties

The steel used in all specimens was CSA Grade 40.21-M 350 W class H. The sections were cold formed from flat-rolled steel and utilized an automatic welding process to produce a longitudinal weld.

The mechanical properties of the structural steel sections after final processing were required to conform to the following:

a) A minimum yield strength of 350 MPa (50.8 ksi)

b) A minimum tensile strength of 450 MPa (65.3 ksi)

c) A minimum of 22% elongation in 50.8 mm (2").

Upon completion of each of the 29 tests, coupons were cut from each specimen (one for each component exclusive of gusset, tie or stiffening plates) remote from the welded seam. These coupons were then subjected to standard tensile tests on a Tinius Olson machine in accordance with the relevant ASTM specification [33].

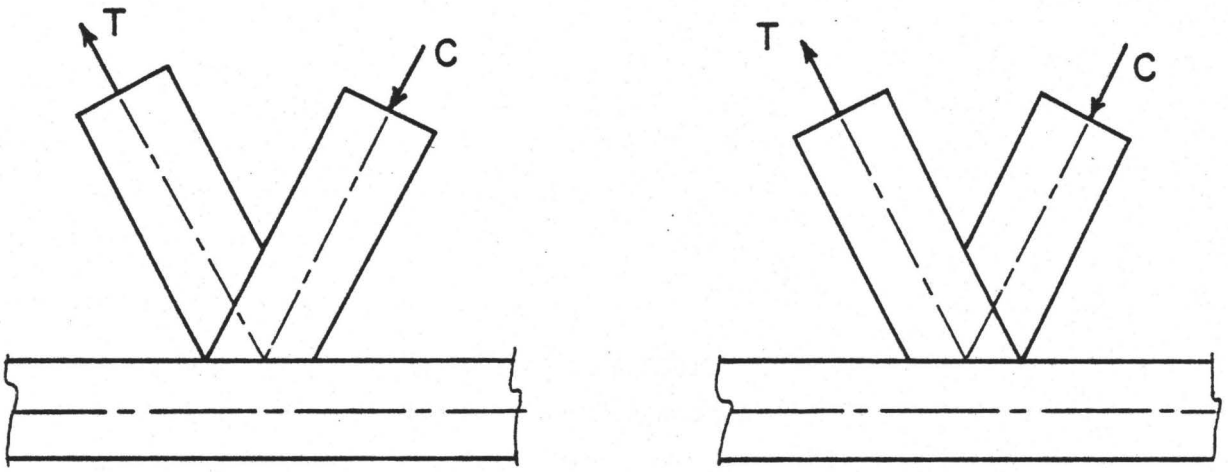

(a) BB2N36C (b) BB2N36C*

FIGURE 2.9 FULL OVERLAPPING IN BACK-TO-BACK JOINT.

Specimen Code Number	Member Length (mm)			Slope of Web Member	Eccentricity e (mm)	Thickness of Stiffening Plate t_s (mm)	General Remarks
	Double Chord $2L_c$	Comp. Web L_{wc}	Tens. Web. L_{wt}				
BB2P56C	2337	1092	1092	2:1	117	0	Gap Joint (g = 50 mm)
BB2P06C	2337	1092	1092	2:1	0	0	44% Overlap
BB2N36C	2337	1092	1013	2:1	-76	0	Ten. Web Above Comp. Web
BB2N36C*	2337	1013	1092	2:1	-76	0	Comp. Web. Above Tens. Web
$BB2P56C_4$	2337	1086	1086	2:1	117	6.35	Gap Joint with Stiffener
$BB2P56C_8$	2337	1080	1080	2:1	117	12.70	Gap Joint with Stiffener
$BB2P56C_{12}$	2337	1080	1080	2:1	117	19.05	Gap Joint with Stiffener
$BB2P56C_{20}$	2337	1067	1067	2:1	117	31.75	Gap Joint with Stiffener

Notes: All chords are 152 x 152 x 6.35 HSS (mm)

All webs were 127 x 127 x 6.35 HSS (mm)

Table 2.5 Dimensions for BB-Type Specimens

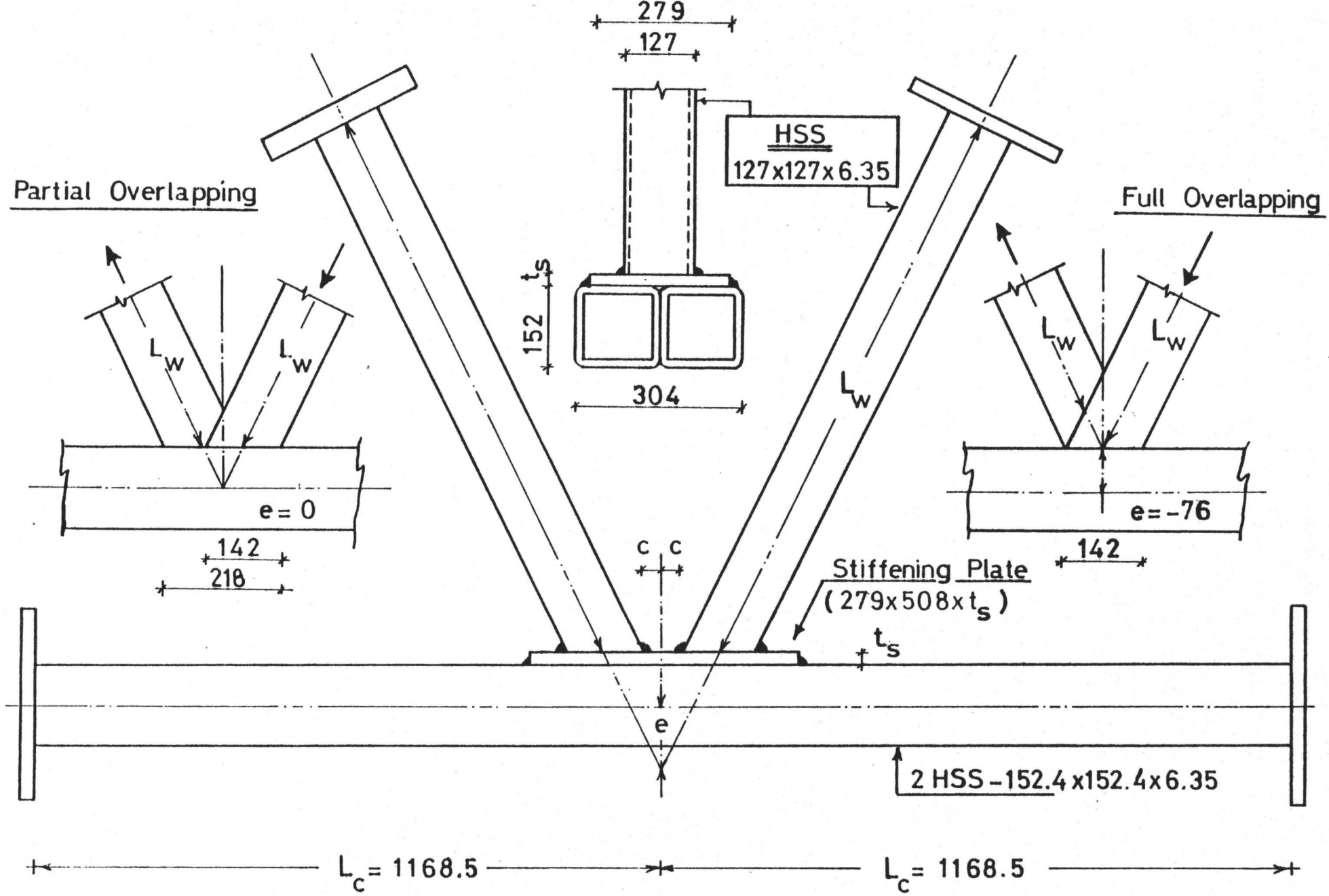

FIGURE 2.10 BACK-TO-BACK CONNECTION (Dimension in mm)

From 110 coupons, the average yield stress was 395.3 MPa (57.33 ksi) with a standard deviation of 26.48 MPa (3.84 Ksi) for the lot.

2.5 Testing Arrangements

A test rig having the following attributes was designed to load the joints:

1. apply a constant axial load to the chord members, either in tension or compression,
2. apply increasing equal loads to the web members, the sign dependent on the preloading conditions as in Figure 2.11
3. account for different eccentricities; and
4. accomodate different slope angles.

Different possibilities were studied in order to design the most economical, safe and practical rig. Wardenier [25], used a semi-circular segmented arch. Jacks could then be positioned on the inside of the frame on any of the segments commensurate with web member angles.

The possibility of using a regular semi-circular arch was investigated also due to its greater versability. However, the loads to which the frame would be subjected necessitated much larger sections for fabrication. Hence this type of loading was ruled out.

A circular rig similar to the one used at the Corby Research Center [15], in which the specimen is tested in a horizontal position was also considered. High cost and large space requirements tended to rule out this method.

The arrangement that was found acceptable consisted of adjustable

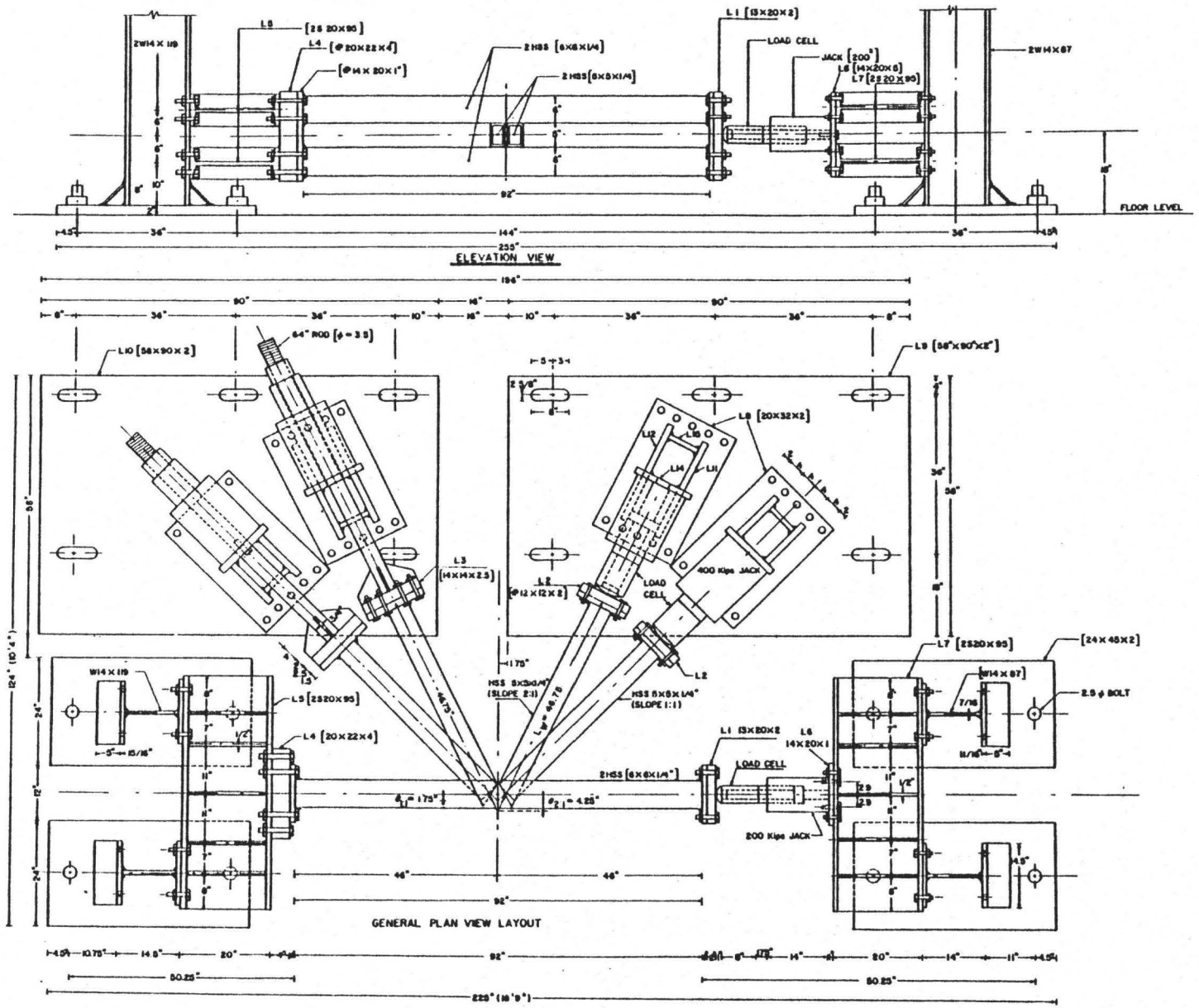

FIGURE 2.11 TESTING RIG.

steel blocks described as horseshoe stands that were bolted to floor plates. These devices carried the reactive forces induced by jack loading to the web members. Floor columns were used to resist chord member preload forces.

A detailed reduced scale drawing is shown in Figure 2.11 with a photograph in Figure 2.12. The specimen was tested in a horizontal position 457 mm (18") above the laboratory floor. Hence any horizontal load would produce minimal bending at the base in comparison with the large diameter rigs described earlier.

2.6 Loading Procedure for Web Members

The two web members were loaded by using two 1792 kN (400 Kips) hydraulic jacks. Each jack was supported in a horizontal position on a horseshoe stand that was bolted to a large plate (1473 x 2286 x 50 mm) that used 10 bolts of 25 mm diameter. The plate was bolted to the floor with six high tensile steel 64 mm diameter bolts and was positioned 25 mm above the floor with six spacers (305 x 305 x 25 mm).

As is evident from Figure 2.11, large slots in the main base plates were needed to permit horizontal adjustment for positioning the jacks to account for different eccentricities. Additionally, minor rotations of the horseshoe stands could be achieved to ensure proper alignment for jack loading. Two sets of holes were drilled in the main plates to allow two orientations. The configuration of these hole patterns was based on testing joints possessing one of two different slope angle (2:1 and 1:1).

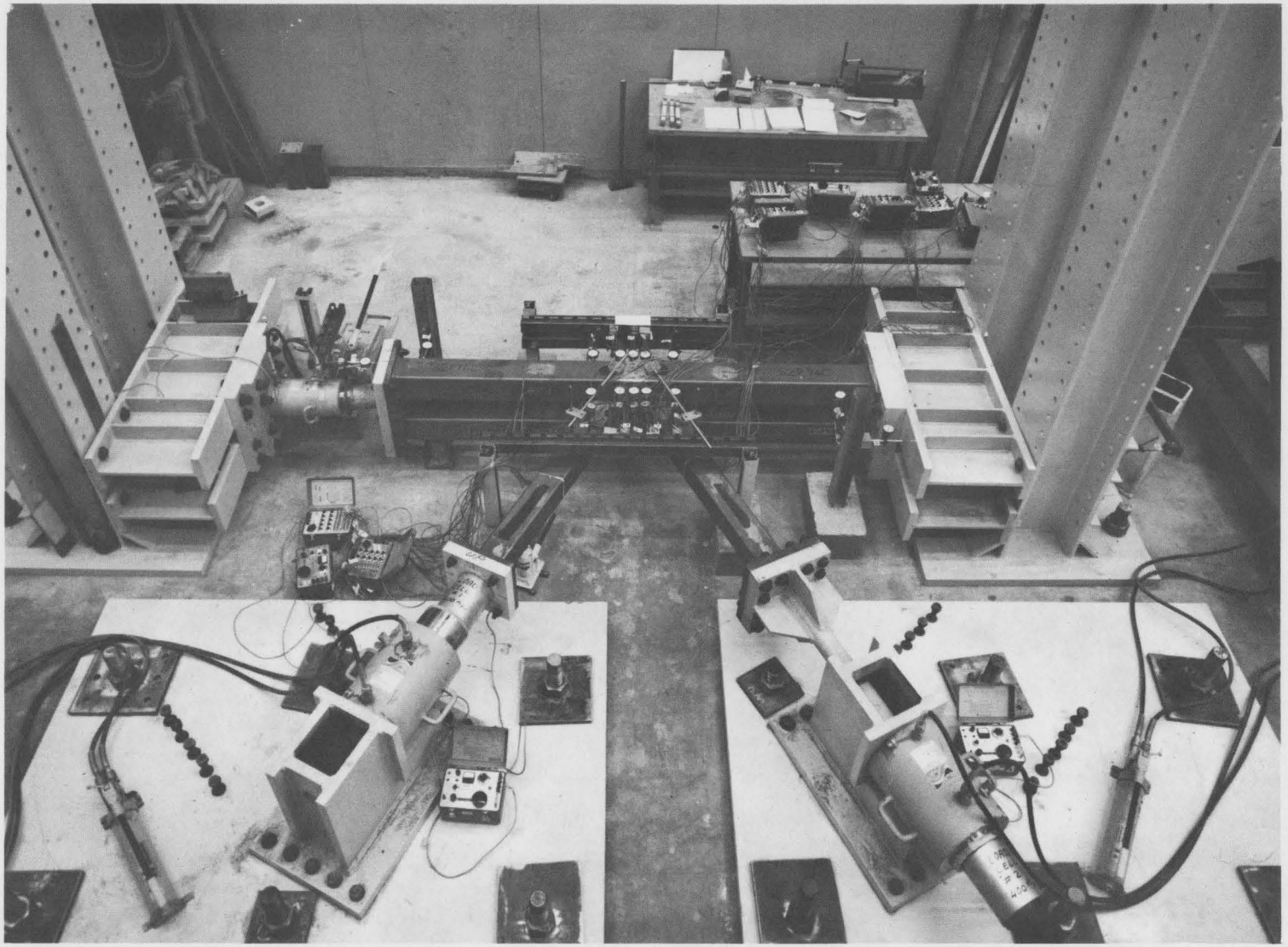

FIGURE 2.12 — PHOTOGRAPH OF THE TESTING RIG

Each horseshoe stand was positioned to load the web member with either a compression axial force or a tensile axial force. In the latter instance, the compressive jack had to be reversed on the stand to apply tensile loading as is the case for the one shown on the left in Figure 2.11.

To alter the direction of loading, it is necessary to turn the horseshoe stand front to back.

2.7 Hydraulic Jack

Three hydraulic jacks were used during the testing program; one was used for the double chord member and two for the web members. The three jacks were fabricated by T.K. SIMPLEX PINE and were single acting models having a central hole to accomodate the use of pull rods. Each jack was provided with four threaded holes at the base to accomodate bolts for fastening.

2.8 Load Cells

Three load cells were fabricated at the Applied Dynamic Laboratory according to requirements of the test program. The load cell which was used for the chord had a capacity of 896 KN (200 Kips) in compression, while the others could support loads of 1792 KN (400 Kips) in compression. These latter two load cells were used with the web member jacks.

The load cells were connected to three strain gauge indicators, from which readings were recorded for prescribed loadings.

2.9 Fastening Device for Tension Loading

Since the jacks used in the experimental program could only be used in compression, a special fastening device was needed for the tension web member. This attachment was comprised of a high strength 90 mm (3.5") rod welded to an end plate 64 mm (2 1/2") thick which used 4 brackets as stiffeners. The end plate accomodated nine 25 mm (1") diameter bolts for attachment to the shoe stand. The other end of the rod was threaded to accept a nut which restrained the movement of the jack that imposed tensile forces on the rod and hence on the web member.

To induce tension in the chord member, the set of I-beams identified as L7 in Figure 2.11 were removed and fastened to the other side of the columns as indicated in Figure 2.13. The end plate of the chord member was provided with a 64 mm (2.5") central hole to accomodate a pull rod of 50 mm (2") diameter with its threaded ends fastened to the end plate of the chord member. The other end restrained the jack and the load cell to produce tension in the rod.

2.10 Measuring Devices

A large number of dial gauges were used for each test to indicate the amount of chord deformation at the joint, the movement of end plates of the chord and the possible movement of the end columns which acted as supporting elements. The arrangement of dial gauges is shown in Figure 2.14.

In addition, two LVDT displacement transducers with a range of ±25 mm were used to measure the relative displacement between the web

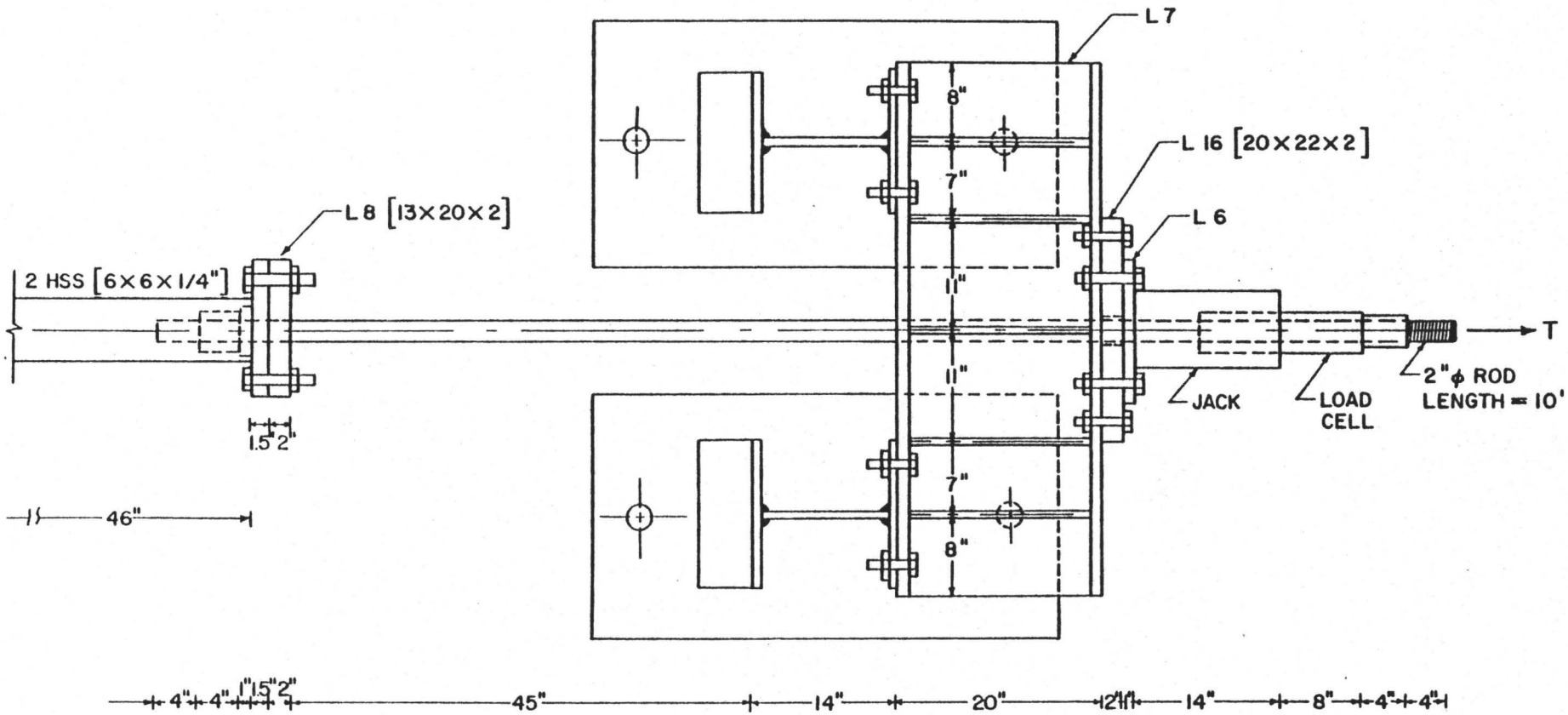

FIGURE 2.13 CHORD TENSION PLAN VIEW

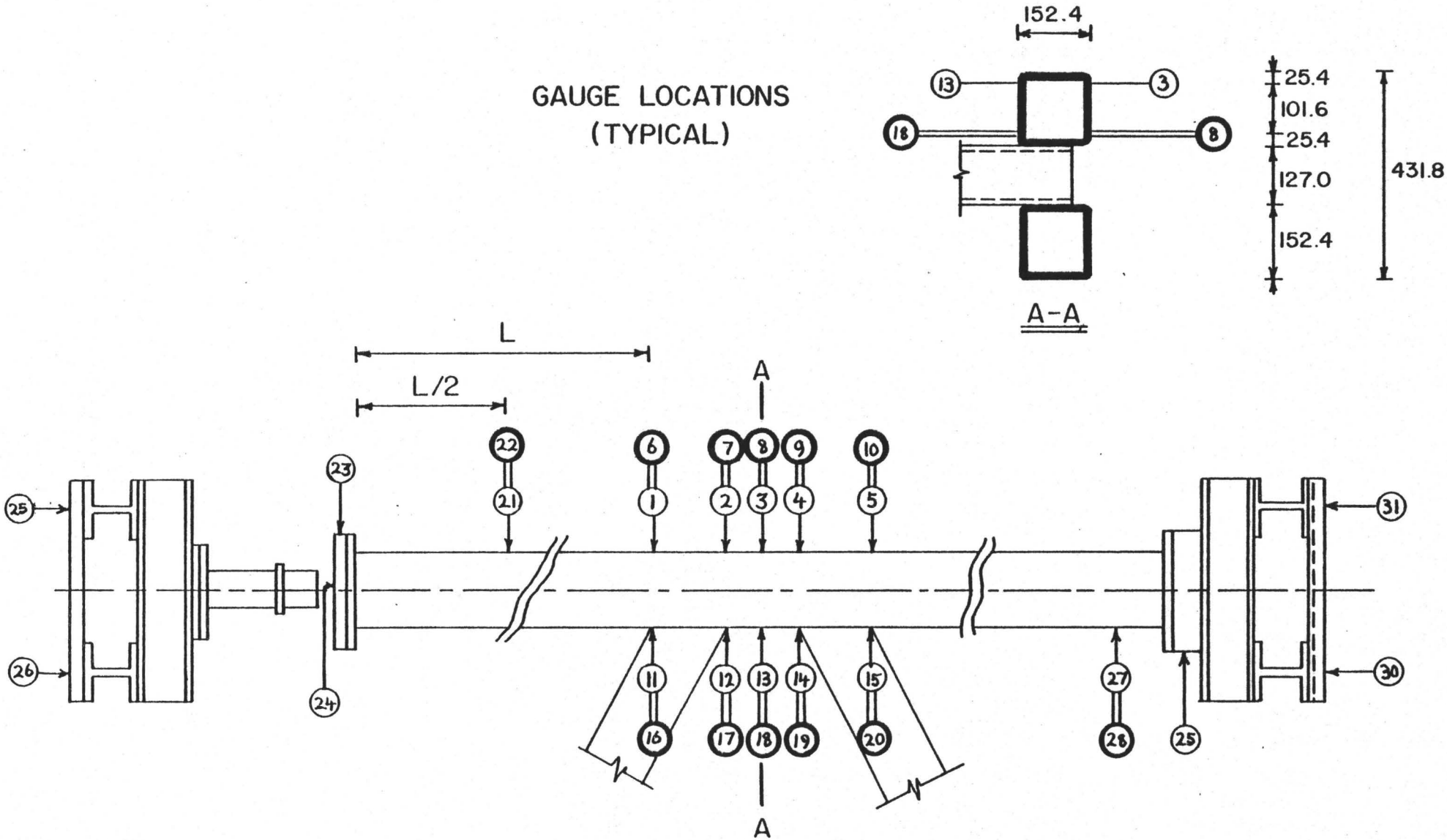

FIGURE 2.14 . DIAL GAUGE ARRANGEMENT (DIMENSIONS IN mm).

members and the double chord for each specimen. A gauge length of 380 mm was used. The purpose of these devices was to assess the overall stiffness of the joint under load. Details are presented in Figure 2.15.

Regular strain gauges and rosettes were used in the testing program. The surface preparation and installation of gauges was done according to the recommendation of the manufacturer. Mounting locations are shown in Figures 2.16 and 2.17. Strain gauges in the former figure, were used for alignment purposes, to prevent loading eccentricity of the chord and web members.

Figure 2.17(a) shows the location of gauges between the two chords for the Standard type joint where four Rosettes were used while Figure 2.17(b) shows the position of the gauges in the web members adjacent to the intersections with the chord members. These latter gauges were mounted to determine how the load would be transferred from the web to the chord member.

Strain gauge measurements were recorded with an Autodata 9 data aquisition system, that at present can monitor 100 channels. Transducer outputs were similarly processed in this way.

2.11 Test Procedure

Prior to testing a given specimen, each of the three load cells was calibrated while the resistance of all strain gauges was checked. In addition a calibration was undertaken for every LVDT transducer after positioning it on the specimen. To help the alignment, mechanical jacks

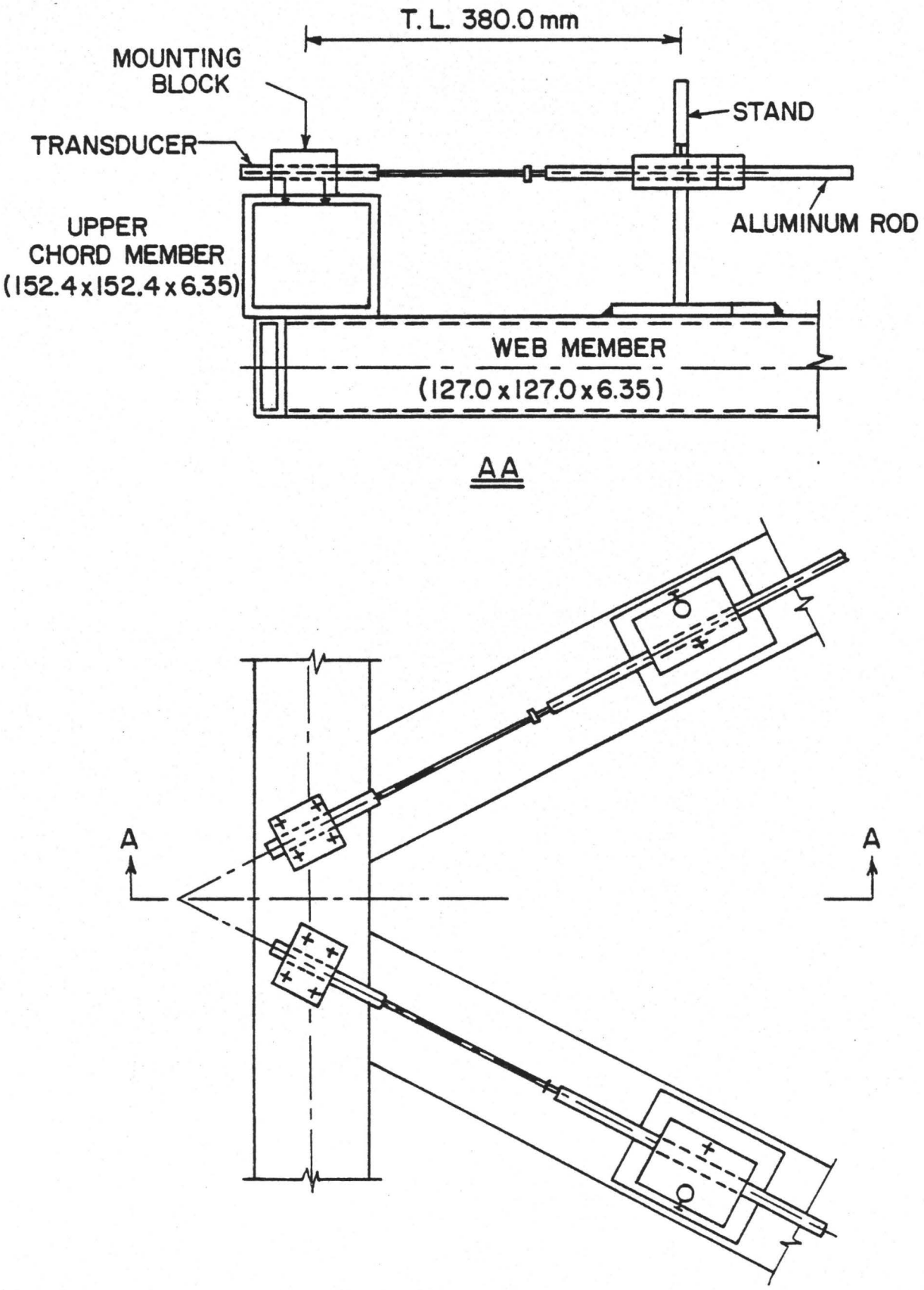

FIGURE 2.15 LOCATION OF THE TWO L.V.D.T. TRANSDUCERS.

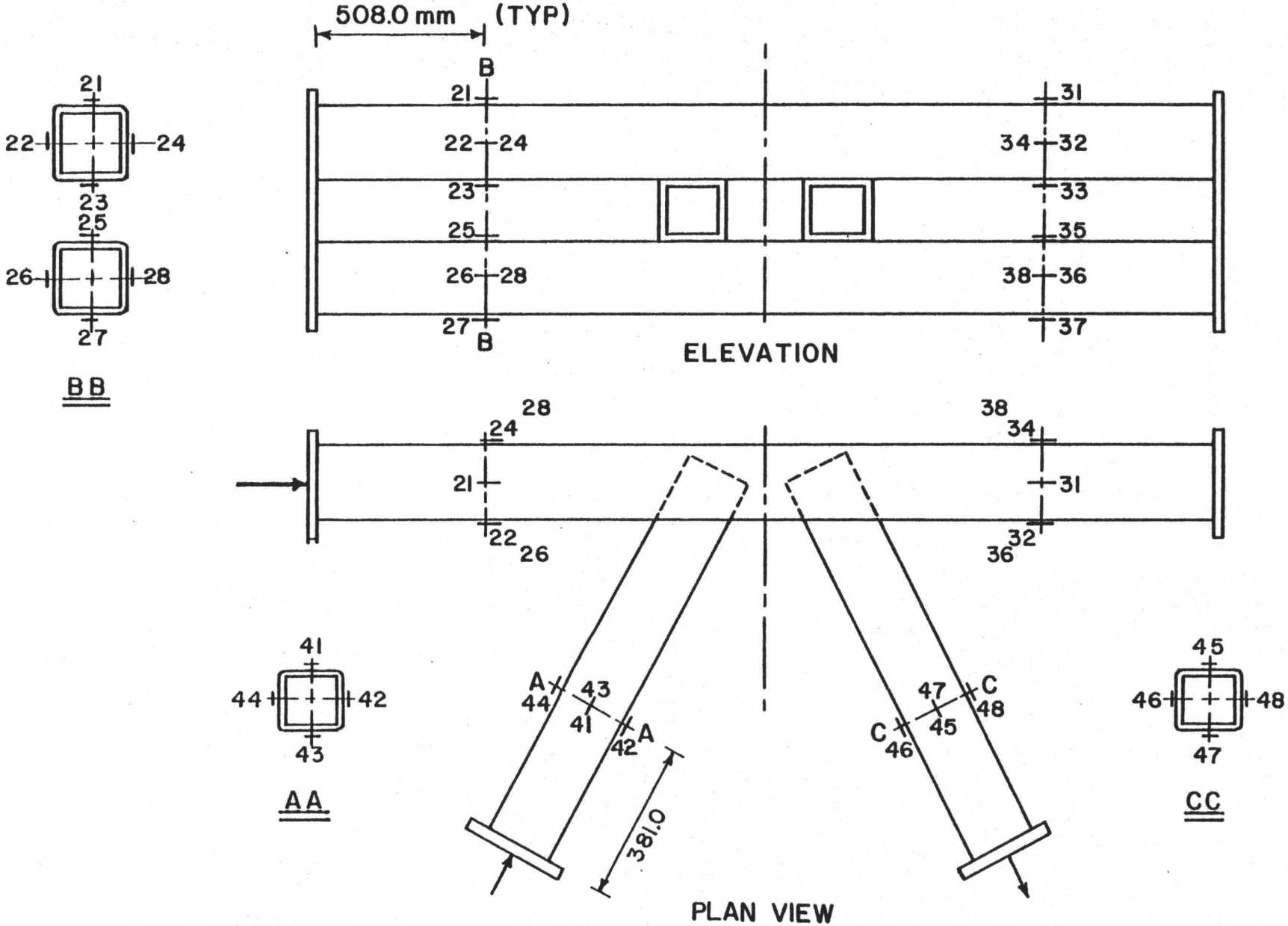

FIGURE 2.16 STRAIN GAUGE LOCATIONS FOR ALIGNMENT.

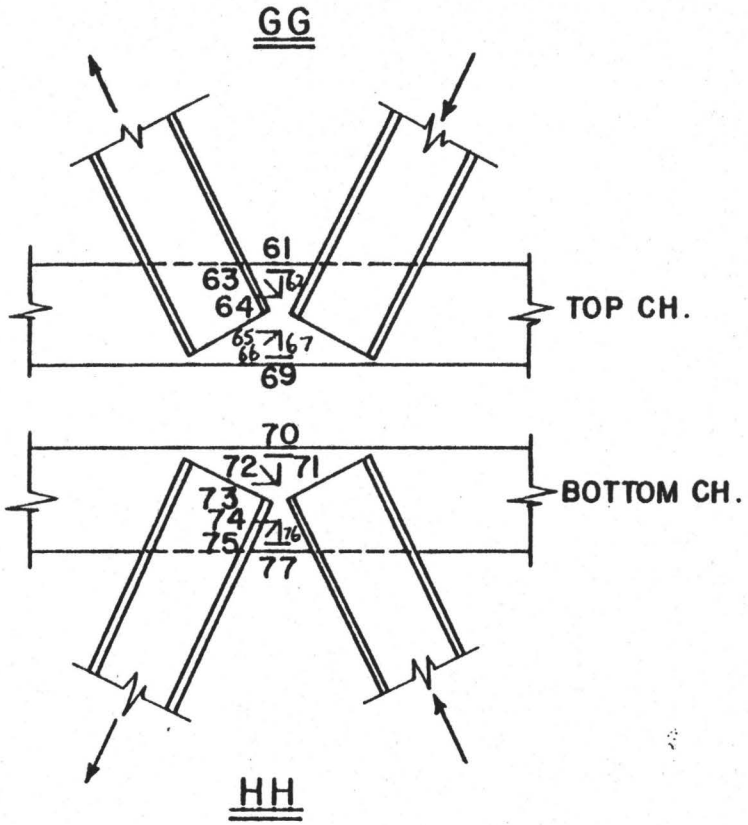

a — Between the Chord Members.

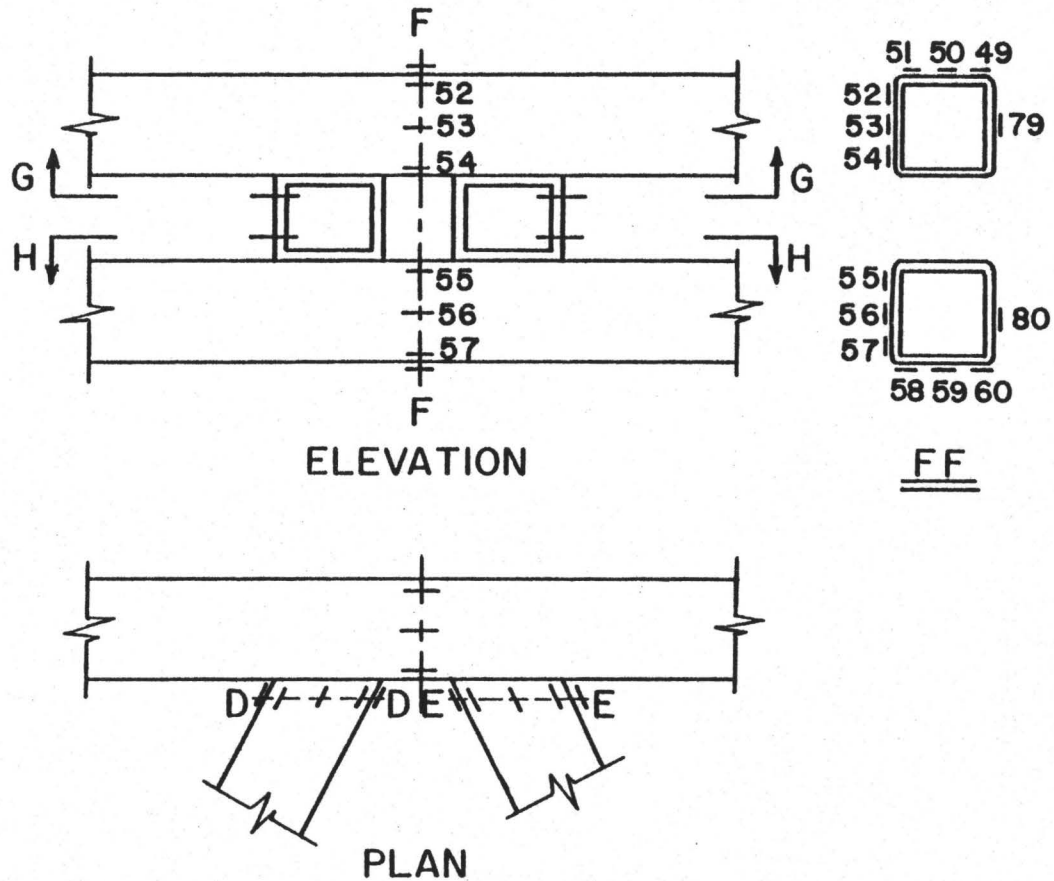

b — Around the Web and Chord Members.

FIGURE 2.17 STRAIN GAUGE LOCATIONS AT THE JOINT.

were used to assist in adjusting the specimen into horizontal position. This effort was facilitated by using rollers between the mechanical jacks and the floor.

Alignment of the chord was performed through a step by step loading and adjustment process. Readings around the periphery of the chord indicated the extent to which uniform loading was applied. When the readings were within 5%, attention was directed to the web members.

The next step was to move the two large plates in order to align the two hydraulic jacks supported by shoe stands with the two web members. Once this first alignment was obtained, three bolts were prestressed to the floor for each plate.

With the chord loaded to its preloading value, the two web members were loaded to 7 or 8% of capacity. Readings around the web periphery were then taken, and if significantly different, the procedure was repeated after realignment. For some specimens it was required to unstress the three floor bolts, adjust the position of the large plates again and repeat the process as before. Once a satisfactory alignment was obtained, the remaining floor bolts for each plate were prestressed to the floor.

To further safe-guard against possible movement of the major plates, spacers were used at various locations. Initial readings were taken throughout for the unloaded case. Preload was then applied to the chord member and a set of readings were obtained. While keeping the load in the chord constant throughout the test, loads were applied incrementally to the web members by an increment of about 5% of the

anticipated capacity. Readings and general observations were recorded at each step. This procedure continued until the specimen failed.

After each test, the specimen was cut to check the dimensions of the HSS and to obtain tensile coupons.

CHAPTER 3

ANALYSIS OF THE EXPERIMENTAL RESULTS FOR THE STANDARD JOINT

3.1 Test Results For Group 1

This group had an eccentricity of 178 mm, a 2:1 slope for the web members and was subjected to five cases of preloading.

The difference that existed between specimens S2P76C and S2P76C* was in fabrication. The two specimens were parametrically identical however specimen S2P76C* exhibited a geometrical imperfection on one side of the two web members. Specimen S2P76C* was therefore tested to determine if the imperfection would cause a premature failure. In fact it did not.

The capacities of the six specimens are shown in Table 3.1, together with the yield stress of the chord and web members, the axial stiffness and the maximum strains at working load.

The mode of failure was essentially the same for all six specimens. It was mainly a shear distortion of the inner two webs of the chord member at the joint, as is shown in Figure 3.1 for specimen S2P76C. After considerable yielding, a crack tended to form between the two webs in the inner web of the chord member, then propagated parallel to the compression web member.

In this group, the effect of chord preloading could be assessed since eccentricity and web angle were held constant. It was found that

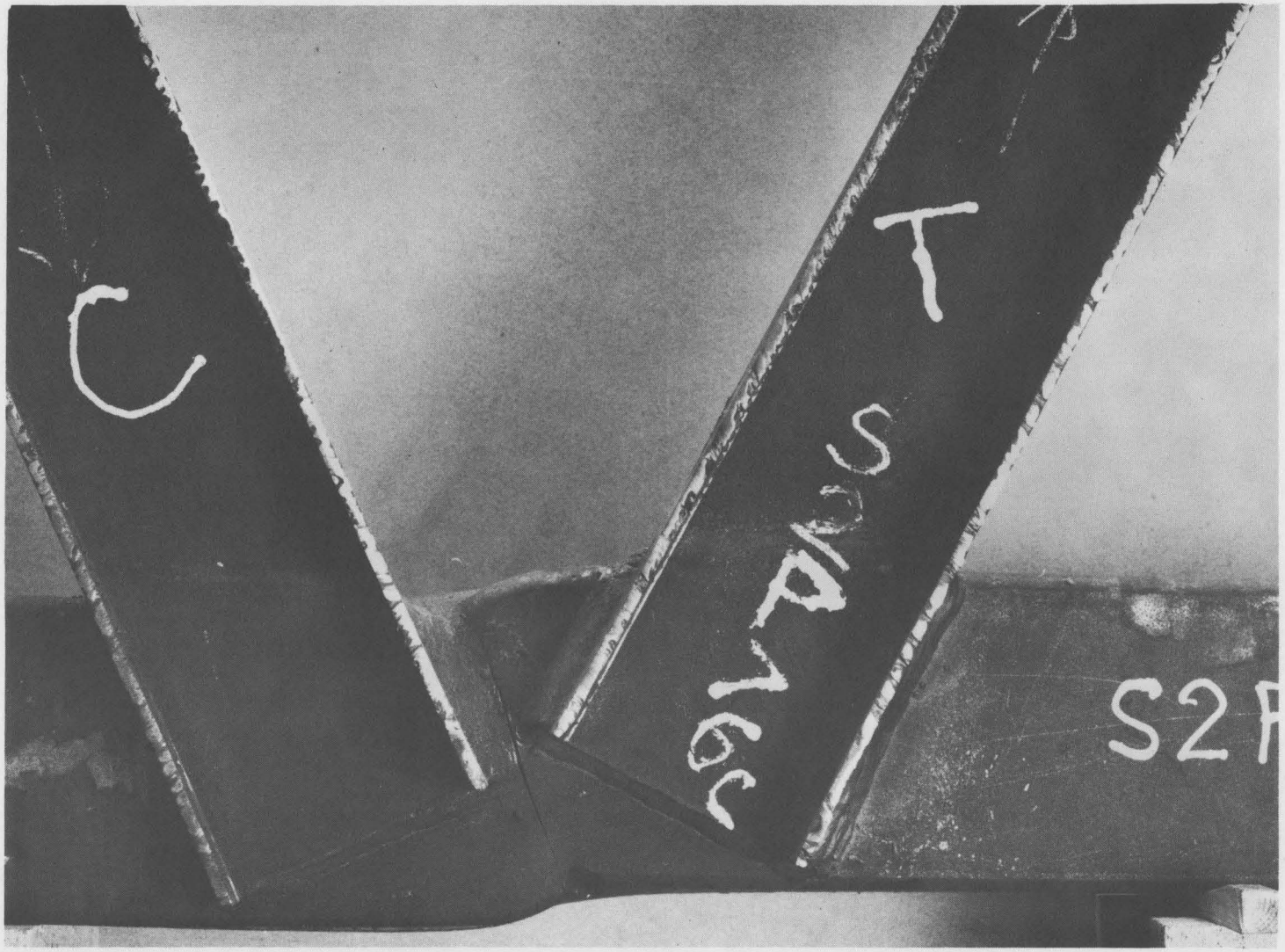

FIGURE 3.1 — FAILURE MODE FOR STANDARD JOINT (GROUP 1)

maximum capacity will be obtained if the magnitude of chord preload is small. As the chord member is loaded to 60% of its yield capacity in either tension or compression the joint strength decreases. Compression preloading causes slightly greater joint deterioration than does tension preloading, perhaps due to higher yield stress values for the chord members of the specimens in tension preloading.

Web force-deformation LVDT transducer curves are shown in Figure 3.2, i.e., the so-called P-Δ curves which will be used to judge the performance of all specimens. The Δ_c and Δ_t displacements were measured from points on the web center line to the center line of the chord (measured along the web). With an increase in preloading, lower capacity and lower web stiffness (P/Δ) were obtained. The preloading effect is shown in Figure 3.3. Note that for group 1 specimens, S2P72C which had the smallest preload, has the largest stiffness and the second best web force capacity as determined by the joint.

While the web member strain distribution was uniform away from the joint, such was not the case at the section nearest the chord. The strains in the inner flanges of the web members were found to be higher than those in the exterior flanges. It was obvious from the experimental strain distribution that the resultant of the web load had shifted closer to the centre of the joint, suggesting that a smaller effective eccentricity, than the prescribed one, had occurred.

The relative movement of the flanges of one of the chord members was measured by using dial gauges positioned along the flange edges

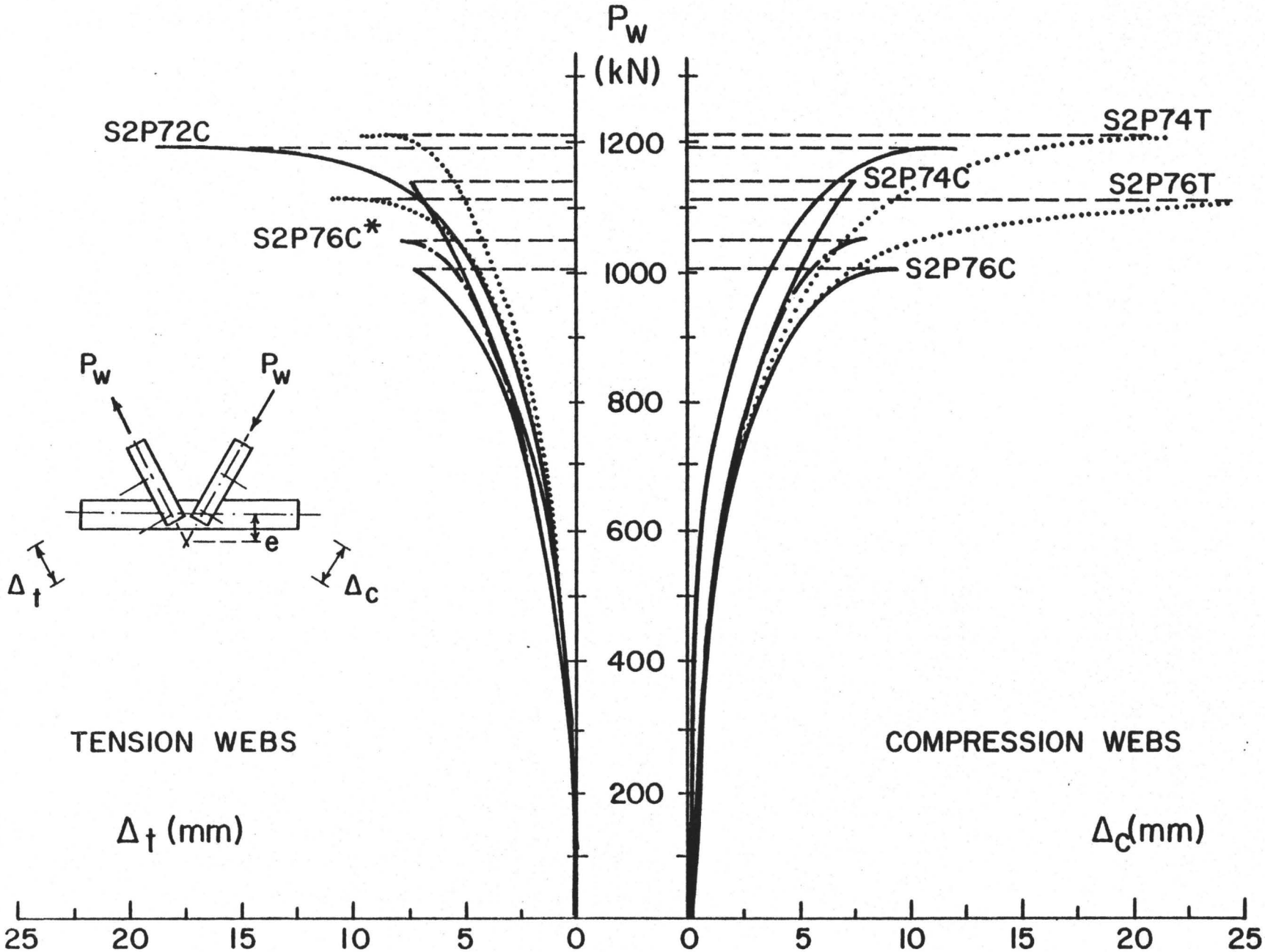

FIGURE 3.2 P_Δ CURVES FOR GROUP1 SPECIMENS

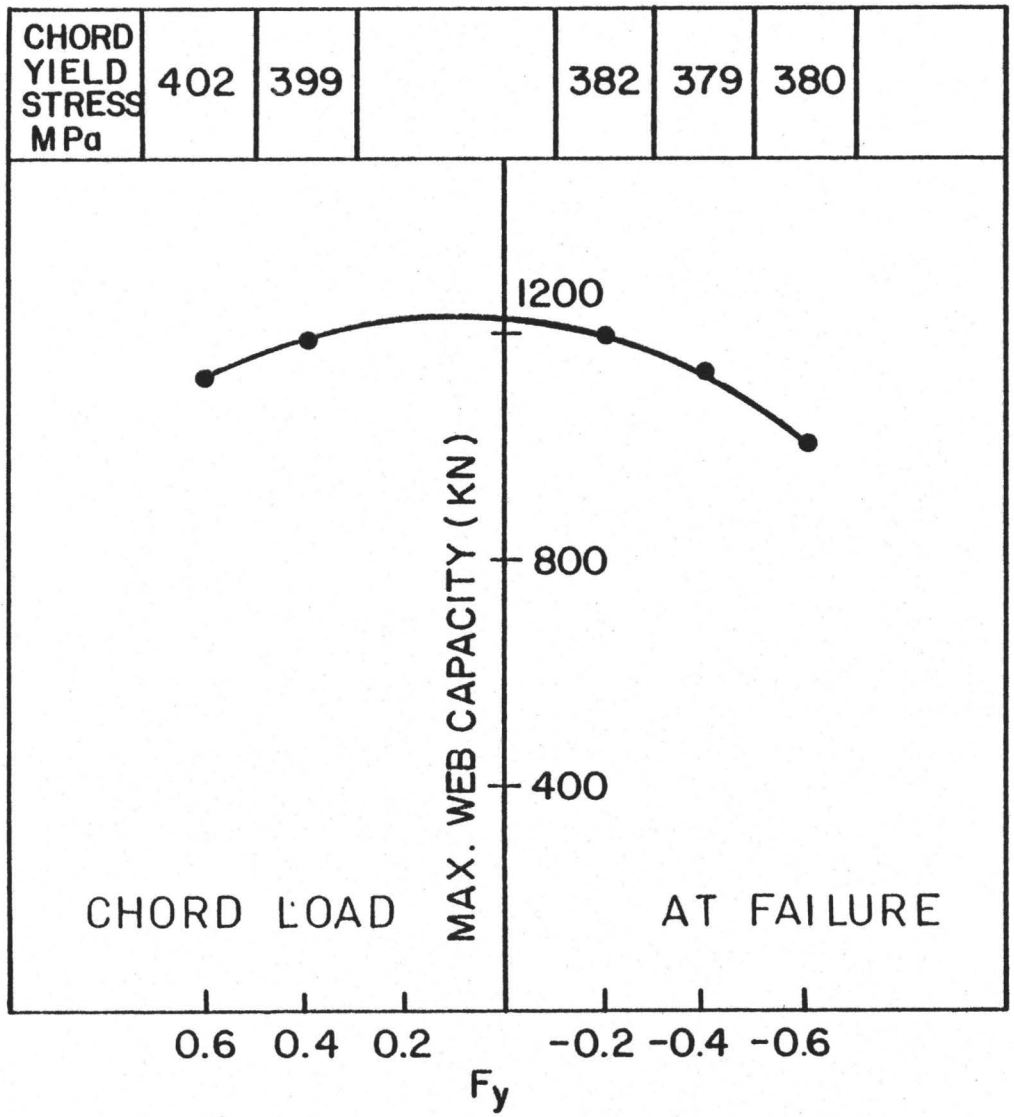

FIGURE 3.3 PRELOADING EFFECT ON GROUP I .

(Figure 2.14). The readings were averaged to obtain the chord deformation, which are shown in Figure 3.4 for the six specimens at the working load level and the ultimate load level. At working load, the chord deformation increased with a larger prescribed increase in preload.

The maximum strain readings in the inner web of the chord members, ε_{max}, were calculated from three gauges 74, 75 and 76. Rosette gauge location is shown in Figure 2.17. It is obvious in Table 3.1 that $|\varepsilon_{max.}|$ at working load increases where the preload is increased. This large amount of strain was mainly caused by shear action as it is clear from $|\gamma_{max.}|$ values.

3.2 Test Results For Group 2

This group had a reduced eccentricity of 10.8 mm, with a 2:1 slope and variable preloadings. The results for the three specimens are shown in Table 3.1. It is obvious that the capacity of this group is significantly higher than the group 1 specimens. The main reason for this increase is attributed to the smaller eccentricity, to be discussed later.

In general, the failure mode was the same for the three specimens, where a shear distortion failure was obvious. Specimens S2P46C and S2P44C had continuous welds between the two web members and the chord member, as opposed to specimen S2P46T which was not bridged in this manner, resulting in a stress concentration at the toes of the web members. This had a weakening effect on the joint and

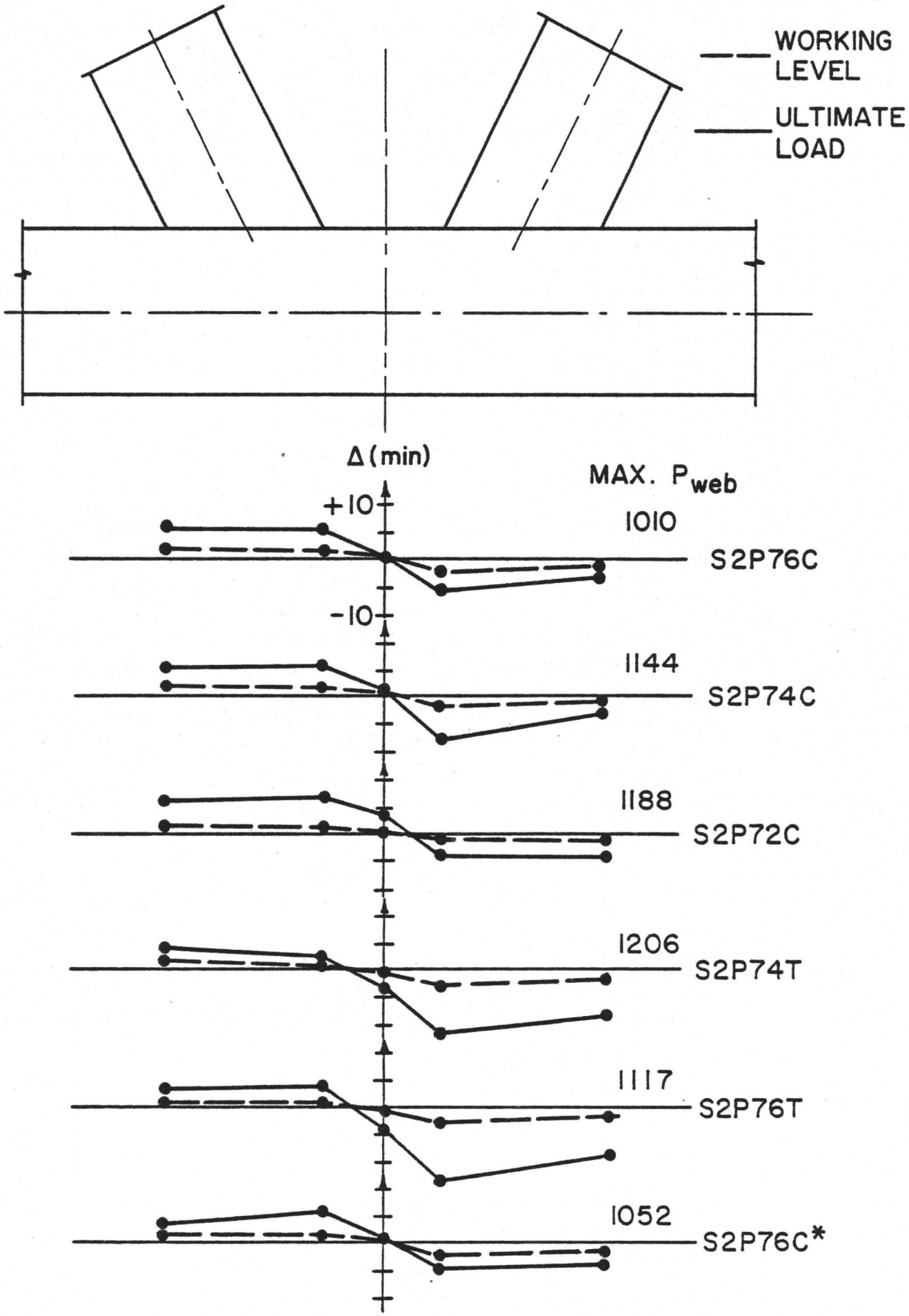

FIGURE 3.4 CHORD DEFORMATIONS FOR STANDARD JOINT GROUP I .

Specimen Code Number	Average Thickness (mm)		Yield Strength (MPa)		$\frac{(P_w)_{ult}}{(P_w)_y}$	At Nominal Branch Working Load					
						Branch Forces & Stiffness				Chord Strains x 10^{-3}	
						Δ_o (mm)		P_w/Δ_o (KN/mm)			
	Branch	Chord	Branch	Chord		Comp.	Tens.	Comp.	Tens.	$\lvert\varepsilon_{max}\rvert$	$\lvert\gamma_{max}\rvert$
S2P76C	6.16	6.25	380	380	0.90	2.07	2.42	359	401	30.8	60
S2P74C	6.18	6.29	371	379	1.05	1.66	2.00	436	548	20.3	39
S2P72C	6.19	6.30	376	382	1.07	0.80	1.15	916	591	19	28
S2P74T	6.22	6.24	373	399	1.09	2.25	2.60	324	516	20.9	33
S2P76T	6.21	6.19	387	402	0.97	2.24	2.60	337	402	24	40
S2P76C*	6.24	6.27	375	388	0.94	2.00	2.35	367	384	32	59
S2P46C	6.18	6.20	368	391	1.17	1.31	1.65	549	1307	9.7	17.5
S2P44C	6.47	6.28	373	396	1.23	.51	.88	1424	2800	6.5	12.9
S2P46T	6.21	6.20	373	388	1.07	1.37	1.72	531	1213	8.5	12.9
S2P16C	6.35	6.38	399	391	1.13	1.66	2.03	468	1766	11.4	21.7
S2P16C*	6.49	6.38	385	384	1.15	1.24	1.60	605	1786	11.5	22.5
S2P16T	6.29	6.37	340	408	1.16	1.61	1.92	411	1742	10.9	17.1

Table 3.1 Test Results for Standard Joints

eventually caused a crack to form after loading was in the plastic range of the joint. A photograph of the failure is shown in Figure 3.5.

By introducing a continuous weld, part of the load in one of the web members is transferred to the other directly through the weld thus bypassing the web of the chord member. This extra weld also increases the area of the cross section which is responsible for resisting shear and axial loads and helping to increase the capacity of the joint.

The failure mode for specimen S2P44C where a continuous weld existed is shown in Figure 3.6.

The P-Δ curves are shown in Figure 3.7 for the three specimens. The effect of preloading is very clear, when comparing the behaviour of specimens S2P46C and S2P44C, where the capacities were 1277 and 1357 KN for a compression preloading of 0.235 and 0.035 F_y respectively. The slope of the curve for S2P44C was greatest which indicates an improvement in joint stiffness.

Specimens S2P46C and S2P46T behaved almost identically up to a web load level of 800 KN, but their maximum capacities were different due to a weld discontinuity for S2P46T as previously mentioned.

From the results shown in Table 3.1, it is obvious that the ultimate capacities for the three specimens were beyond the yield limit in addition to which Δ_o at working load was smaller than for the group 1 specimens. This result is an indication of better stiffness and capacity for the group 2 specimens as compared with their group 1 counterparts.

The same strain distribution as obtained for group 1 was found

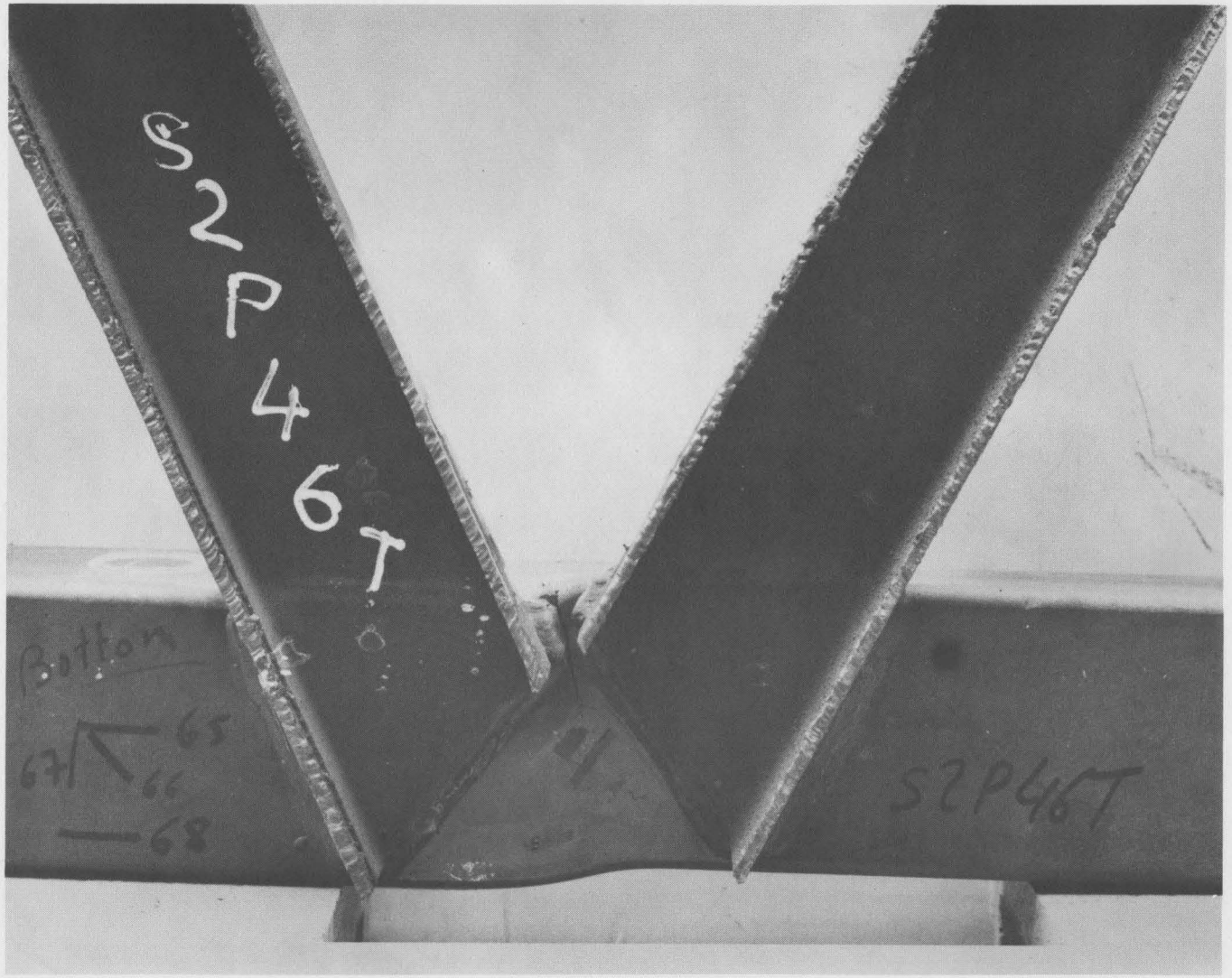

FIGURE 3.5 — DISCONTINUITY OF WELD, CAUSED A CRACK FOR S2P46T

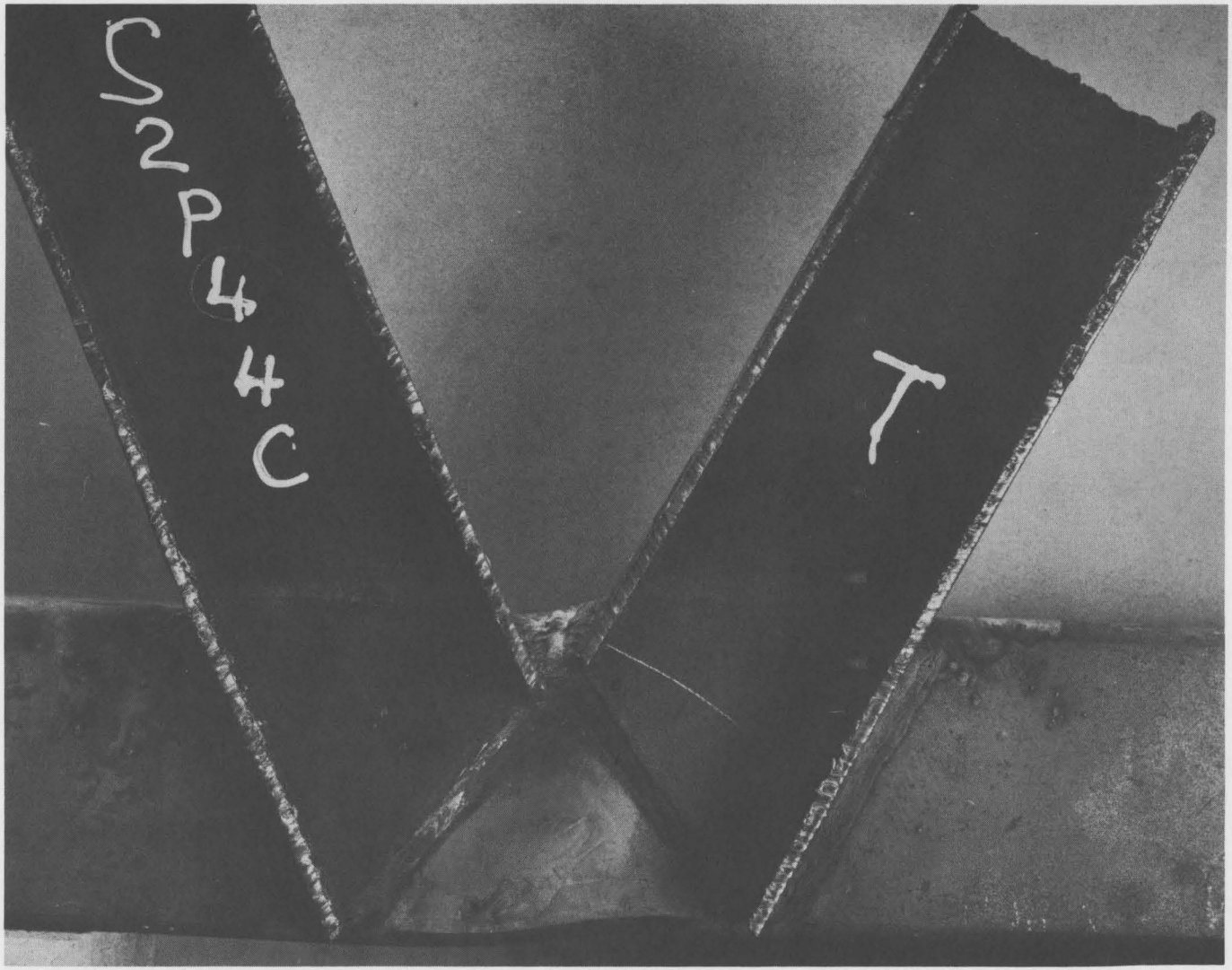

FIGURE 3.6 — CONTINUOUS WELD FOR S2P44C

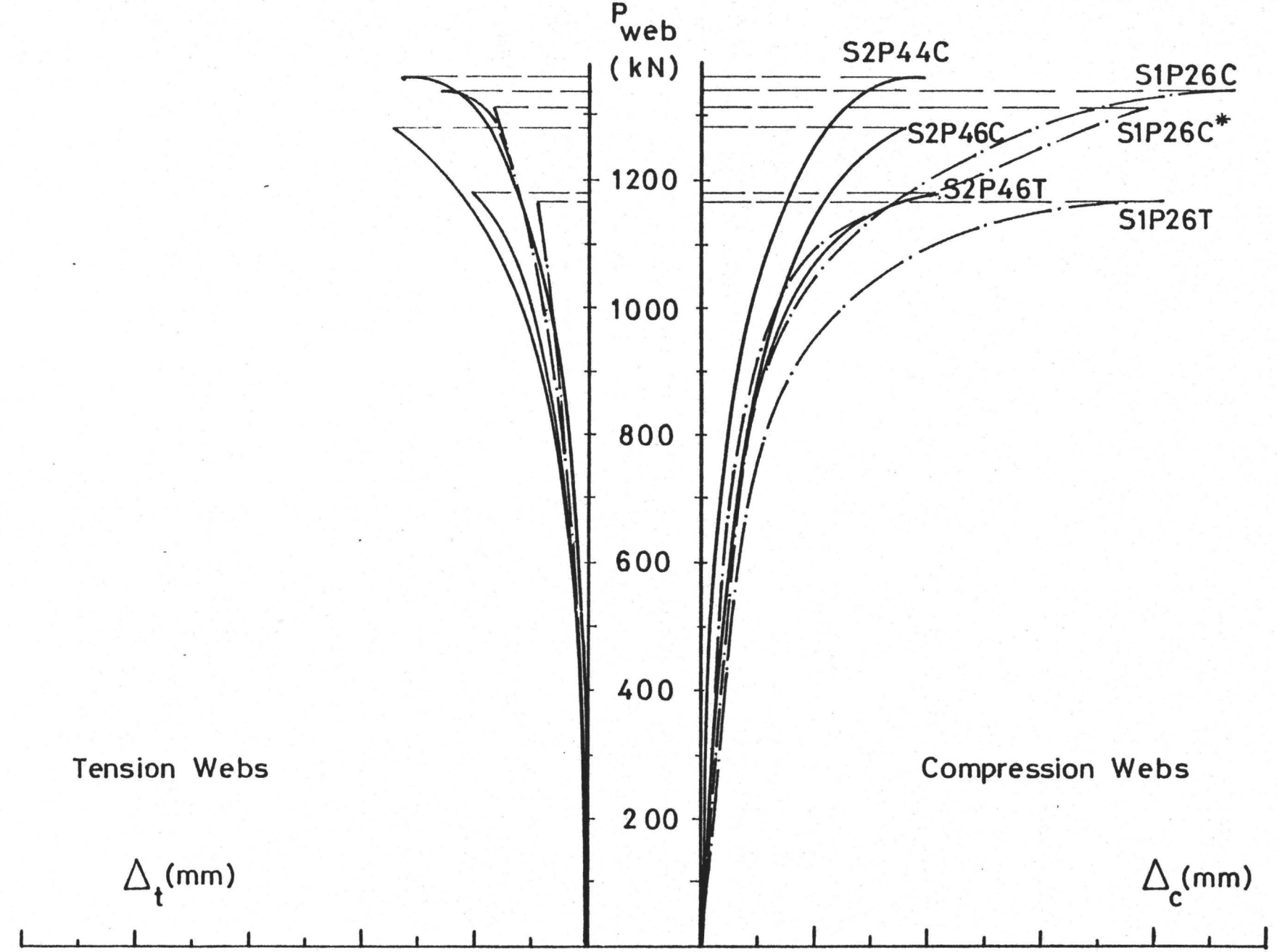

FIG.3.7 P-Δ Curves for STANDARD Joint, Groups 2 and 3

for group 2. The resultant loads in the web members shifted toward the center of the joint producing in effect a smaller eccentricity.

In general the chord deformations for group 2 specimens were smaller than the deformations for group 1. This was due to the smaller eccentricity as well as the weldment between the web members. The two web members being closer to each other, helped to restrain the amount of deformation at the joint. In addition the deformation between the two web members for specimens S2P46C and S2P44C was much smaller than the deformation obtained for S2P46T. Final deformations for the three specimens are shown in Figure 3.8.

3.3 Test Results For Group 3

In this group the angle the web members made with the chord was 45°. The 1:1 slope reduced the joint eccentricity to 45 mm. Originally, three cases of preloading were scheduled for this group: 0.235 Fy and 0.035 Fy in compression and 0.235 Fy in tension. Since it was established that 60% chord yield level was critical and to provide more confidence in testing repeatability, two identical load tests were done in group 3. Specimens S1P26C and S1P26C* gave virtually identical results in capacity as indicated in Table 3.1, although some difference was evident in the deformation readings during testing caused by temporary plate uplift of one of the jack supports. This is evident from Figure 3.7.

The results of Table 3.1 show that the ultimate capacities for

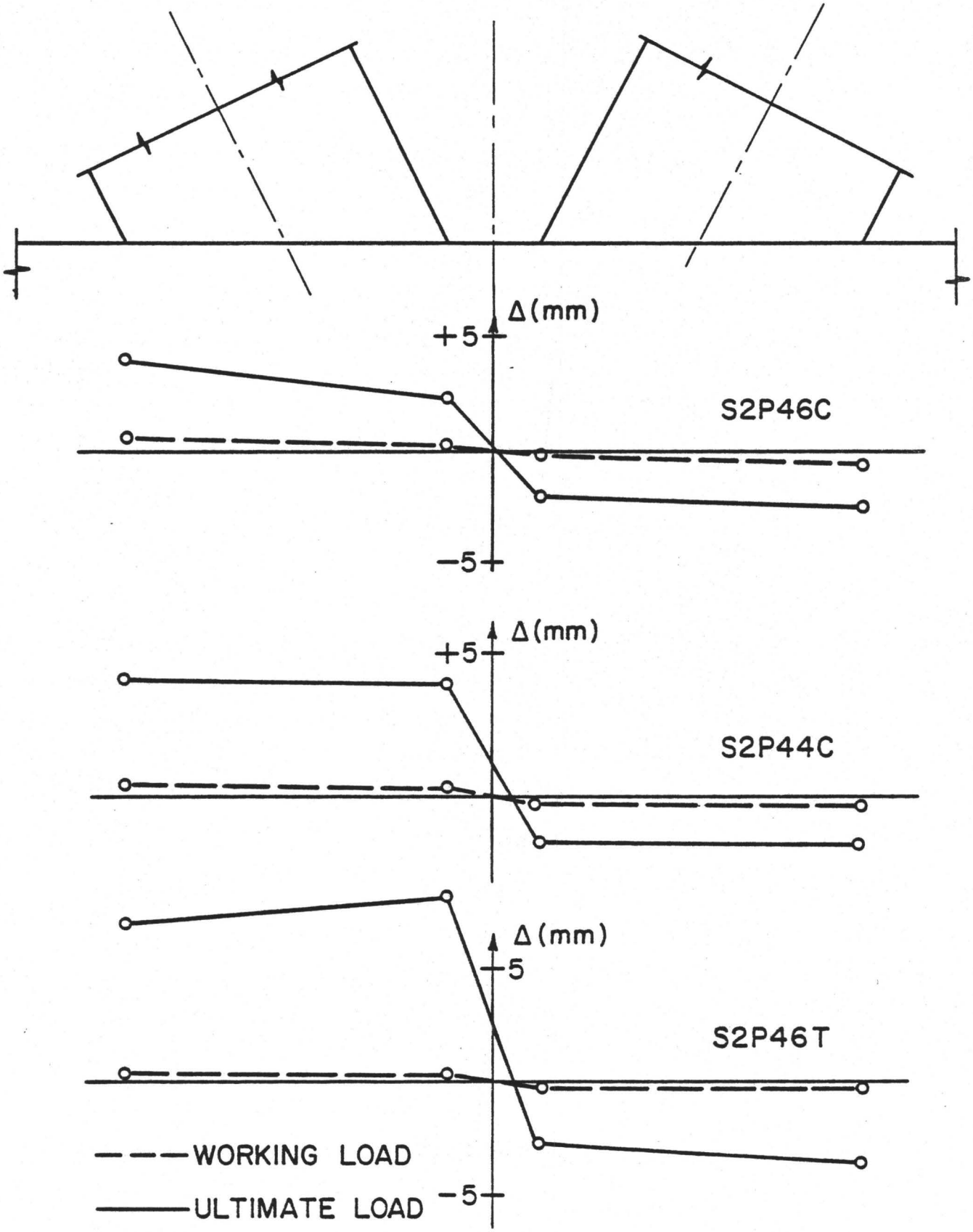

FIGURE 3.8 CHORD DEFORMATION FOR GROUP 2.

the three specimens were at least 13% more than the yield load of the web member, assuming a uniform distribution of axial stress.

The failure mode was the same for the three specimens, where a small shear distortion was noted. Subsequently, compression web buckling occurred at about the same time as a crack was observed to develop in the weld or in the inner web of the chord member. It seems, then, that the joint itself had adequate strength. By comparing the maximum capacities of the three specimens: it will be noticed that the capacity of SIP26T (1170 KN) is much smaller than for SIP26C (1340 KN). The reason for this large difference was due to a lower yield stress for SIP26T (340 MPa) in comparison with SIP26C (399 MPa). From Table 3.1 it is obvious that the two specimens had almost the same ratio for $(P_{ult}/P_Y)_{web}$, 1.16 and 1.13 respectively. The failure mode for specimen SIP26T is shown in Figure 3.9.

The strain distributions around the web members were similar to the distributions obtained for groups 2 and 1.

The chord deformations for the three specimens are shown in Figure 3.10. A considerable difference existed between the deformation plots of SIP26C and SIP26C*; this was due to the different clearances (c) between the two web members of 17 and 10 mm respectively. The web members were closer to each other in SIP26C*, hence any movement would be more restrained than for SIP26C.

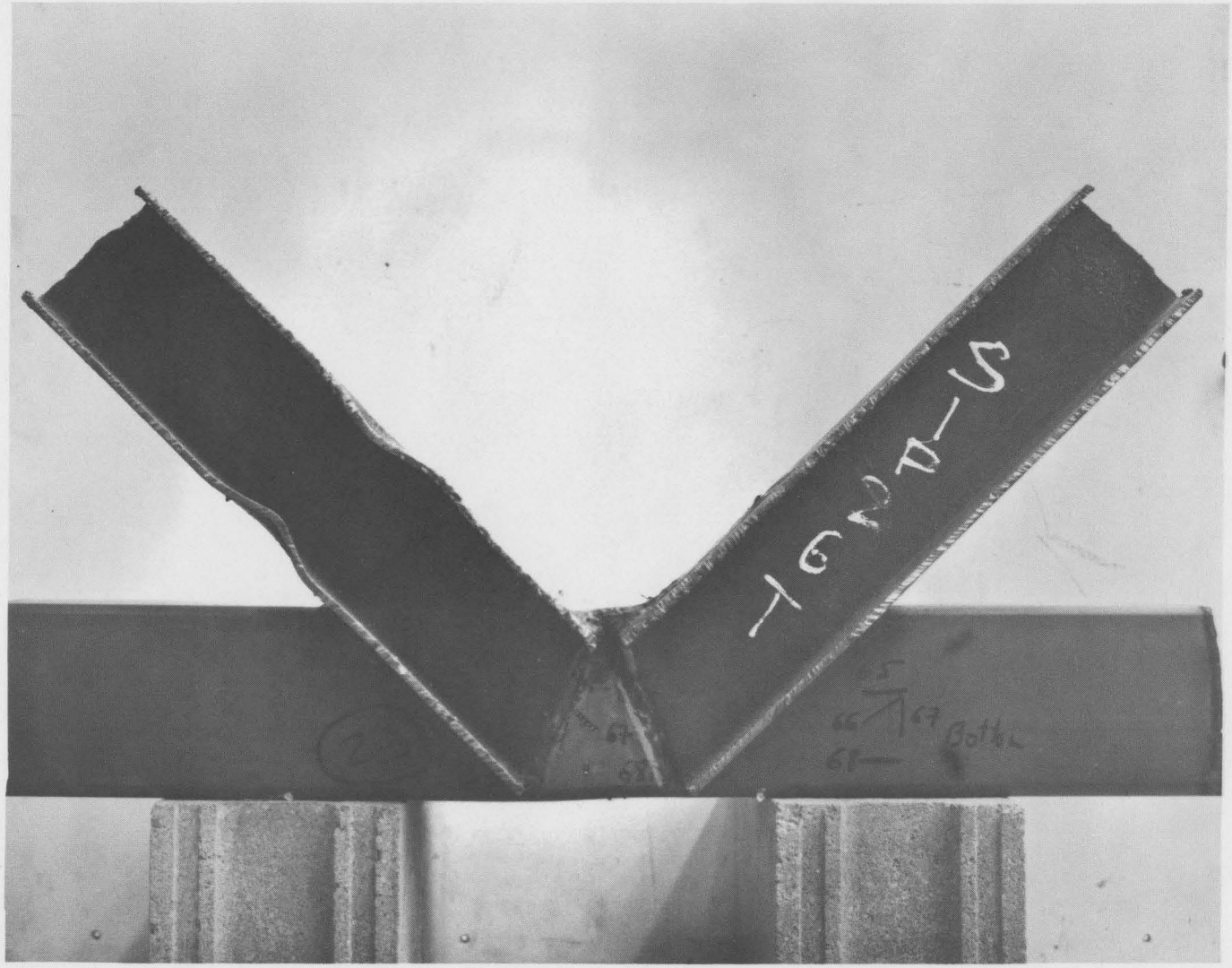

FIGURE 3.9 — MODE OF FAILURE FOR SIP26T

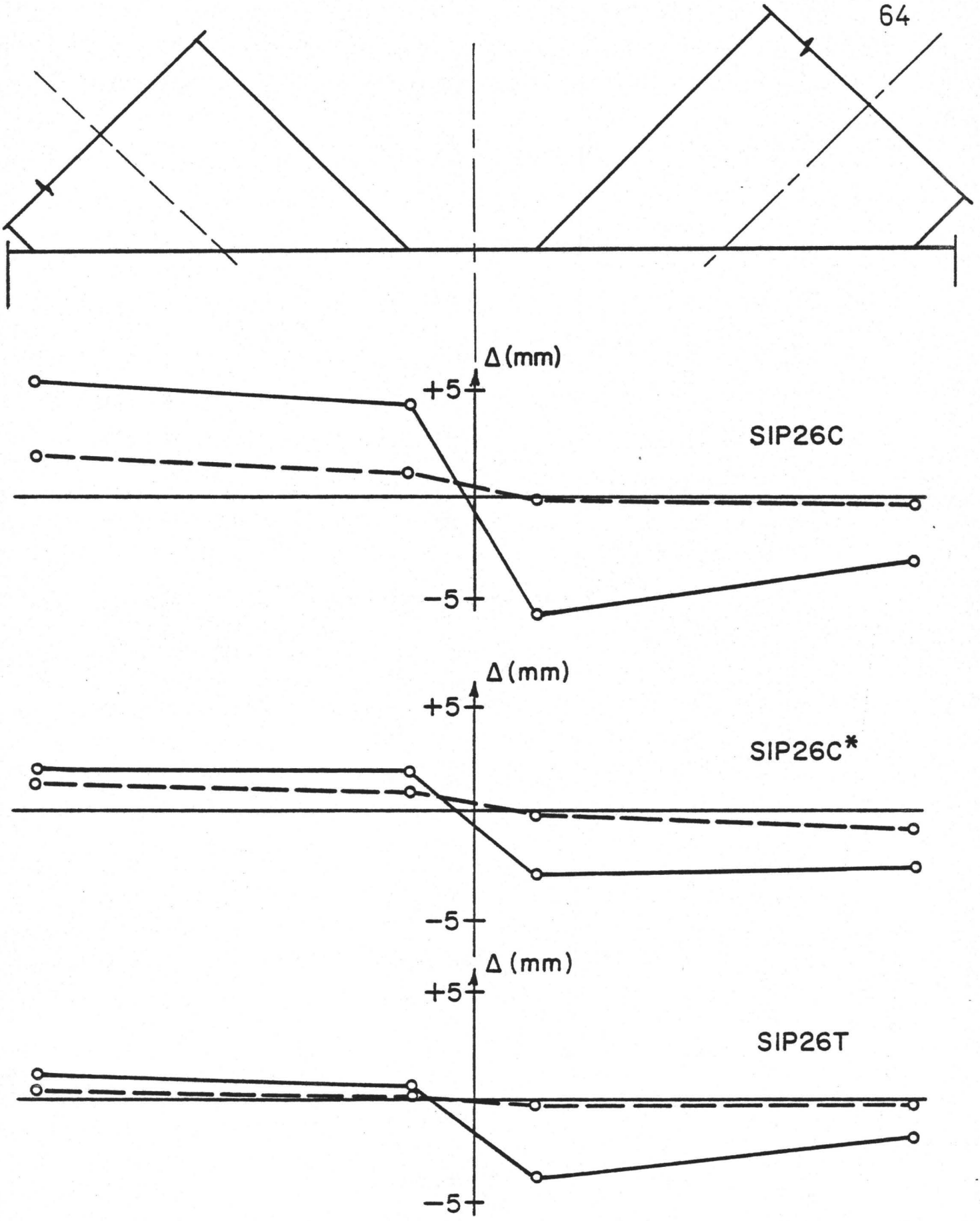

FIGURE 3.10 CHORD DEFORMATION FOR GROUP 3.

3.4 Effect of Eccentricity, Preloading and Slope Angle

The effect of eccentricity is very obvious when comparing the results of specimens S2P76C with S2P46C, and S2P74C with S2P44C, where the capacities were improved for the latter joints by 26% and 19% respectively. The increase in capacity was smaller for the tension preloading case (6%) due perhaps to the discontinuity in the weldment between the web members. All the parameters were the same for the specimens in groups 1 and 2, except for the eccentricity where it was 178 and 108 mm respectively. The reduction in the eccentricity was obtained by having an extra cut at the end of the web member as is shown in Figure 3.11.

By using a 2:1 slope, the minimum eccentricity which may be obtained when using 2 HSS 152x152x6.35 for chord members and one HSS 127x127x6.35 for web members is 108 mm. This eccentricity is considered large for a single chord connection, however when it was used for the double chord connection, the ultimate capacity was above the yield load for all the specimens.

The eccentricity may be reduced only if the slope angle is reduced as it was shown in Figure 2.5.

A 45^{o} angle was used for specimen SIP26C* with a 45 mm eccentricity. It is obvious from Figure 3.12 that the stiffness of the smaller angle specimen was higher, which indicates smaller chord deformation.

By increasing the chord preloading the maximum capacity of the specimen is reduced as was indicated in Section 3.1. However the amount

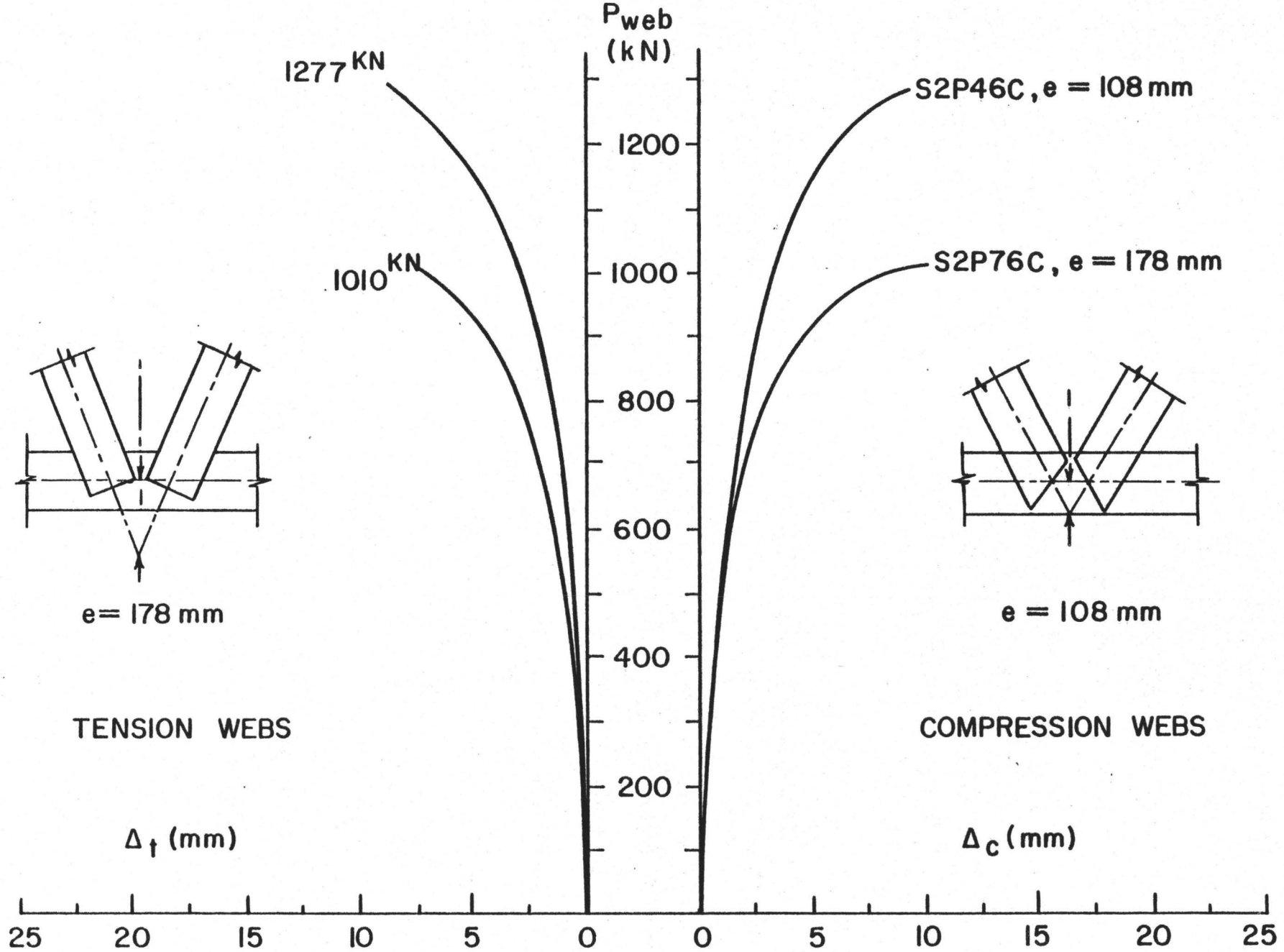

FIGURE 3.11 EFFECT OF ECCENTRICITY.

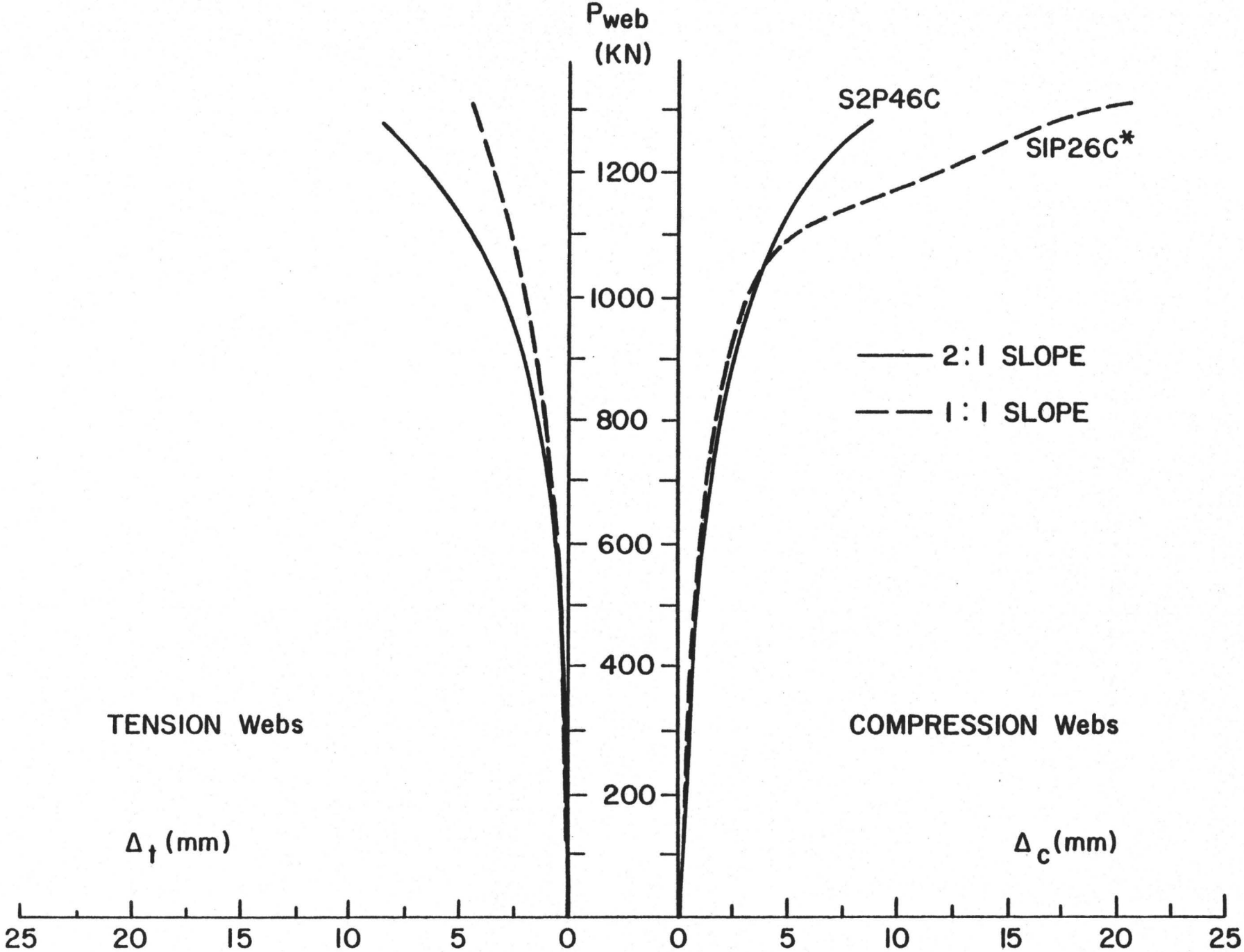

FIGURE 3.12 EFFECT OF SLOPE ANGLE.

of reduction is not as significant as for the case when the eccentricity was changed.

It is evident from the results that chord preload and eccentricity are significant parameters. The former quantity depends on loading conditions and, as such, cannot be as readily controlled as fabrication parameters.

Not unexpectedly, joint strength and stiffness are both improved with decreasing eccentricity.

3.5 Strain Distribution in the Vicinity of the Joint

Shear distortion was the main mode of failure for the standard joint. Also a crack occurred in the plastic zone, after which severe shear deformation was obvious. Since a considerable amount of welding was used (11 to 14 mm) especially at the intersection of the web members with the chord; it was thought useful to check if the weld had any effect on the parent material. Before discussing the weld effect, strain distribution in the chord between the web members will be outlined first.

Figure 3.13 shows the strain distribution at the most critical stressed area for specimen S2P76T. The shape of the curves was similar for all specimens. Four rosettes were used to identify strains in the elastic range to assess the extent of the deformation at working load. It is evident from Figure 3.13 that the diagonal gauges had much higher readings than the horizontal or vertical gauges. This behaviour was mainly caused by the high shear forces which were transferred through the web of the chord member.

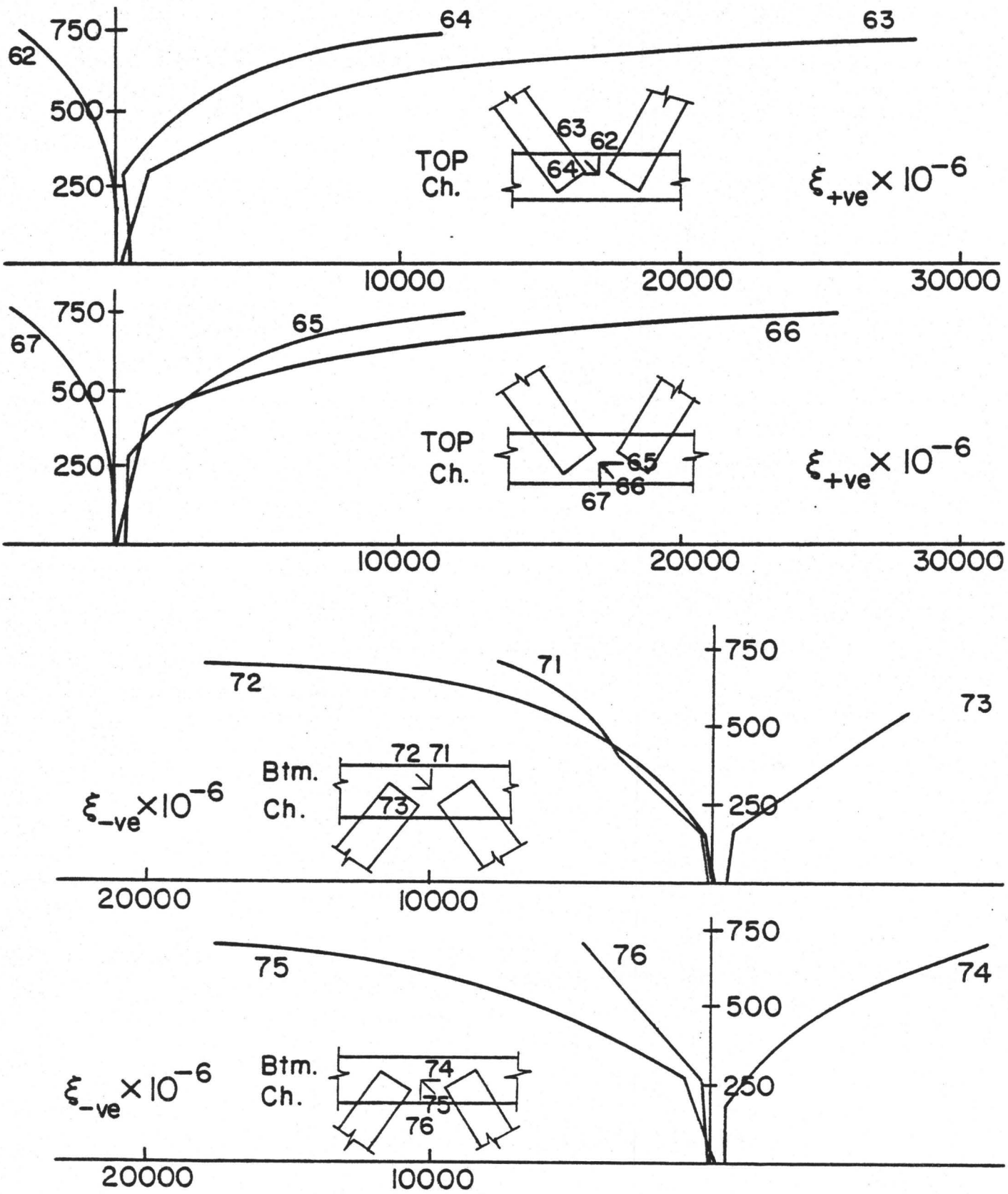

FIGURE 3.13 ROSETTE READINGS AT THE JOINT FOR S2P76T.

The principal strains, ε_{max}, and the maximum shear strain γ_{max} at working load are given in Table 3.1 for the 12 specimens.

Weld effect was checked for specimen S2P72C. A 15 mm wide strip was smoothly cut at the vicinity of the crack in the inner web of the chord member.

Two samples were taken from this strip and examined by optical metallography. These samples were cut in a way to include both the parent material and the weld itself. Metallographic examination at 300X as shown in Figure 3.14, indicated that the grain distribution of the weld material was very similar to the grains of the parent material. No disturbed area was observed or detected, which is an indication that the weld was satisfactory and did not cause any change in the material properties.

A fractographic examination was also necessary to find out if the crack was due to a brittle or a ductile failure. Two other samples were cut and checked under the scanning electron microscope, where different magnification factors were used with the highest equal to 2400X. Scanning electron micrographs are shown in Figure 3.15 and suggest that the behaviour of the material was ductile and that the crack did not initiate by unstable (brittle) crack growth.

From the above two sets of tests it was concluded that the weld did not have any severe effect and did not precipitate the failure of the joint or the occurrence of the crack. This was also evident with the high capacities obtained by most of the standard joint specimens.

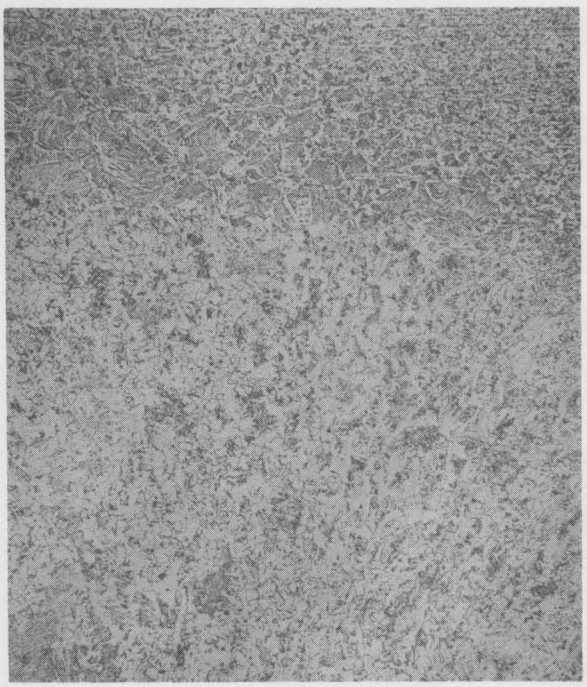

a) 30X Cross Section of Sample

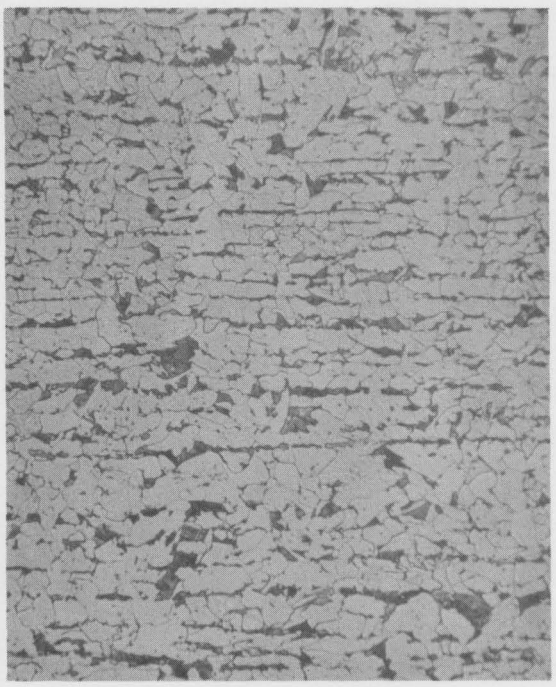

b) 300X Nondisturbed Material

c) 300X Grain Growth near Weld

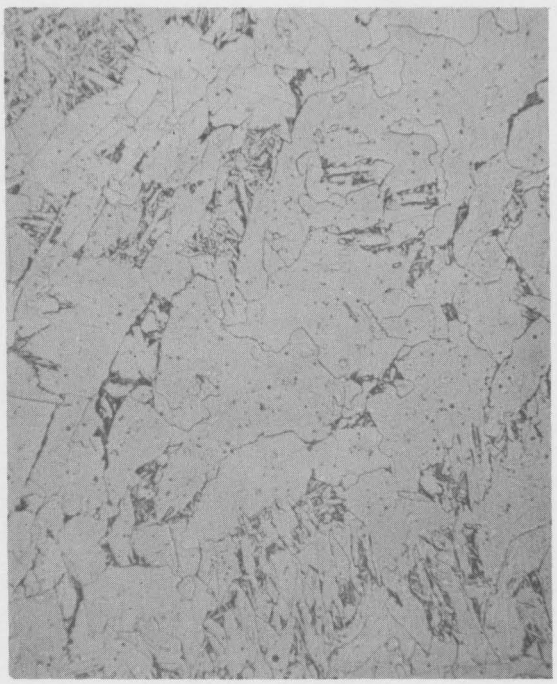

d) 300X Weld Material

FIGURE 3.14 — METALLOGRAPHIC EXAMINATION FOR SPECIMEN S2P72C

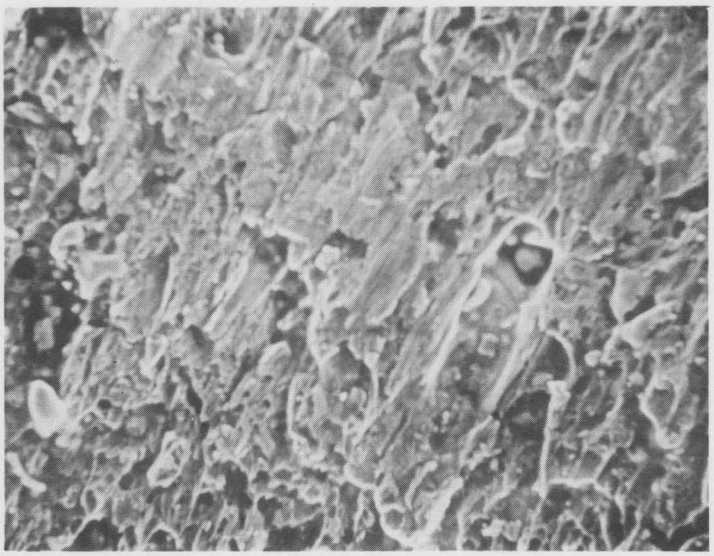

a) 600X Parent Metal

b) 2400X Parent Metal

FIGURE 3.15 — SCANING ELECTRON MICROGRAPHS FOR SPECIMEN S2P72C

CHAPTER 4

EXPERIMENTAL RESULTS OF THE CHANNEL, BOLTED AND BACK-TO-BACK JOINTS

4.1 The Channel Type

The channel type specimens were divided into two groups. The five specimens of group 4 had zero eccentricity with varying preloading from ±23.5% of chord yield. Group 5 was composed of a single specimen having a negative eccentricity of 76 mm and a preloading of -.235 of chord yield.

Two specimens from group 4, C2P06C and C2P04C, had 6.35 mm thick chords. These joints had low strength capacity and stiffness as can be seen from low $(P_w)_{ult}/(P_w)_y$ values in Table 4.1 and the slopes of the P_{web}/Δ_o curves in Figure 4.1. The ultimate load for both specimens was lower, than the web yield load by 29 and 21% respectively. A large chord deformation, shown in Figure 4.2(a), was observed at the end of the tests and was the result of a pushing effect on the inner webs of the chord and a pulling action on the outside webs of the chord. No obvious deformation was detected on the web members for either specimen. From the P-Δ curves of these two joints, it appears that the preloading affected the final capacity. The capacity increased by 8% when the preloading was decreased from -0.235 to -0.035 of yield chord. Both specimens had almost the same stiffness (85 KN/mm) which was much weaker than the one obtained from the standard joint (359 KN/mm).

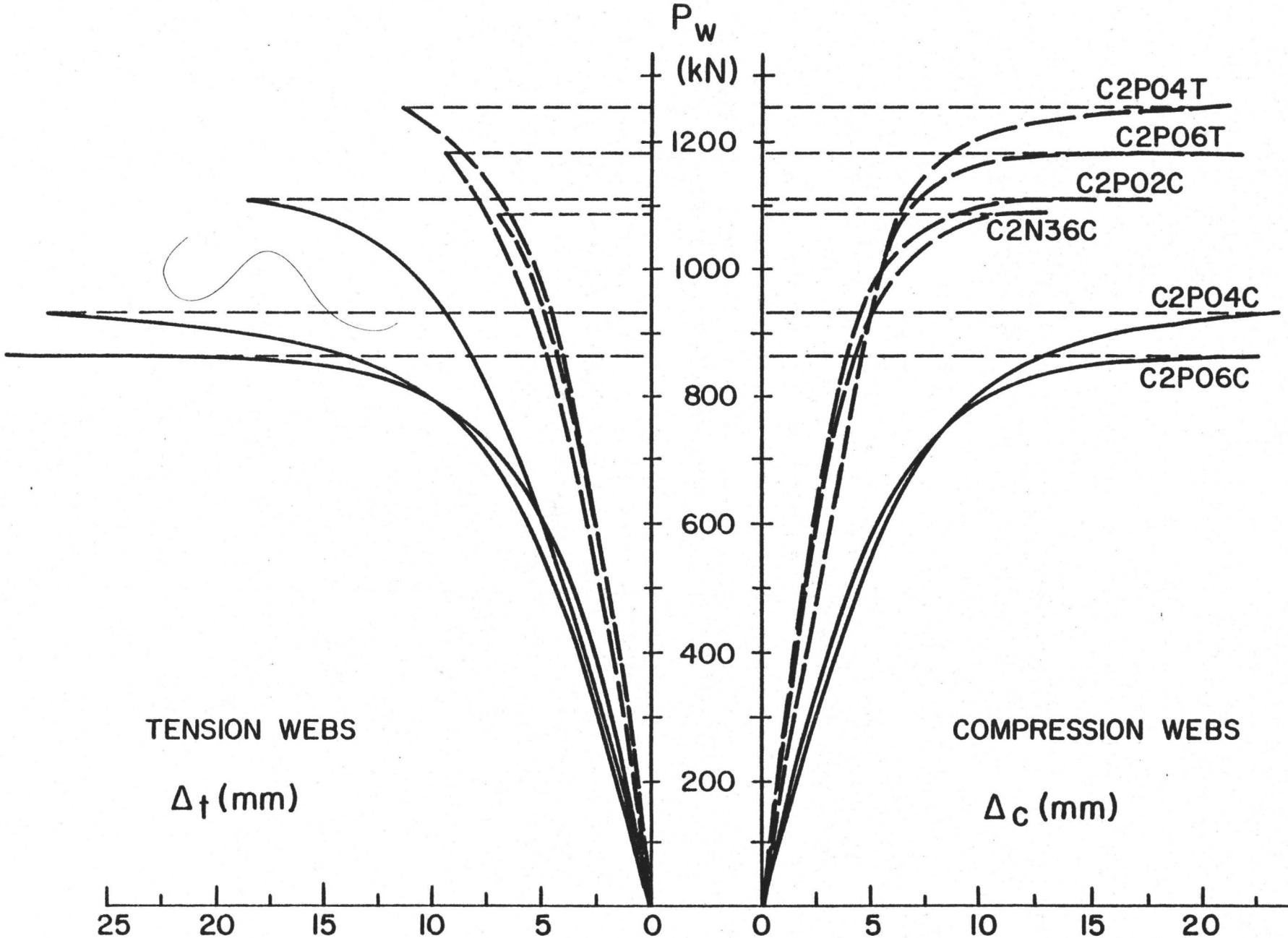

FIGURE 4.1 P_Δ CURVES FOR CHANNEL TYPE JOINTS.

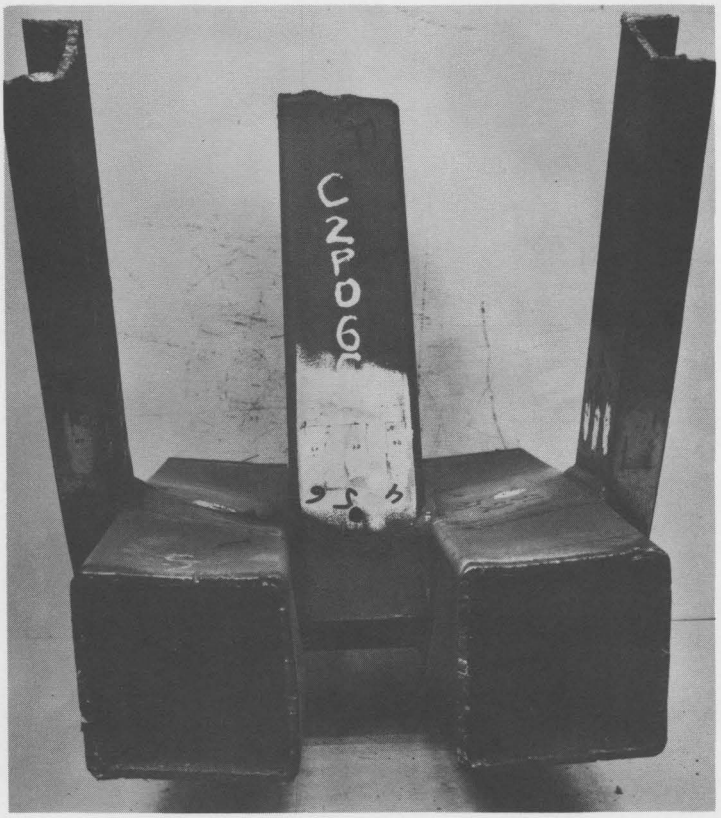

a) DOUBLE CHORD H.S.S. 152 x 152 x 6.35

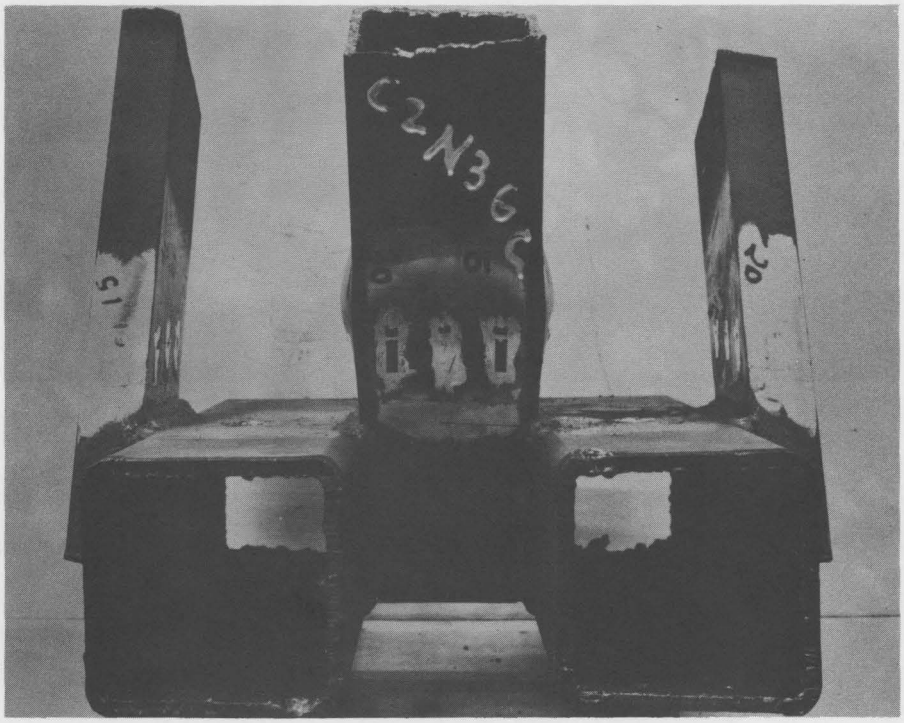

b) DOUBLE CHORD H.S.S. 152 x 152 x 9.53

FIGURE 4.2 — MODE OF FAILURE OF CHANNEL TYPE

Since group 4 specimens did not have any eccentricity, the above results are an indication of a poor performance for this type of joint when a 6.35 mm thick chord is maintained. As such, two specimens C2P04T and C2P06T were fabricated from 152 x 152 x 9.53 mm HSS chords. The strengths increased, however, at the expense of the additional material.

A completely different mode of failures was obtained when the larger thickness was used for the chord member. The failures were local buckling of the compression web member near its intersection with the chord members as shown in Figure 4.2(b). There were no obvious signs of shear or torsional duress in the chord members as was the case when the smaller thickness was used for the chords.

Specimen C2P06T had a 37% higher capacity than specimen C2P06C while C2P04T had an improvement of 35% over the capacity of C2P04C. From the results in Table 4.1, it is obvious that the stiffnesses improved when the 9.53 mm thick chord was used, but remained below that of the standard joint. The web yield load was surpassed by both specimens. Also, the joint capacity increased by 6% when the preloading was reduced from +0.235 to +0.035 of yield chord. Specimen C2P02C used a double chord, having one member from each thickness, its result was a performance between the other pairs as evidenced from Figure 4.1. The mode of failure is shown in Figure 4.3. Note that the deformation for the 6.35 mm chord was similar to the one shown in Figure 4.2(a) for specimen C2P06C while the thicker chord suffered no obvious deformation. As a result specimen C2P02C failed by local buckling of the compression member precipitated by bending due to the nonsymmetry of the load

Specimen Code Number	Average thickness (mm)		Yield strength (MPa)		$\frac{(P_w)_{ult}}{(P_w)_y}$	At Nominal Branch Working Load					
						Branch Forces & Stiffness				Chord Strain x 10^{-3}	
						Δ_o (mm)		P_w/Δ_o (KN/mm)		$\lvert\varepsilon_{max}\rvert$	$\lvert\gamma_{max}\rvert$
	Branch	Chord	Branch	Chord		Comp.	Tens.	Comp.	Tens.		
C2P06C	6.36	6.37	414	405	0.71	9.51	9.50	85	85	6.404	12.248
C2P04C	6.20	6.41	400	410	0.79	9.32	9.10	84	86	3.314	6.228
C2P02C	6.22	6.43	352	363	1.07	2.67	5.76	257	119	1.770	2.812
		9.06		402						0.480	0.676
C2P04T	6.24	9.05	390	369	1.09	3.83	3.24	199	236	0.372	0.593
C2P06T	6.20	9.07	374	363	1.07	3.55	3.46	206	211	0.630	1.008
C2N36C	6.17	9.2	409	445	0.90	3.71	3.52	215	227	0.335	0.532

Table 4.1 Test Results for Channel Joints

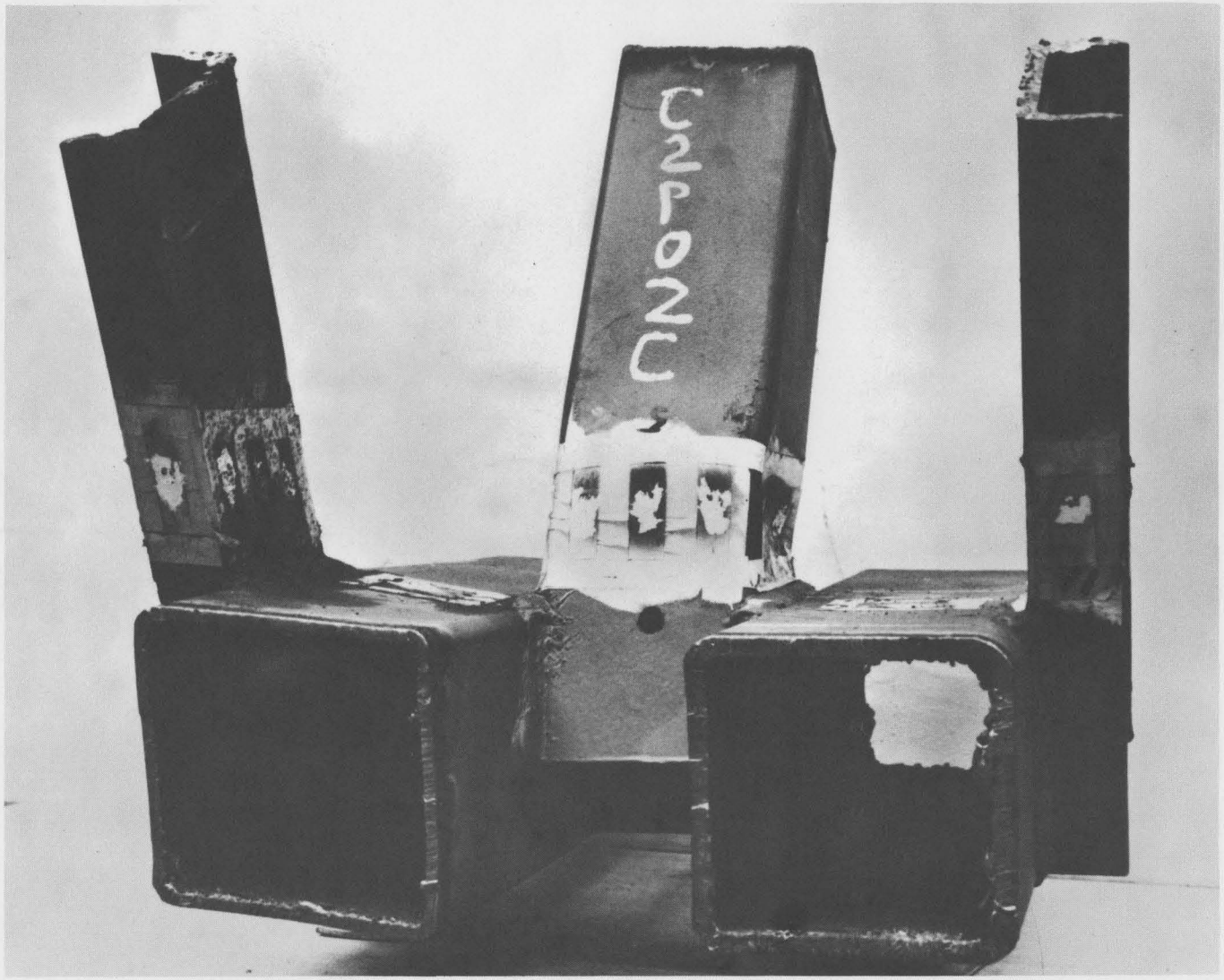

FIGURE 4.3
FAILURE MODE FOR SPECIMEN C2P02C

distribution.

Specimen C2N36C was used to assess the effect of employing a negative eccentricity. It possessed good stiffness qualities, although its strength capacity was somewhat lower (16%) than the others having the same chord thickness. The mode of failure was similar to specimen C2P06T and C2P04T and is shown in Figure 4.2(b).

The strain distributions around the web members of the C-type joints near their intersections with the chord members were symmetrical and the strain readings were in general very near one another. There was no detectable shifting in the resultant web forces at the junction with the chord as was the case with the Standard Type specimens.

The maximum shear strain γ_{max} in the flange of the chord members is shown for the different thickness specimens in Figure 4.4. For the smaller chord thickness, C2P06C, the strains became nonlinear when the web load reached about 37% of its working load, while for the larger chord thickness, C2P06T, the strains remained elastic even as the web member load reached its working value. It is evident then that the torsion produced in the channel type joint can only be adequately resisted if a larger chord thickness than was used for the S-type is employed. In the case of specimens C2P04T, C2P06T and C2N36C the chord essentially behaved elastically up to failure and the deformation was virtually eliminated upon removal of the load.

Figure 4.5 shows the relative displacement of the inside web of the chord with respect to the outer chord web for specimens C2P06C and C2P06T during different stages of loading. The relative displacement at

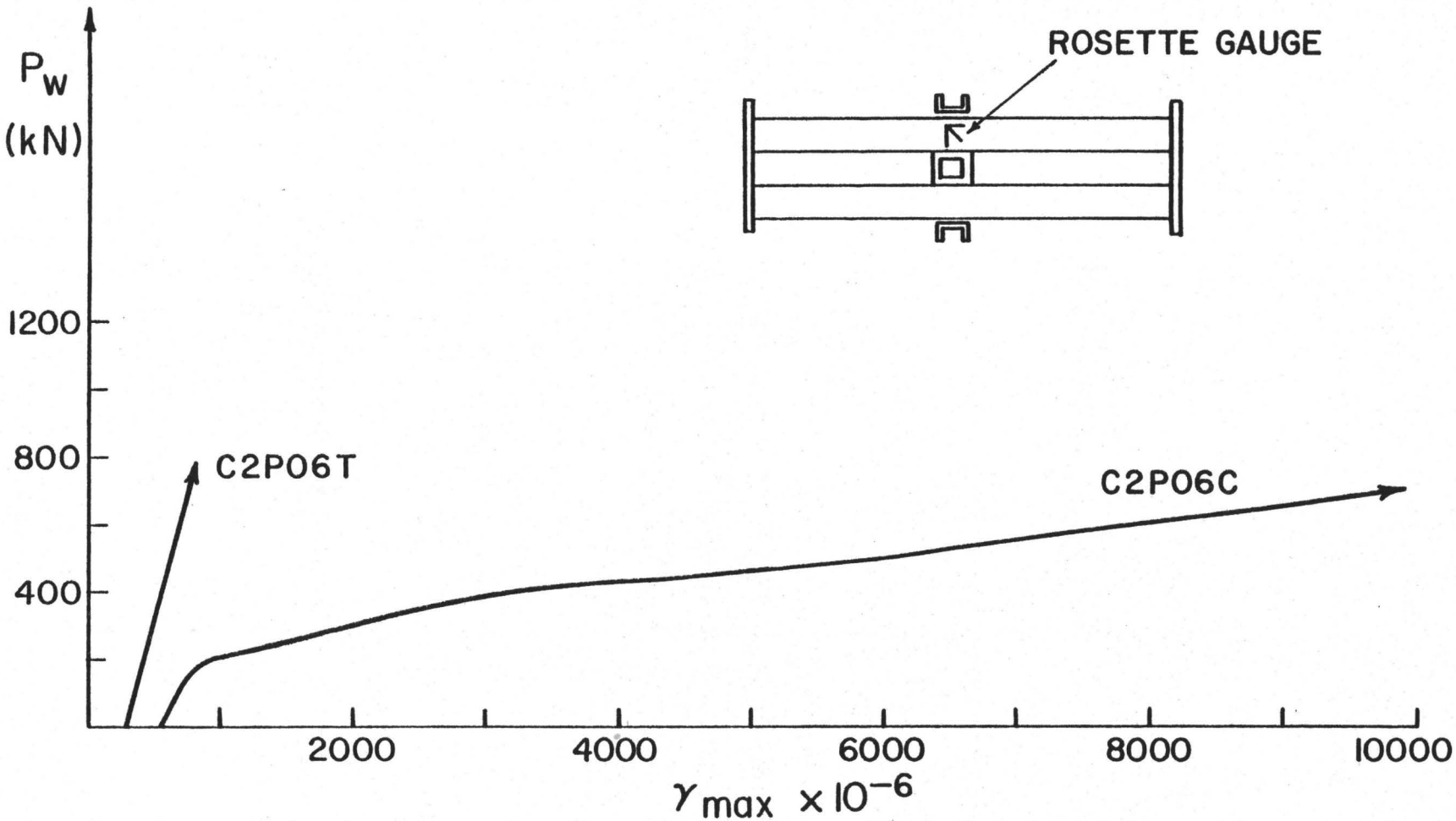

FIGURE 4.4 MAXIMUM SHEAR STRAINS FOR C2P06C & C2P06T.

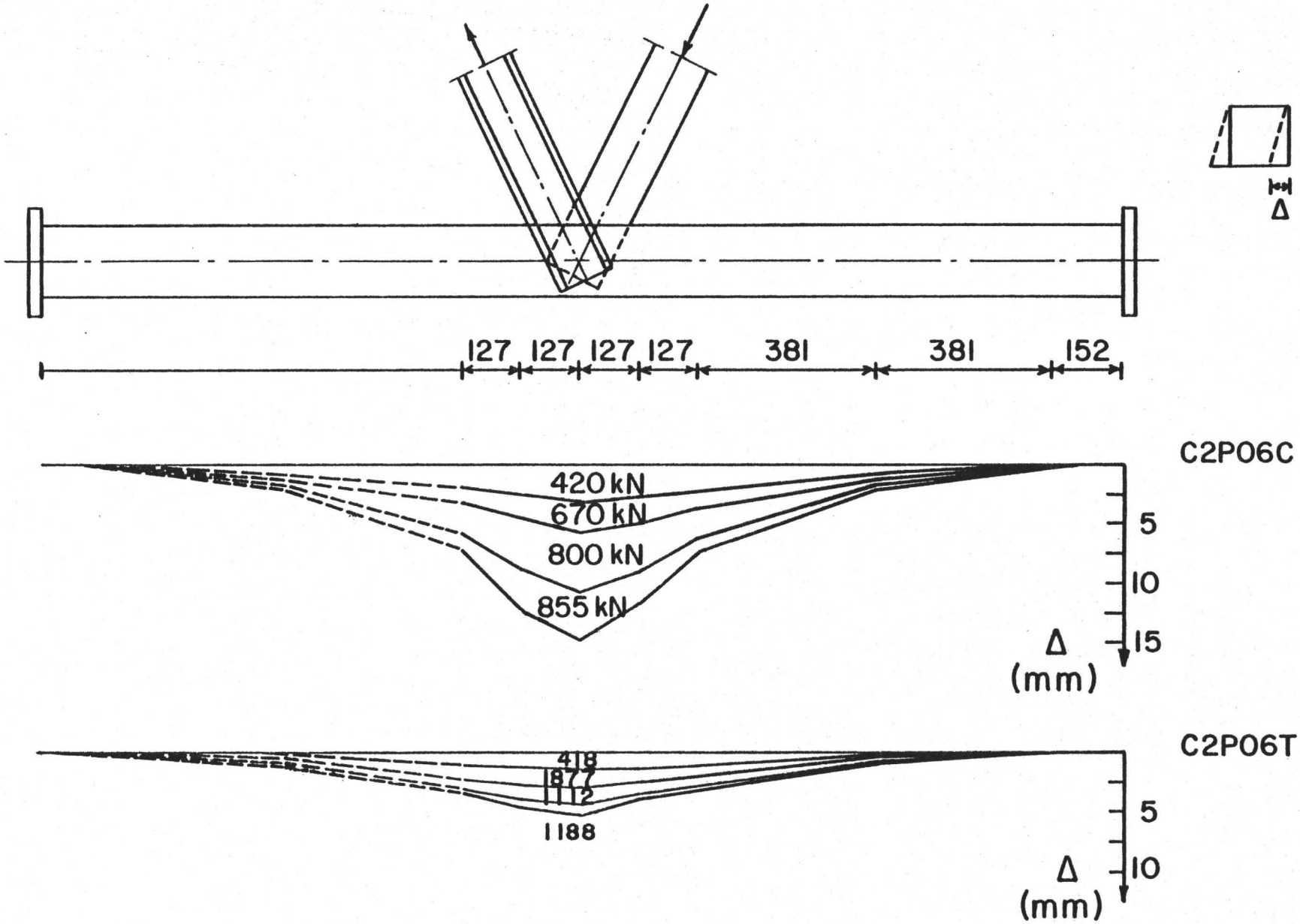

FIGURE 4.5 CHORD DEFORMATIONS FOR SPECIMENS C2P06C & C2P06T.

working load was 7.5% of the HSS chord width for C2P06C and 1.7% for C2P06T, while it was 10% and 3.6% respectively at ultimate. The curves also show that there were some relative displacements far from the joint which was not the case for the standard type.

4.2 Bolted Type Joints

The bolted type joint has application for large spans where field erection procedures must be followed. Constraints on transport will often necessitate some form of on-site assembly. Group 6 comprises three joints: B02P06C, B02P04C and B02P06C*. All chords were 2-HSS 152 x 152 x 9.53 sections although the 6.35 mm size had been specified. The specimen labelled B02P06C* utilized two flat bars spanning the chords on the side remote from the gusset plates and are described as tie plates (see Figure 2.8). For the other two specimens these plates were omitted. The results of the tests are given in Table 4.2. Note that the capacity was beyond the web yield load for the three specimens. The P-Δ curves for the bolted type are presented in Figure 4.6. In general the stiffness for this type was better than for the standard type by 30%. It is also to be observed that the tie plates greatly stiffen the joint. Indeed, the P_w/Δ_o value is more than three times that of its untied counter-part and the joint capacity is improved by about 2%.

By strain gauging the tie plates it was found that they transferred forces of up to 40 KN in tension and compression. The build up of the bar forces with the applied web member loading is shown in Figure 4.7.

Specimen Code Number	Average thickness (mm)		Yield strength (MPa)		$\frac{(P_w)_{ult}}{(P_w)_y}$	At Nominal Branch Working Load					
						Branch Forces & Stiffness				Chord Strain x 10^{-3}	
						Δ_o (mm)		P_w/Δ_o (KN/mm)		$\lvert\varepsilon_{max}\rvert$	$\lvert\gamma_{max}\rvert$
	Branch	Chord	Branch	Chord		Comp.	Tens.	Comp.	Tens.		
B02P06C	6.18	9.32	390	461	1.08	1.83	1.33	417	574	0.8	1.05
B02P06C*	6.29	9.32	393	453	1.10	0.53	0.33	1449	2327	0.66	0.85
B02P04C	6.26	9.38	390	457	1.14	1.43	1.13	534	675	0.36	0.51

Table 4.2 Test Results for Bolted Joints

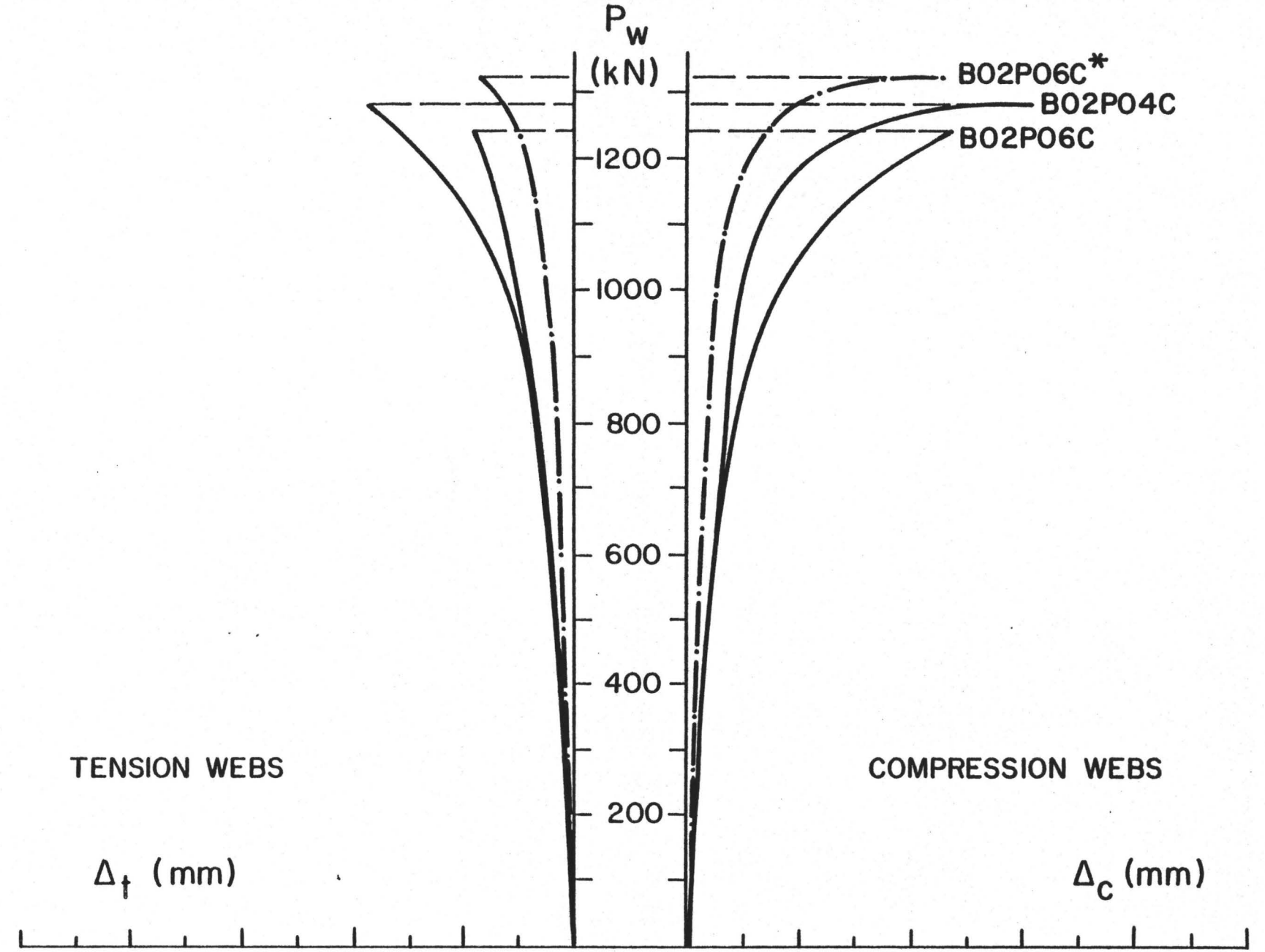

FIGURE 4.6 P_Δ CURVES FOR BOLTED JOINTS.

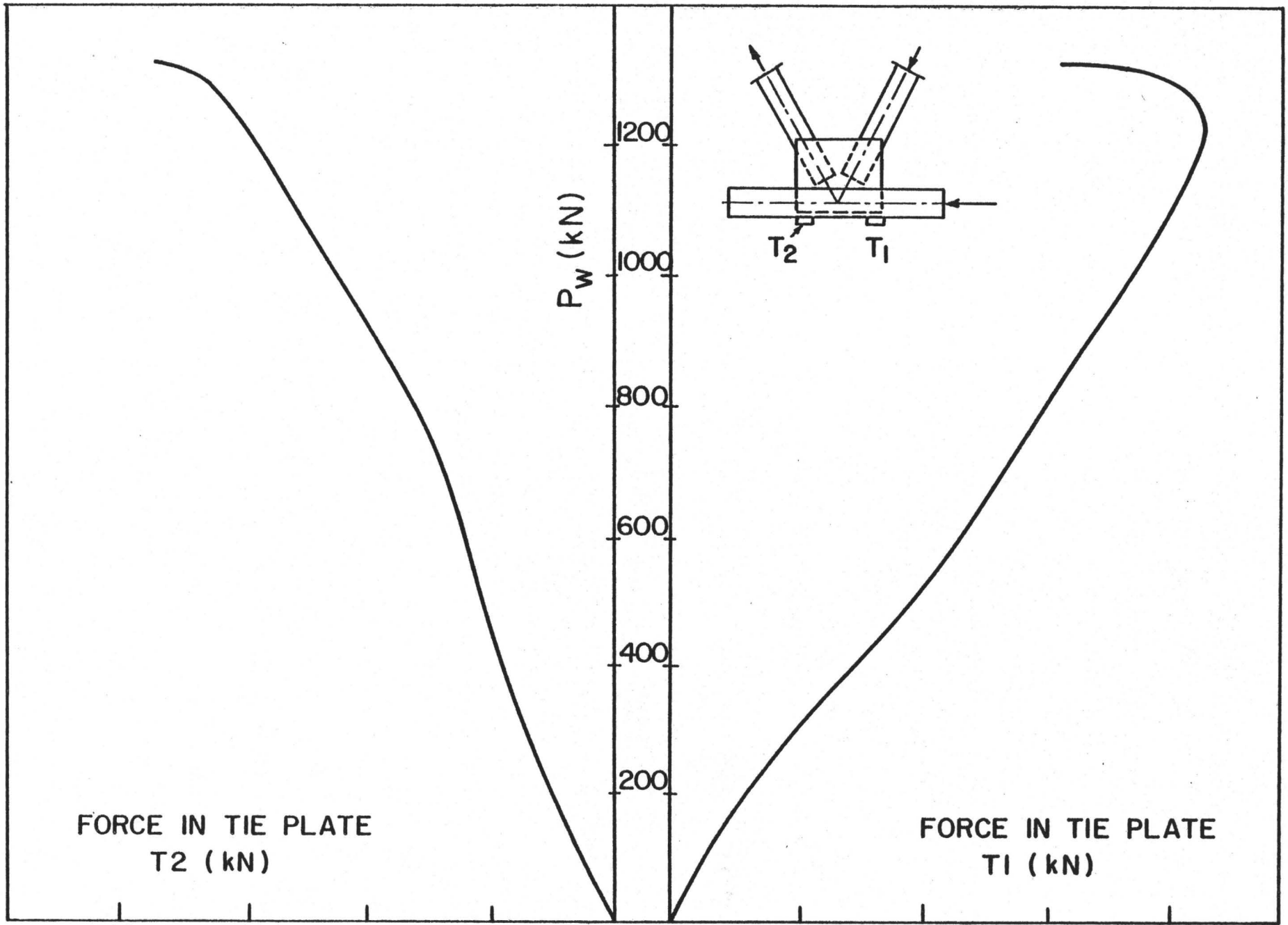

FIGURE 4.7 RESULTING LOAD IN THE TIE PLATES OF THE BOLTED JOINT.

Failure was caused by buckling of the compression web in each instance. No obvious deformation was observed in the chord members or in the gusset plates. Photographs of the bolted specimen B02P06C are given in Figure 4.8.

Twelve gauges were mounted on each web member near the joint as indicated in Figure 4.9. Readings obtained for face B of the web member were similar to those of face A, indicating that there was very little shift in the prime stress lines as occurred for the standard joints. Also, pair readings for gauges 3 & 6, 2 & 5, and 1 & 4 matched closely, indicating that the stresses were uniformly distributed along the depth of face B or along each flange of the web member. While the strain readings for gauges 3, 6, 9 & 12 had very large inelastic values at failure, gauges 2, 5, 8 & 11 just started to yield. The remaining four gauges remained in the elastic range.

Readings of all the rosette gauges were in the low elastic range throughout the tests which indicated that the chord members were not significantly affected by the web loads.

There was no obvious chord deformation detected during or after testing of the three specimens. Using the dial gauge readings, the maximum displacement was only 1.2 mm for specimen B02P06C. This negligible amount of deformation was due to the presence of the gusset plates, suggesting that the web jack forces were transferred from one diagonal to the other without affecting the chord members.

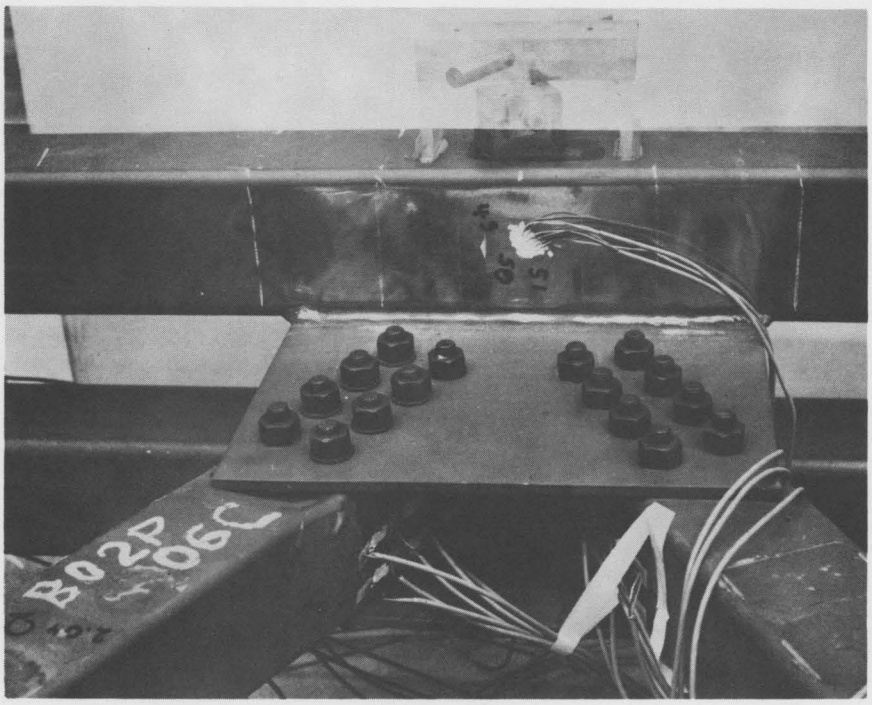

a) PLAN VIEW

b) ELEVATION VIEW

FIGURE 4.8— BUCKLING FAILURE OF BOLTED TYPE

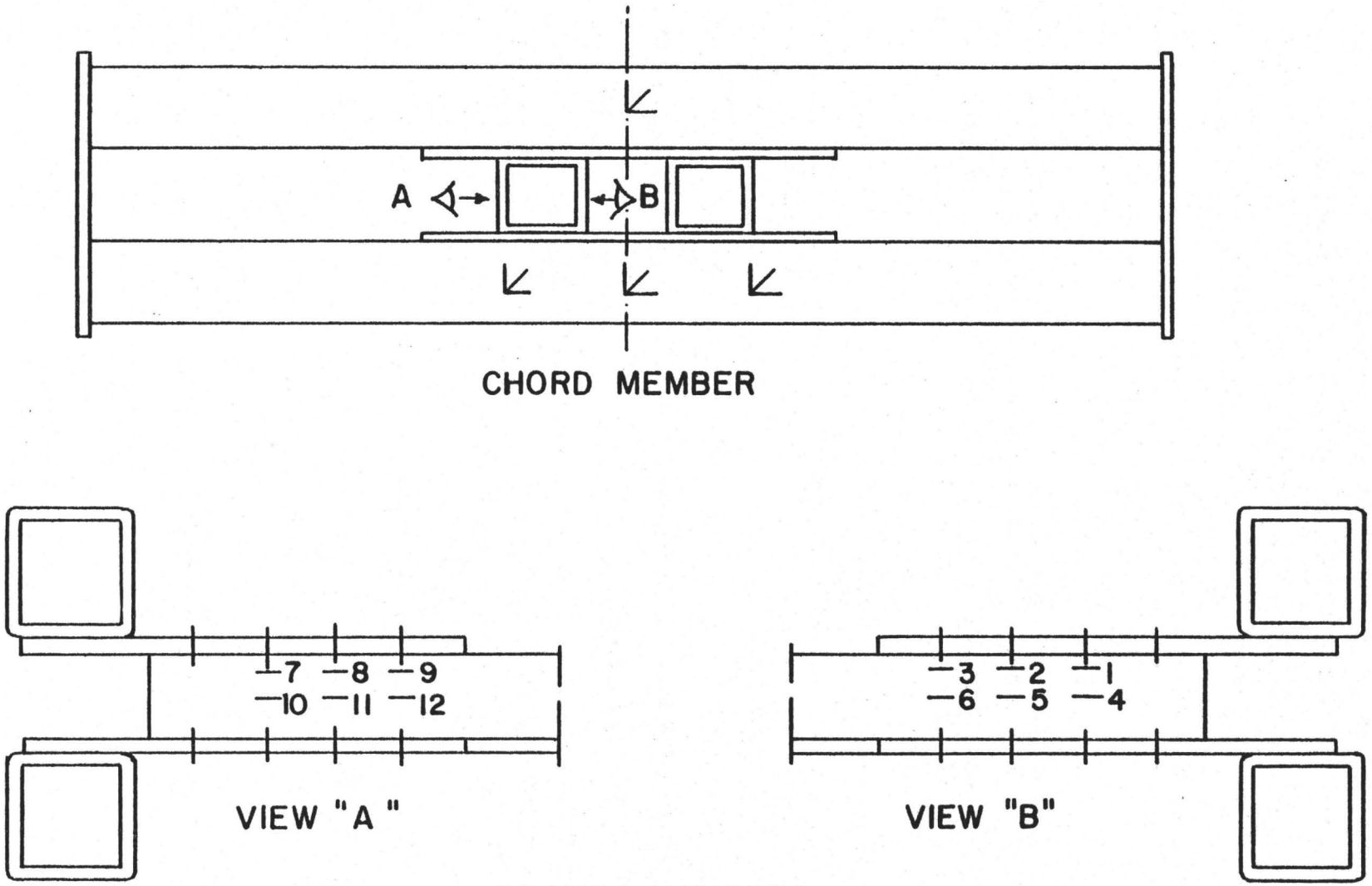

FIGURE 4.9 LOCATIONS OF GAUGES FOR BOLTED CONNECTIONS.

4.3 The Back-to-Back Joints

Eight specimens were tested in group 7 to study the performance of the back-to-back joint type. The following four specimens, BB2P56C, BB2P06C, BB2N36C and BB2N36C*, did not have any strengthening or stiffening device. The remaining four specimens, $BB2P56C_4$, $BB2P56C_8$, $BB2P56C_{12}$ and $BB2P56C_{20}$ each utilized a stiffening plate connected to the chord. Four different thicknesses (6.35, 12.7, 19.05 and 31.75 mm) were used to investigate the optimal sized plate to be used for a given chord thickness.

The same preloading and different eccentricities (117, 0 and -76 mm) were used for specimens without reinforcement device, i.e. those involving gap, partial overlap and full overlap. All specimens had the same slope angle. An eccentricity of 117 mm was used for all specimens having stiffening plates, to compare their behaviour with specimen BB2P56C which was without reinforcement. The results of the eight tests are summarized in Table 4.3.

Specimen BB2P56C possessed a gap joint with an eccentricity of 117 mm. A tearing failure occurred in the inner webs of the chord members when the load in the web member reached 675 KN or 60% of its yield load. The mode of failure is shown in Figure 4.10(a), where the prying action is obvious around the tension web member. Most of the load in the web members was transferred through their flanges and not through the webs as for the previously described types of joint. The reason was due to the existence of the inner webs of the double chord, which acted as a stiff support. The double chord web thickness was

Specimen Code Number	Average thickness (mm)		Yield strength (MPa)		$\frac{(P_w)_{ult}}{(P_w)_y}$	At Nominal Branch Working Load					
						Branch Forces & Stiffness				Chord Strain x 10^{-3}	
						Δ_o (mm)		P_w/Δ_o (KN/mm)		$\lvert\varepsilon_{max}\rvert$	$\lvert\gamma_{max}\rvert$
	Branch	Chord	Branch	Chord		Comp.	Tens.	Comp.	Tens.		
BB2P56C	6.18	6.17	383	414	0.6	-	-	-	-	-	-
BB2P06C	6.09	6.21	388	391	0.84	1.0	0.8	738	916	0.9	0.9
BB2N36C	6.18	6.21	388	400	0.91	0.8	0.038	916	20000	1.1	1.1
BB2N36C*	6.25	6.41	400	430	1.00	0.4	0.3	1862	2444	0.6	0.9
$BB2P56C_4$	6.34	6.42	394	411	0.44	-	-	-	-	-	-
$BB2P56C_8$	6.25	6.23	394	398	0.74	2.4	8.0	316	96	12.8	25.3
$BB2P56C_{12}$	6.15	6.21	396	392	1.09	0.5	0.5	1487	1487	1.1	2.1
$BB2P56C_{20}$	6.20	6.19	374	386	1.19	0.5	0.4	1622	2086	0.7	0.8

Table 4.3 Test Results for the Back-to-Back Joints

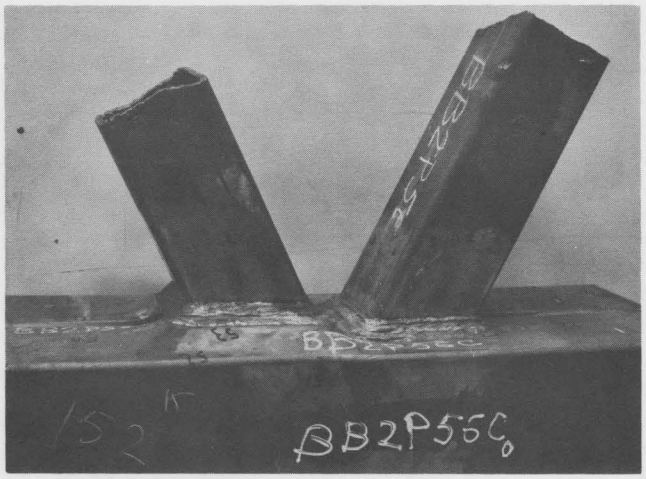

a) UNREINFORCED

b) STIFFENING PLATE 6.35 m m

c) STIFFENING PLATE 19.05 m m

FIGURE 4.10— BACK-TO-BACK TYPE AT FAILURE

insufficient to resist even the working load of the webs.

Specimen BB2P06C had a partial overlapping joint with no eccentricity. The chord deformation was much smaller than for BB2P56C. No tearing or post yield cracking occurred in the chord. The partial overlapping helped in some measure to directly transfer diagonal forces from one web to the other. A capacity of 965 KN was obtained which was higher than that of the first specimen by 43% but less than the yield load by 16%. The failure was due to cracks in the weld between the two webs which were observed to commence when the load was equal to 940 KN. No cracks were evident at working load. However, by bevelling the end plates of the tension web members which are parallel to the compression web, a stronger weld would be expected, thus creating a stronger joint.

Specimen BB2N36C had a negative eccentricity with full overlapping. The tension web was welded to the compression web. The mode of failure that was obtained was buckling of the compression web just above its connection with the tension member. The capacity was higher than for the previous two but was still less than the yield value by 9%. The chord member was almost intact and no deformations were observed visually. No cracks in the weld between the two web members were evident at failure.

Specimen BB2N36C* was exactly the same as specimen BB2N36C except that the compression web was welded to the tension web. A higher capacity of 1184 KN compared with 1050 KN for BB2N36C was obtained, thus attaining the yield load. No chord deformation was visually apparent, nor were there cracks in the weld between the web members. The specimen

failed by local buckling of the compression web member.

In the P-Δ curves shown in Figure 4.11, the weak performance of the gap joint is obvious. Overlapping in general improves the joint's stiffness and increases its capacity while the welding of the compression web to the tension web improves the capacity and the stiffness of the joint.

Another possible solution to attempt to increase and improve the capacity of the back-to-back joint was by using stiffening plates between the chord and the web members. The thickness of the plate appeared to be a very important factor in affecting joint capacity.

Specimen $BB2P56C_4$ utilizing the thin (6.35 mm) plate suffered extensive yielding to its connecting plate. Considerable plate deformation was evident adjacent to the periphery of the tension member. The stiffening plate, which was welded around its boundary exhibited upward movement. After only a few increments of load, the occurence of two cracks in the plate was observed at 500 KN, one located between the two webs and near the tension member while the second was on the opposite side of the tension member. There was no evidence of major distress in the chord. The lowest capacity, 516 KN, in the 29 tests was obtained for specimen $BB2P56C_4$. The mode of failure is shown in Figure 4.10(b).

Specimen $BB2P56C_8$ possessed a 12.7 mm stiffening plate, which helped to increase the capacity to 868 KN, 68% higher than for the previous specimen but short of the yield load by 26%. The mode of failure was similar to specimen $BB2P56C_4$. The improved capacity was due to the increased stiffness provided by the thicker plate.

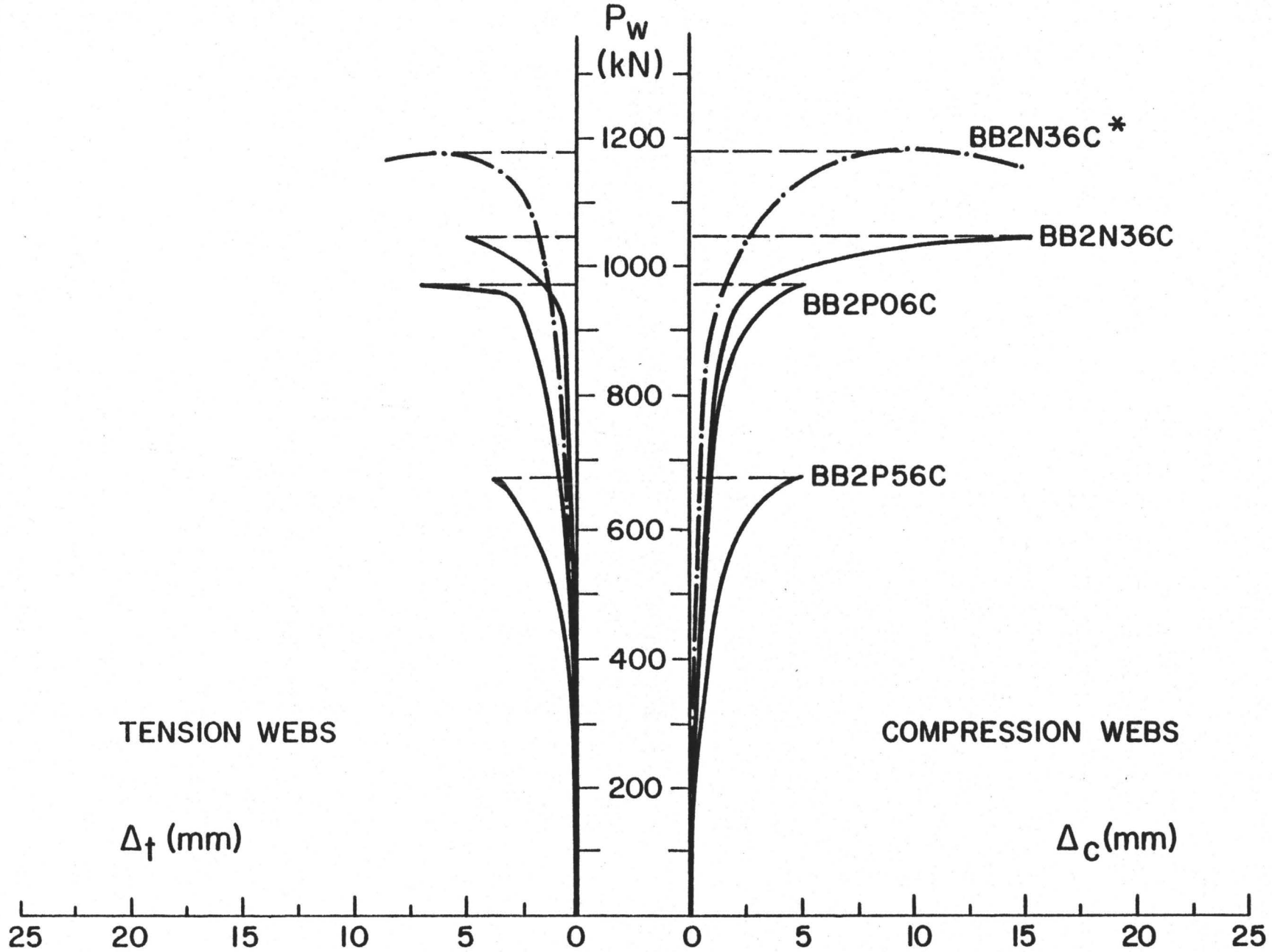

FIGURE 4.11 P_Δ CURVES FOR UNREINFORCED BACK_TO_BACK JOINTS.

Specimens BB2P56C_{12} and BB2P56C_{20} had thicker stiffening plates of 19.05 and 31.75 mm respectively. Their performances were completely different from those of the previous two specimens. There was no noticeable plate deformation or tearing in either case. The specimens failed by local buckling of the compression web members. The web member yield load was therefore reached for these two cases. The P-Δ curves are shown in Figure 4.12 and the failure mode for specimen BB2P56C_{12} is shown in Figure 4.10(c).

Strain readings in the stiffening plate for specimens BB2P56C_4 and BB2P56C_8 were in the inelastic range as determined by the permanent plastic deformation on unloading. The strain readings in the stiffening plates for specimens BB2P56C_{12} and BB2P56C_{20} were elastic throughout.

Large permanent chord deformations were obtained for specimens BB2P56C (gap joint), BB2P56C_4 and BB2P56C_8. When thicker stiffening plates were used, the strains were negligible and disappeared after terminating the test. When the full overlapping joint was used, very small deformations were obtained.

Figure 4.13 shows the shape of the chord after deformation for four specimens. It is evident that the gap joint had the largest deformation at ultimate load, where the relative displacement was 18 mm. For BB2N36C*, the deformation at ultimate was minimal.

From the strain readings around the periphery of the web member near its intersection with the chord, the percentage of load which was transferred through the flanges or the webs of the web member was calculated and is shown in Table 4.4 for all the specimens. For the

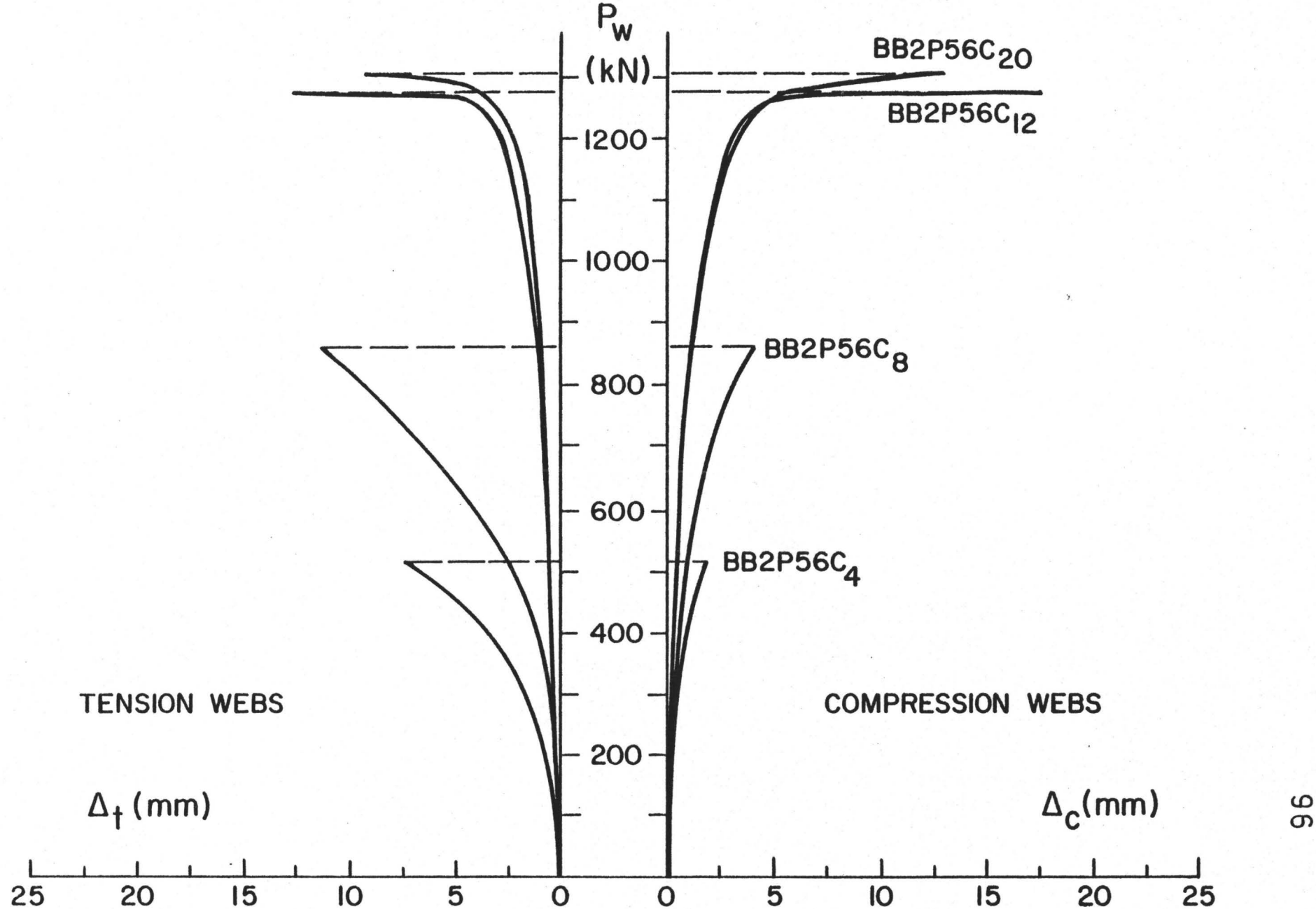

FIGURE 4.12 P_Δ CURVES FOR REINFORCED BACK-TO-BACK SPECIMENS.

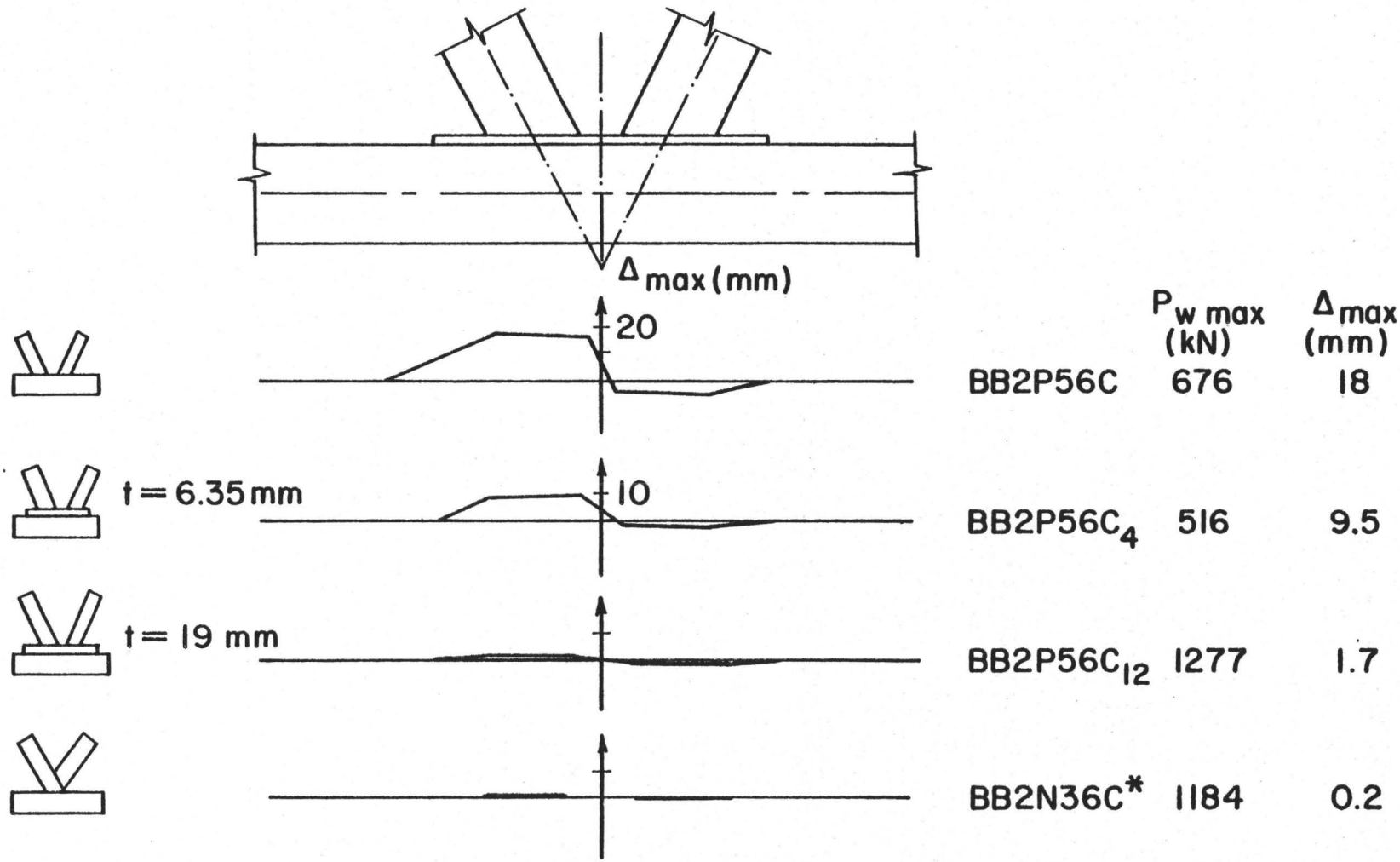

FIGURE 4.13 CHORD DEFORMATION FOR BACK-TO-BACK JOINTS.

Specimen	Tension Web Member % of Load Taken by		Compression Web Member % of Load taken by	
	Flanges	Webs	Flanges	Webs
BB2P56C	85	15	78	22
BB2P06C	41	59	52	48
BB2N36C	48	52	46	54
BB2N36C*	52	48	49	51
$BB2P56C_4$	80	20	74	26
$BB2P56C_8$	68	32	69	31
$BB2P56C_{12}$	60	40	57	43
$BB2P56C_{20}$	53	47	53	47

Table 4.4 Branch Member Load Distribution at the Joint

unreinforced gap joint specimen, most of the load was transferred through the flanges of the web members, while for the full overlapped joint, the load was equally transferred by the flanges and the webs. When stiffening plates were used, larger portions of the web load were taken by the flanges when t_s was equal to 6.53 and 12.7 mm. For larger thickness plates the web load was almost equally distributed. Better joint performance occurred when the web load was equally transferred through its flanges and webs.

CHAPTER 5

DISCUSSION AND COMPARISON OF EXPERIMENTAL RESULTS

5.1 Capacity and Stiffness of Joints

A comparison between the 4 different types of joint will now be made for the simplest joint from each type. Consider specimens S2P46C from the Standard, C2P06C from the Channel, B02P06C from the Bolted and BB2P56C from the Back-to-back categories. Note that the preloading and slope angle are the same for all. The joint stiffness for the channel type was the lowest in this group and was due to the fact that the branch members at the joint were connected to different webs of the double chord, resulting in extensive torsional strain. On the other hand, the stiffness of the Bolted and Standard joints had equally high values and were the best for this group. The stiffness of the back-to-back joint was in the intermediate range, much better than the channel type, but somewhat lower than the other two connections. The P-Δ curves are shown in Figure 5.1 and the results of the four specimens are summarized in Table 5.1.

The ultimate capacities of the standard and bolted connection exceeded the yield load by 17% and 8% respectively, whereas the channel and back-to-back were insufficient by 29% and 40% respectively. At working load, the maximum Δ_o for the compression member was 9.51 mm for the channel type whereas it was only 1.31 mm for the standard type.

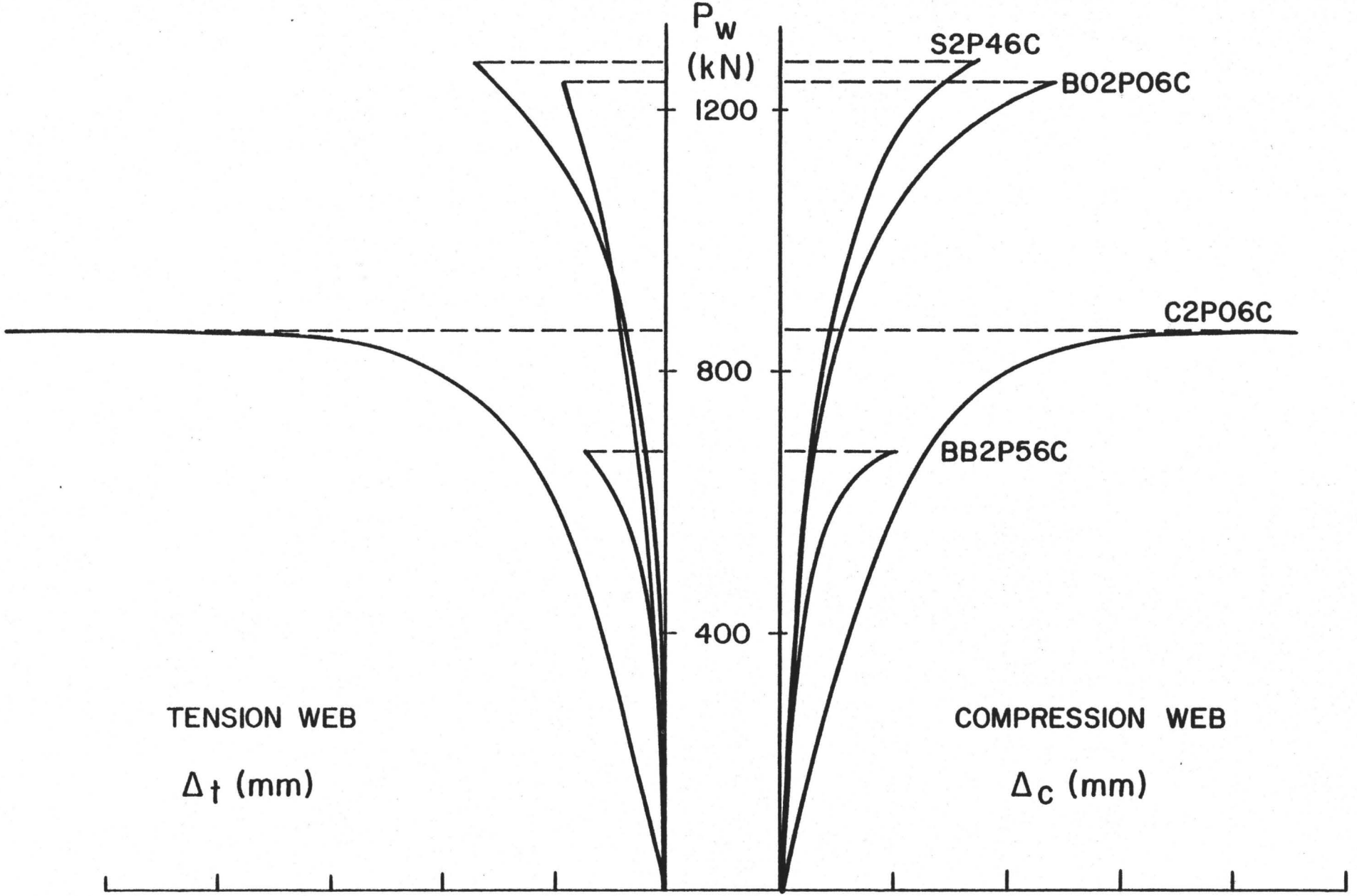

FIGURE 5.1 P_Δ CURVES FOR DIFFERENT JOINT TYPES.

Specimen Code Number	Yield Strength (MPa)		$\frac{(P_w)_{ult}}{(P_w)_y}$	At Nominal Branch Working Load					
				Branch Forces and Stiffness				Chord Strains x 10^{-3}	
	Branch	Chord		Δ_o (mm)		P_w/Δ_o (KN/mm)		$\lvert\varepsilon_{max}\rvert$	$\lvert\gamma_{max}\rvert$
				Comp.	Tens.	Comp.	Tens.		
S2P46C	368	391	1.17	1.31	1.65	549	1307	9.7	17.5
C2P06C	414	405	0.71	9.51	9.50	85	85	6.4	12.25
B02P06C	390	461	1.08	1.83	1.33	417	574	0.8	1.05
BB2P56C	383	414	0.60	N/A	N/A	N/A	N/A	N/A	N/A

Table 5.1 Test Results Comparison Between Four Different Types of Joint

This is an indication of how much more effective is the latter joint than the former in stiffness. At failure, the minimum chord deformation was observed in the bolted joint, followed by the standard, the back-to-back and the channel in that order. It is also obvious from the last column in Table 5.1, that joint B02P06C was the only specimen in which its chord member was not highly stressed in shear, due to the presence of gusset plates which transferred most of the load directly from one web member to the other.

5.2 Discussion

Each of the various joint types with its particular advantages and disadvantages is described below.

(a) Standard Type

The standard type joints are easy to fabricate, aesthetically attractive and have excellent strength capacity. Simple fillet welding at the joints, using normal design criteria for weldments, appears to be quite adequate.

Of the twelve joints tested, only three were unable to attain the yield load of the webs. Nonetheless, even the poorly designed joints having large eccentricities had ultimate strengths within 10% of web member yield. End cutting the webs to permit closer positioning to the truss node point will reduce the gap, and hence the eccentricity. Such a reduction in "e" from 178 mm to 108 mm tended to increase joint strength by as much as 20%. Furthermore, bridging the webs with weldment at their nearest position tended to transfer directly stress from one web member to the other, a desirable feature for the joint

performance. A study of this transfer mechanism was not attempted in this investigation.

A smaller slope angle for the web member reduces the joint eccentricity but the capacity is not significantly increased because the joint is subjected to a higher axial load which minimizes the effect of reducing the eccentricity. In practice, the smaller slope angle will result in a longer diagonal members for deeper trusses. Hence the capacity of the web member may be reduced by strut buckling if the slenderness ratios exceed the critical value, i.e. if the member buckling controls their design. It appears that 45° slope angle will be appropriate for shallow trusses and 2:1 slope can be used for deeper trusses.

The chord preloading had an influence on joint capacity. Increasing the chord preload, either in tension or compression, has the effect of reducing joint strength. The difference was about 18% between -23.5% and +16.5% of chord yield. In an actual truss, the maximum web forces are likely to be nearer the truss ends, rather than mid span, and hence reduced joint strength due to preloading may not be of major concern.

Chord deformation is reduced by, decreasing the eccentricity, slope angle and by having continuous weld between the web members. The maximum shear strain "γ_{max}" is significantly reduced in the chord member if the eccentricity is reduced.

Overall, then, stiffness, capacity and final deformation were among the best obtained in this program.

(b) Channel Type

To achieve an equivalent capacity for the channel type joint, the chord thickness had to be increased by 50%. The regular double chord size of 152 x 152 x 6.35 mm was not adequate because of excessive torsional distortion and shear stresses that led to failure. This joint type does not appear to possess sufficient design strength and economy to be competitive with the standard type. By increasing the chord thickness by 50% the stiffness of the joint was improved, but was nonetheless insufficient to reach the stiffness value of the standard type. Joint capacity was not reduced when negative eccentricity was introduced; in fact there was a slight decrease in strength.

(c) Bolted Type

The bolted type specimens hold promise when large trusses pose problems in delivery to the site and in assembly because of their size. Negligible chord deformations were observed although thicker chords than specified were fabricated for the test program. High capacity was obtained with very good joint stiffness. The use of tie plates improved the joint stiffness and increased its capacity from 1246 KN to 1326 KN. The load between the two web members is mainly transferred through the gusset plate and not through the chord. For good performance an adequate gusset plate is needed to transfer the large web member forces that can be developed.

(d) Back-to-Back Type

Comparing the results of BB2P56C with specimen S2P76C it appears that the back-to-back gap joint is indeed very weak. The web forces are

mainly transferred by the inner two webs of the chord members. Hence, when designing a gap joint the thickness of the chord member needs to be a primary parameter in determining the capacity of the joint particularly if the width ratio λ^* between the branch and chord members is ≤ 0.5.

Packer [31], concluded that for lapped single chord joints the ultimate strength of the joint increases linearly as the amount of lap increases up to the strut squash load.

For double chord joints, it was found that 100% overlapping increases the capacity significantly, particularly if the compression web is welded to the tension member. For the reverse case, i.e. when the tension web has been welded to the compression member, part of the compression member is subjected to a combination of compressive stresses due to the diagonal member force and tensile stresses in a perpendicular direction due to the web pulling effect of the tension diagonal. The resulting maximum shear stress becomes larger than in the former situation thus creating a yield zone which can precipitate an early local buckling failure.

The performance of the back-to-back joint is improved by using a stiffening plate with adequate thickness. If the thickness is insufficient, a lower capacity than the unreinforced gap joint will be obtained. Therefore the thickness of plate is very important in the design of plate reinforced back-to-back joints. For example the pulling force for specimen $BB2P56C_4$, was resisted by a 6.35 mm plate, welded along its outside periphery to the chord. This joint was more flexible

and weaker than without the presence of the plate (BB2P56C). By using Shenouda's recommendations [4,31], a 22 mm thick plate will be adequate to provide a strong joint for an equivalent single chord joint. The adequate thickness for the stiffening plate was found to be 19.05 mm from the test, i.e. three times the thickness of the chord member. Very good performance was attained with this joint although its final cost will be shown to be considerably higher than the cost of the standard joint.

5.3 Cost Estimate for Specimen Fabrication

In design, cost is always a consideration. The cost will be briefly discussed to ascertain the potential for the joints that were tested. An estimate of the cost of fabrication of the joint was performed by CANRON and is shown in Table 5.2. The least expensive connections were the standard type. The bolted joint was the most expensive.

The most economical joint, was the standard joint S2P46C where its fabrication cost was $82.5 and its ultimate capacity was beyond the yield load by 17%. The joint stiffness was not the best but it was reasonably good. The cost of the channel joint was slightly higher but its stiffness was very low and its ultimate capacity was 29% less than the yield load.

The bolted joint had almost the same stiffness properties of the standard joint with a slightly lower ultimate capacity but its cost of fabrication was 75% larger. By using tie plates, the stiffness of the joint is improved by 380%, and higher capacity is also obtained, but the

Type of Joint	Specimen Number	Average P_w/Δ_o (KN/mm)	Cost of Joint Fabrication $	$\frac{(P_w)_{ult}}{(P_w)_y}$	Stiffening Device
Standard	S2P76C	380	77.0	0.90	-
	S2P46C	928	82.5	1.17	-
	S1P26C	1117	78.5	1.13	-
Channel	C2P06C	85	90.0	0.71	-
Bolted	B02P06C	496	144.2	1.08	-
	B02P06C*	1888	167.0	1.14	Tie Plates
	BB2P56C	N/A	86.6	0.6	-
	BB2P06C	827	117.6	0.84	Partial Overlap
Back	BB2N36C*	2153	103.1	1.00	Full Overlap
To	$BB2P56C_4$	N/A	110.38	0.44	6.35 mm Plate
Back	$BB2P56C_8$	206	125.85	0.74	12.7 mm Plate
	$BB2P56C_{12}$	1487	149.60	1.09	19.05 mm Plate
	$BB2P56C_{20}$	1854	160.00	1.19	31.75 mm Plate

Table 5.2 Cost Estimate for the Specimens

cost of fabrication is twice the cost of the standard joint.

For the back-to-back joint, the gap joint is the cheapest one, but possesses a low joint capacity. By overlapping the diagonals, the capacity and the stiffness of the joint are improved, the cost increases too. The full overlapped joint with 25% more fabrication cost than the standard joint had just reached the yield load at failure while the standard was 17% beyond it. By using an adequate thickness for the stiffening plate, the yield load was exceeded, but the fabrication cost was larger by 80% and 93%.

Figure 5.2 shows graphically the cost penalties encountered in using either bolted or back-to-back connections rather than the standard joint. In fact, BB2N36C* is even inferior to S2P46C in strength although its cost is 24% higher.

5.4 Comparison Between Single and Double Chord K-Joint

The most economical double chord joint was specimen S2P46C where simple fillet weld was used. This standard joint comprises 2-HSS 152 x 152 x 6.35 mm for chord members and 1-HSS 127 x 127 x 6.35 mm for web members. To compare the performance of the double and single chord joint, the chords need to be equivalent in area and section modulus, if strength is used as a basis for structural performance.

For a single chord gap joint, the chord member is comprised of 1-HSS 200 x 200 x 9.53 mm and the web members from 1-HSS 127 x 127 x 6.35 mm. Cross-sectional properties are shown in Table 5.3. By having a 25 mm gap, the joint eccentricity will be 76 mm which is still smaller

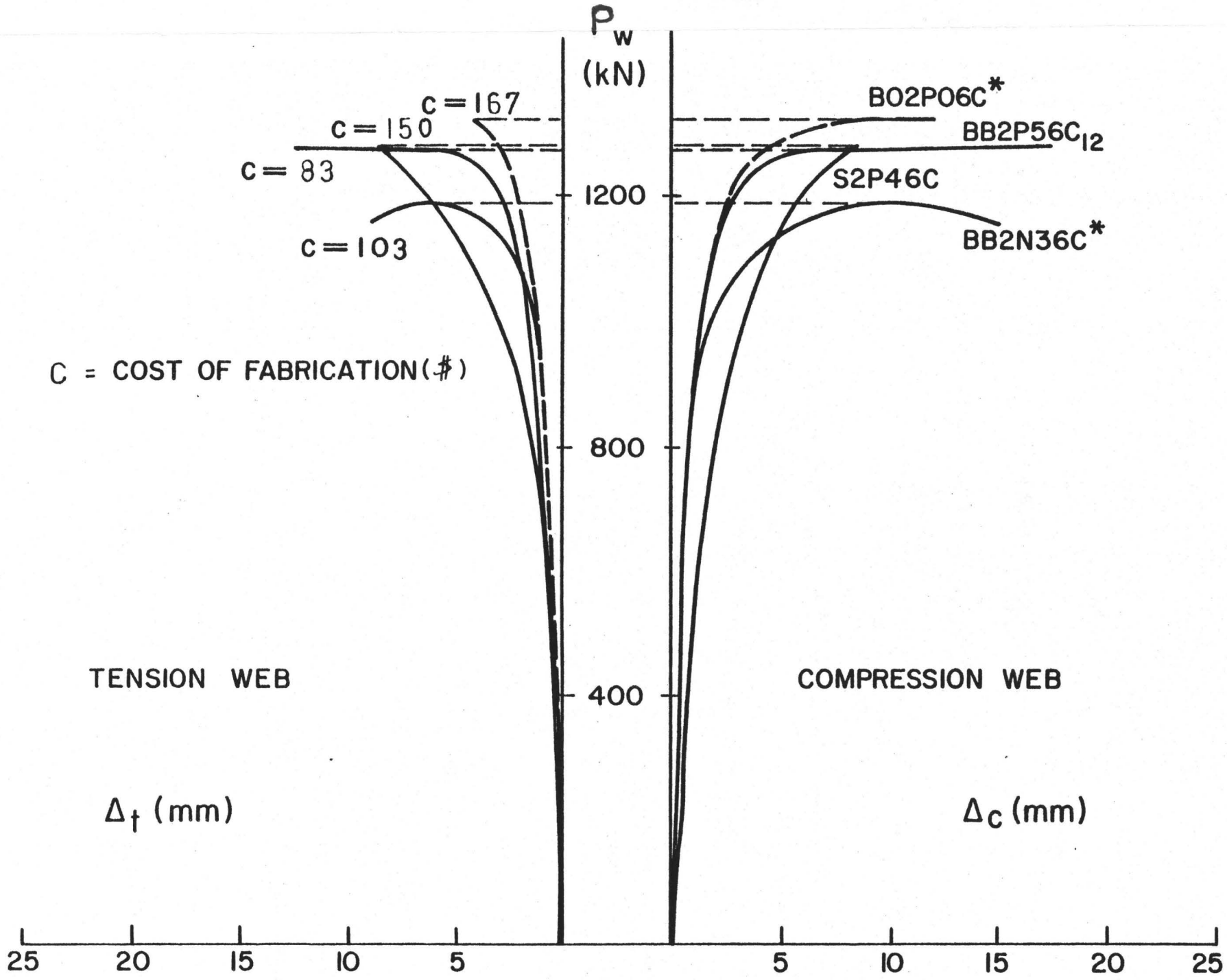

FIGURE 5.2 P_Δ CURVES FOR BEST JOINTS.

Double Chord Joint	Cross Section Properties	Single Chord Joint
2-HSS 152 x 152 x 6.35	Chord Member	1-HSS 200 x 200 x 9.53
7220	Area (mm^2)	7150
136.5	Mp (KN.m)	180
1-HSS 127 x 127 x 6.35	Web Member	1-HSS 127 x 127 x 6.35
12.7	Clearance or Gap	25.4
108	Eccentricity	76

Table 5.3

Single and Double Chord Joint Properties

than 108 mm for the double chord joint. From the LSD code [9], for gap joint, the factored vertical resistance (R_v) for the above chord section is 267 KN. For a 2:1 slope angle, the maximum capacity allowed by the code [9] for the web members would be 299 KN. Comparing this value with the ultimate capacity for S2P46C, 1277 KN, which was obtained from the test, it appears that the behaviour of the double chord joint is much better. The positioning of the joint components during fabrication is much easier for the double chord, and even with larger eccentricity the double chord had much larger capacity.

Most of the tests, which were done on single chord HSS Warren type connections, used small sizes of HSS for chord or web members. Relatively few specimens have been fabricated from large HSS, as for example by Wardenier [25] who utilized 197 x 197 mm sections for chords and branch members.

The results of tests on a few large scale single chord joints are shown in Table 5.4. The dimensions are not an exact match of that proposed in Table 5.3, but provide some basis for comparison. All the specimens had a slope angle of 45° while the yield stresses were somewhat lower than those of the double chord connections reported here. Wardenier [25] concluded that the influences of the angle θ on the joint strength is in accordance with the function $1+\sin\theta/2\sin\theta$, that is $N_u = N(1+\sin\theta)/2\sin\theta$, where N is the joint strength if $\theta = 90^{\circ}$. From this conclusion, it is obvious that if all the specimen shown in Table 5.4 had had a 2:1 slope their capacities should have been even lower than the values shown in the table. It appears, therefore, that the capcity

Test Number	W-RR-178	W-RR-177	Gap	Lap	Lap
Reference	Wardenier	Wardenier	Corby	Corby	Mang
Chord Member	197 x 197 x 8.05	197 x 197 x 8.05	258 x 258 x 8.5	258 x 258 x 8.5	260 x 260 x 8.8
Comp. Web	125 x 125 x 6.5	197 x 197 x 8.05	100 x 100 x 6	100 x 100 x 6	100 x 100 x 5
Tens. Web	125 x 125 x 6.5	197 x 197 x 8.05	100 x 100 x 5	100 x 100 x 5	100 x 100 x 6.3
Preload (KN)	0	0	700	0	700
g^*/b_o	0.1	0.2	0.1	-0.33	-0.33
θ	45^o	45	45	45	45
$F_{y_{chord}}$ (MPa)	312	312	306	317	359
Ult. P_w (KN)	710	950	445	582	800
Failure	Local Buckling of comp. web	Shear Failure of the chord	Chord Failure and cracking in the toe of the weld	Buckling of comp. web	Buckling of the the chord & web bending of the tension & comp. web

Table 5.4 Single Chord Experimental Results
(c.f. P_w = 1277 KN for S2P46C)

g^* = Gap between toes of branch members

b_o = Width of the chord member

of the double chord (1277 KN) considerably surpasses that of the single chord.

From an extensive series of tests mentioned earlier, an empirical equation derived by Wardenier [25] is as follows:

$$(P_w)_{ult.} = 12.7 \times Fy \times t_o^2 \times \gamma^{0.5} \beta \frac{1 + \sin\theta}{2 \sin\theta} f_5(n) f_6 \left(\frac{h_o}{b_o}\right) \qquad (5.1)$$

where $(P_{web})_{ult.}$ = ultimate load of the branch member

Fy = yield strength

t_o = chord wall thickness

γ = $b_o/2t_o$

b_o = width of chord

β = mean width ratio between branches of chords

= $b_1+b_2/2b_o$

b_1 & b_2 = width of branches

θ = angle between bracing and chord.

$f_5(n)$ = 1 for $0 < n < 0.6$

= $1 - 0.8|n|$ for $n < 0$

n = N/A_oFy

N = axial load in chord (additional)

A_o = cross section chord area

$f_6(h_o/b_o)$ = 1 for $h_o/b_o \geq 1$

= h_o/b_o for $h_o/b_o < 1.0$

h_o = depth of chord member.

Substituting the corresponding section properties of the equivalent single chord joint into eqn. (5.1), it yields to

$$\gamma = \frac{203}{2 \times 9.53} = 10.65$$

$$\beta = \frac{127 + 127}{2 \times 203} = 0.63$$

$$\theta = 63^{o}\ 435$$

$$\sin \theta = 0.8944$$

$$f(\theta) = \frac{1 + \sin \theta}{2 \sin \theta} = 1.059$$

$$n = \frac{-534}{7150 \times .345} = -0.2164$$

$$f_5(n) = 1 - 0.8 \times 0.2164 = 0.83$$

$$\frac{h_o}{b_o} = 1 \text{ therefore } f_6\left(\frac{h_o}{b_o}\right) = 1$$

$$(P_w)_{ult.} = 12.7 \times .345 \times (9.53)^2\ (10.65)^{1/2} \times 0.63 \times 1.059 \times 0.83 \times 1$$

$$= 719 \text{ KN}$$

By comparing the predicted single chord capacity with the 1126 KN as the average for the double chord joint, it appears that the capacity of the double chord is 56% larger than the predicted value using Wardenier equation. Comparing Wardenier's prediction with the capacity allowed by LSD Code [9], it was found that the code had used a factor of safety of 2.4.

The mean ultimate static strength of SHS to SHS single chord gap joints can also be expressed by the empirical equation derived by Packer [31]

$$(P_w)_{ult} = \sigma_y^0\ (b_o)^{0.3}\ (t_o)^{1.7}\ [3.8 + 10.75\ (\frac{b_1}{b_o - 2t_o})^2]$$

$$\left[1 - \left|\frac{N + 2\,(P_w)_{ult}\cos\theta}{\sigma_y^0\, A_o}\right|\right]^{1/2} \frac{1}{\sin\theta} \qquad (5.2)$$

where the c's and w's refer to the chord and web members respectively. By using the equivalent single chord previously used, equation (5.2) gives $(P_w)_{ult.}$ = 669 KN. A similar disparity in strength applies to overlapped joints. The mean ultimate static strength of single chord lap joints, Packer [31], for the equivalent chord above gives a value no more than 55% that of the 3 overlapped back-to-back joints.

The fabrication cost of the single chord joint is similar to the fabrication cost of the Back-to-Back double chord gap joint [40]. Since standard double chord joints are more economical and have capacities over 50% higher, the double chord concept indicates potential for improved structural performance and at a somewhat reduced fabrication cost in comparison with the single chord.

CHAPTER 6

DOUBLE CHORD T-JOINT CONNECTIONS

6.1 Vierendeel Trusses of HSS

Unlike K-type trusses, the members in a Vierendeel truss are subjected to predominantly bending action. This type of structure is susceptible to very high end member stresses since axial forces play a less significant role in distributing the loads.

In general, these trusses have tended to be difficult to design and unsightly in appearance because of the need for heavily reinforced joints. With the advent of HSS, the potential for these trusses had greatly increased as it is now possible to design Vierendeel trusses which are both reasonably structurally efficient and aesthetically pleasing.

In recent years several researchers have looked at Vierendeel joints in HSS. In 1966, Jubb and Redwood [23] indicated that full moment transfer can be achieved at an equal width connection ($\lambda^* = 1$, see Figure 6.1) without any stiffening device, but for $\lambda^* < 1$ there is a considerable reduction in joint stiffness. This latter fact was also confirmed by Lazar and Fang [34] and Duff [35]. Cute et al. [36] indicated that for unreinforced connections with $\lambda^* < 1$, the branch member width-to-chord thickness ratio b/t_c has a significant effect and it is unlikely that even the yield moment M_y of the branch member can be developed unless $b/t_o \leq 16$.

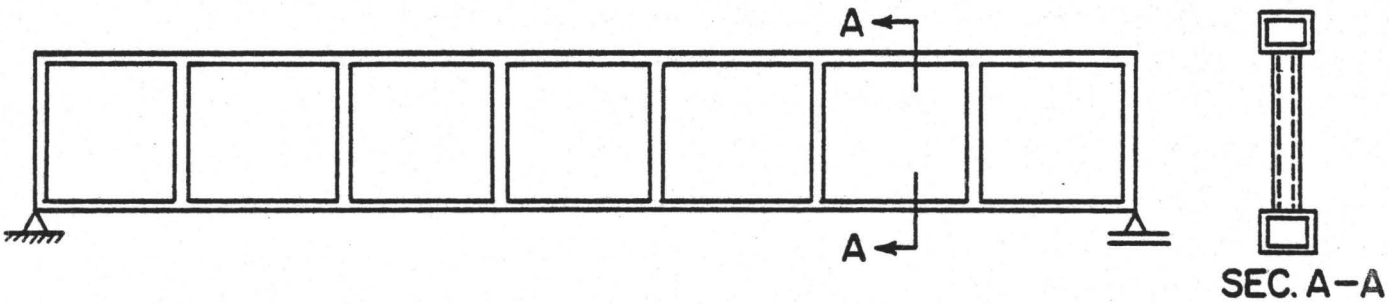

VIERENDEEL TRUSS

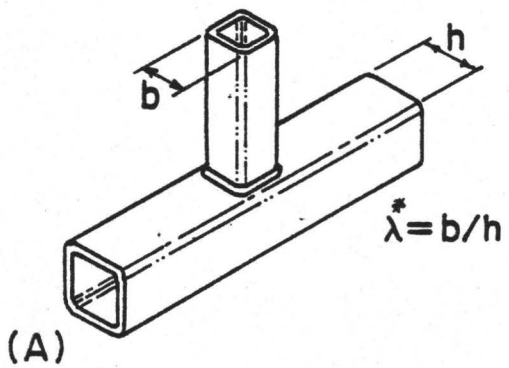

FIGURE 6.1 UNREINFORCED SINGLE CHORD T-JOINT CONNECTION.

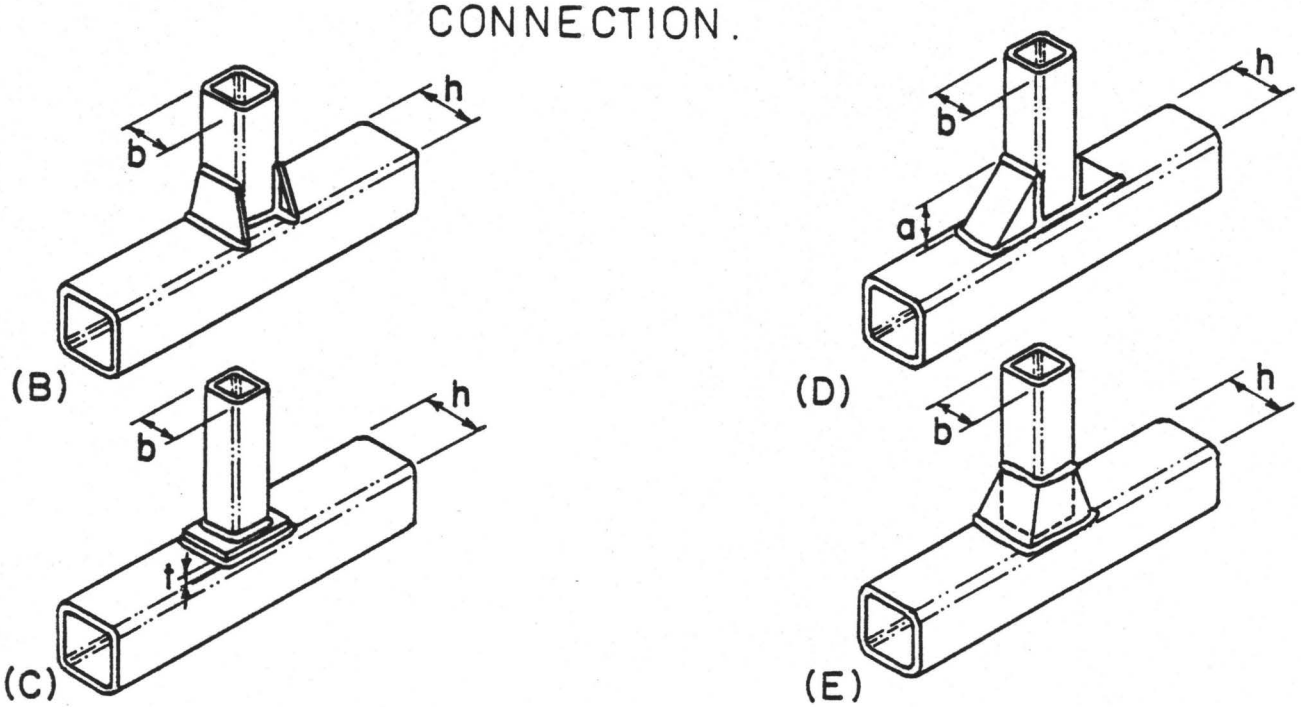

FIGURE 6.2 REINFORCED SINGLE CHORD T-JOINT CONNECTION.

6.2 Types of Single Chord T-Joint Composed of HSS

In order to encourage the design and use of Vierendeel trusses, Brady [37] and El-Zanaty [38] conducted extensive experimental programmes on the branch member moment transfer of equal and unequal width connections using various strengthening devices. Korol et al. [39] summarized their results.

The following five types of joints shown in Figures 6.1 and 6.2 were investigated. These are: the Unreinforced type, Branch Flange Reinforced Connection, Chord Flange Stiffener, Haunch Connection and the Truncated Pyramid. Each type will be briefly described together with its merits and weaknesses:

i) Unreinforced Type (A) joints did not perform adequately and hence, in general, necessitate some form of reinforcement. Even the equal width connections tested did not attain the branch member's plastic moment capacity.

ii) the Haunch Type (D) of connection provides adequate stiffness and strength at reasonable cost and is recommended for non-architectural applications. A haunch size, equivalent to the width of the branch member, gives good performance and permits the use of branch off-cuts during fabrications.

(iii) the Chord Flange Stiffener Connection, Type (C), also performed well for plate thicknesses in excess of the chord thickness and represents an aesthetically pleasing joint type.

(iv) the Truncated Pyramid, Type (E), is a very efficient joint with excellent stiffness qualities, but the high cost of fabrication

and its unsightly appearance may mitigate against its use in most applications.

(v) the Branch Flange Stiffener Connection, Type (B), did not perform as well as the other reinforced joint types since very high stresses in the flange plate corners tended to cause a somewhat premature weld failure.

6.3 Introduction of the Double Chord T-Joint as a New Concept

Since some form of strengthening device for the single chord T connection is required, fabrication costs or undesirable obtrusiveness may tend to rule out this option. Hence the possibility of using an unreinforced double chord single web member arrangement to meet the necessary joint requirement was investigated as shown in Figure 6.3. Such a concept suggested itself because the mating webs of the double chord act to stiffen the section under both branch moment and axial load. The final appearance remains attractive in keeping with the architectural objectives of an unobstructed view.

6.4 Double Chord T-Joint Tests

The main purpose of the experimental program was primarily to see whether the load transfer mechanism was similar to that of the back-to-back K joint case and secondarily to see what possibilities existed for this type of joint in Vierendeel trusses. The effect of welding the

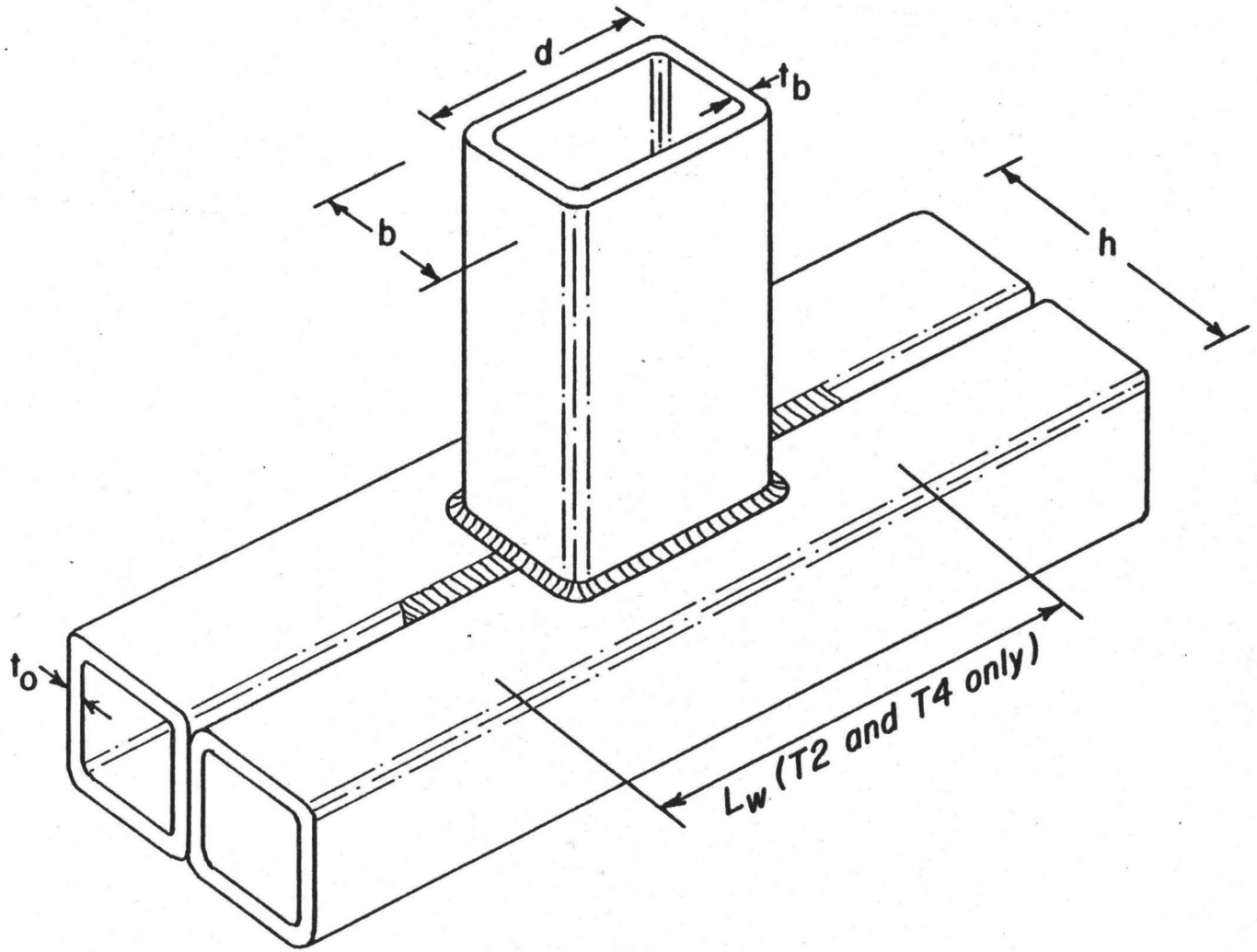

FIGURE 6.3 DOUBLE CHORD T-JOINT CONNECTION.

back-to-back chord members together near the joint was investigated. The performance of the double chord T joint connection was compared with that of the single chord specimen.

Specimen Details

Four prototype specimens were tested under static loading conditions. These specimens were fabricated at McMaster University Applied Dynamics Laboratory under typical shop conditions.

Each specimen consisted of a 1220 mm long single branch member connected to an 2130 mm long double chord member. In each case, 2 HSS 152.4 x 152.4 x 6.35 mm were used for the chord section, while branch member sizes 254 x 152.4 x 7.13 mm and 177.8 x 127.0 x 4.78 mm were selected, each for two specimens. The branch members were fillet welded to the chord sections. Specimens with similar geometries (T1 and T2, or T3 and T4) were identical to each other except for chord member connecting welds both top and bottom as shown in Figure 6.3. The length of weld, L_w, for specimen T2 and T4 was 305 mm. Specimens details are presented in Table 6.1.

Material Properties

The steel used for the HSS specimen was CSA grade 40.21-M 350 W Class H, cold formed. Upon completion of the tests, coupons were cut from each chord and branch member. These coupons were then subjected to standard tensile tests on the Tinius Olson machine in accordance with the relevant ASTM specification [33]. The yield stresses for both branch and chord members were obtained from the tensile test and are shown in Table 6.1.

Specimen Number	Branch Member HSS (mm)	Chord Member 2 HSS (mm)	Weld Length Between Chords (mm)	Yield Strength (MPa)		Branch Plastic Section Modulus Z_x (10^3 mm^3)	λ	b/t_o	b/t_b
				Branch	Chord				
T1	254 x 152 x 7.13	152 x 152 x 6.35	-	386	370	458	0.5	24	21.4
T2	254 x 152 x 7.13	152 x 152 x 6.35	305	370	347	458	0.5	24	21.4
T3	177 x 127 x 4.78	152 x 152 x 6.35	-	345	377	167	0.42	20	26.6
T4	177 x 127 x 4.78	152 x 152 x 6.35	305	347	352	167	0.42	20	26.6

Table 6.1 Details for Double Chord T-Type Connection

Test Procedure

The four specimens were tested using the same experimental technique and apparatus used by Korol et al. [39] in their single chord T-joint tests. The testing apparatus is shown in Figure 6.4 as well as the dial gauge arrangement.

The load was applied to the branch member by a hydraulic jack positioned 1118 mm from the top flange of the chord member which was used in conjunction with a 225 KN capacity load cell. Strain gauges were used to assess the strain distribution at the base of the branch member. The horizontally applied load, P, was monotonically increased until joint failure occurred.

Results

Load-deflection curves for the four specimens are shown in Figure 6.5. As it is evident from Table 6.2, the larger specimens, T1 and T2 reached ultimate moments that were considerably less than the computed fully plastic moment, Mp, based on nominal 345 MPa yield. The smaller T3 and T4 joints performed much better, attaining 88% and 98.4% of their nominal Mp values respectively.

The specimens possessing the interchord welding were found to have greater strength and stiffness than those not so treated. For the 254 x 152 x 7.13 mm branch members, the ultimate moment of T2 exceeded that of T1 by about 17%, whereas for the smaller web members, the difference was 12%. It is evident that some form of connection between the chords has a desirable effect on structural performance.

The geometrical parameters which affect overall joint strength

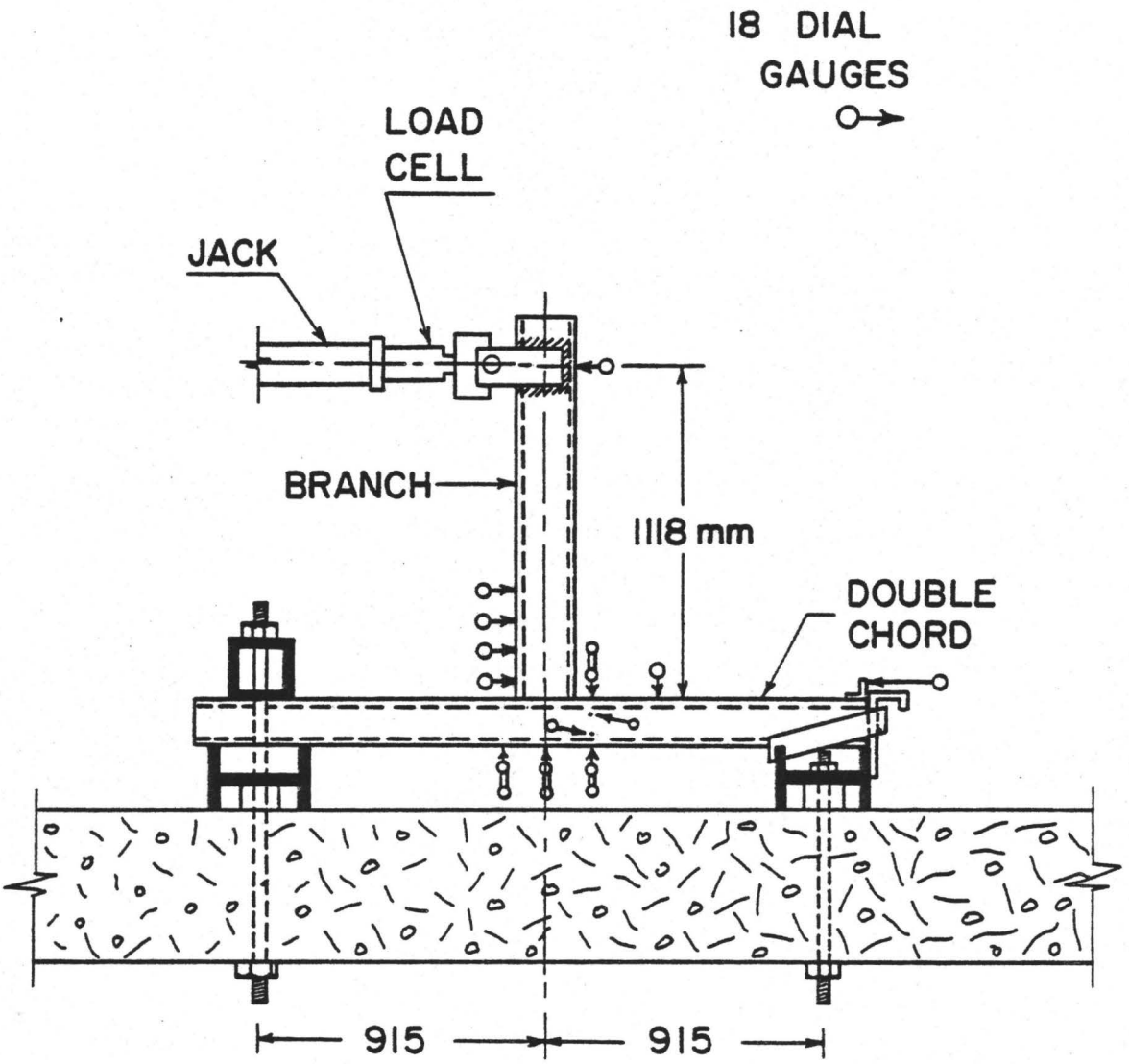

FIGURE 6.4 TESTING APPARATUS FOR T-JOINT SPECIMENS.

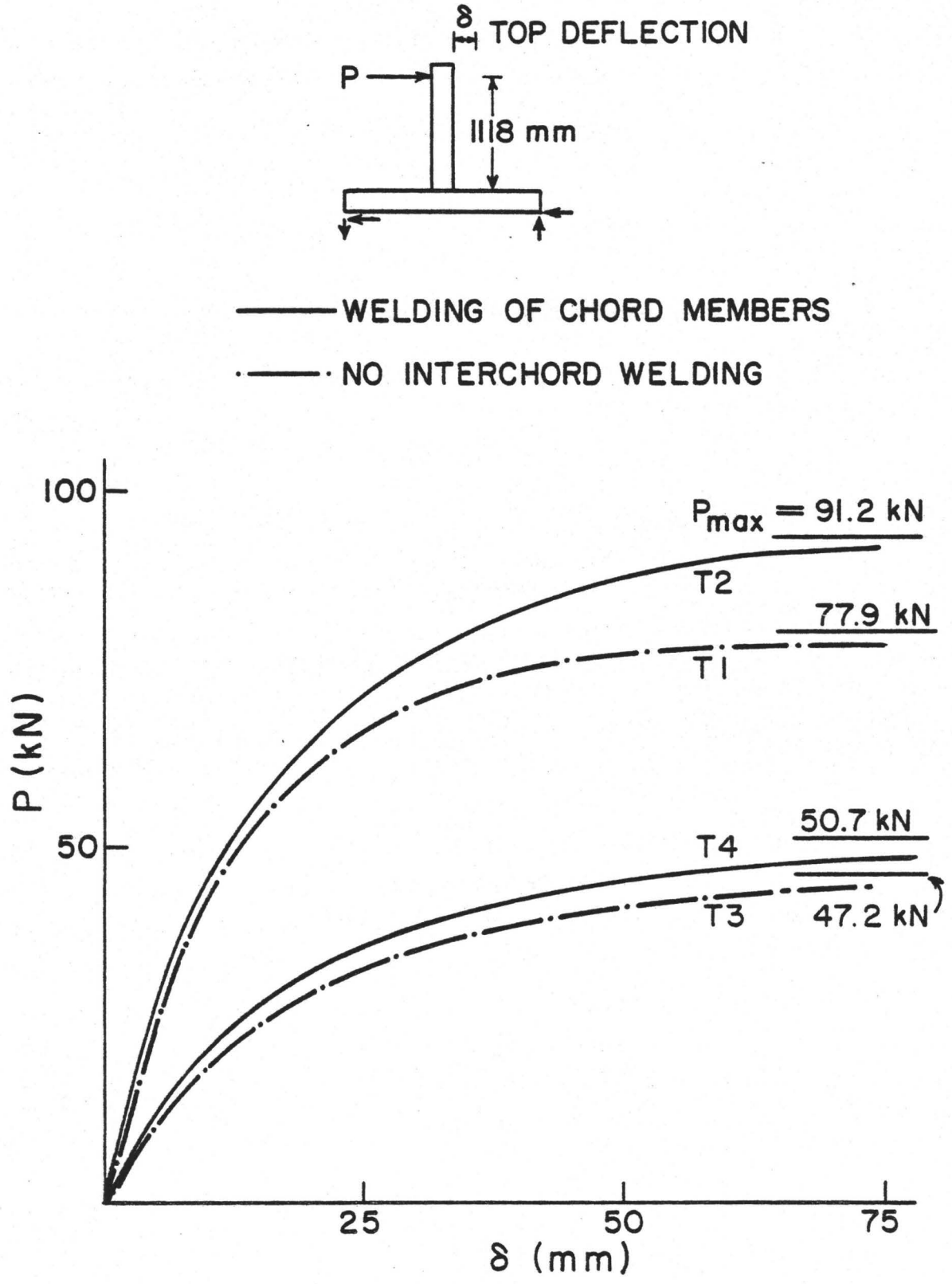

FIGURE 6.5 P-δ CURVES FOR DOUBLE CHORD T-JOINT CONNECTION.

Specimen Number	Plastic Moment Mp (KN.m)	Maximum Moment (KN.m)	Ultimate Moment as % of Mp	Failure Mode
T1	158.2	87	55.0	Chord Web Tearing
T2	158.2	102	64.4	Chord Web Tearing
T3	57.6	50.8	88.0	Branch Flange Buckling
T4	57.6	56.7	98.4	Branch Flange Buckling

Table 6.2 Double Chord T-Joint Results

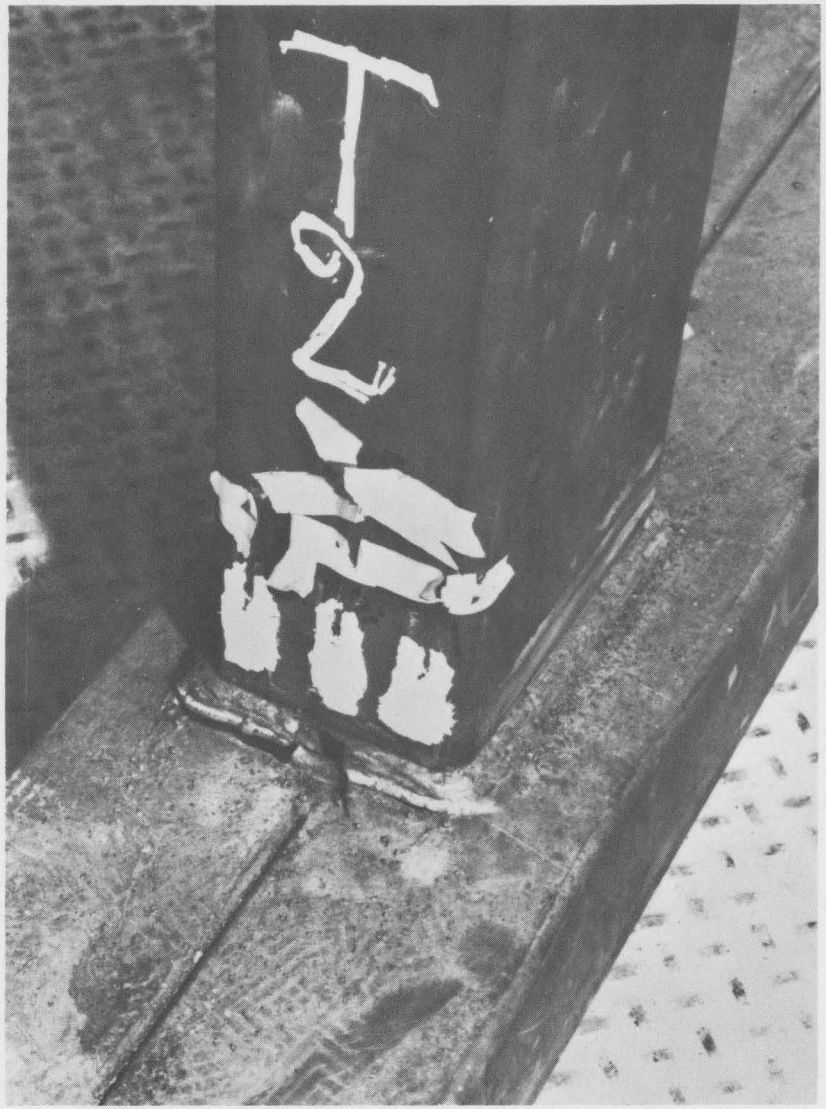

a) Tension side

b) Compression side

FIGURE 6.6 — FAILURE MODE FOR SPECIMEN T2

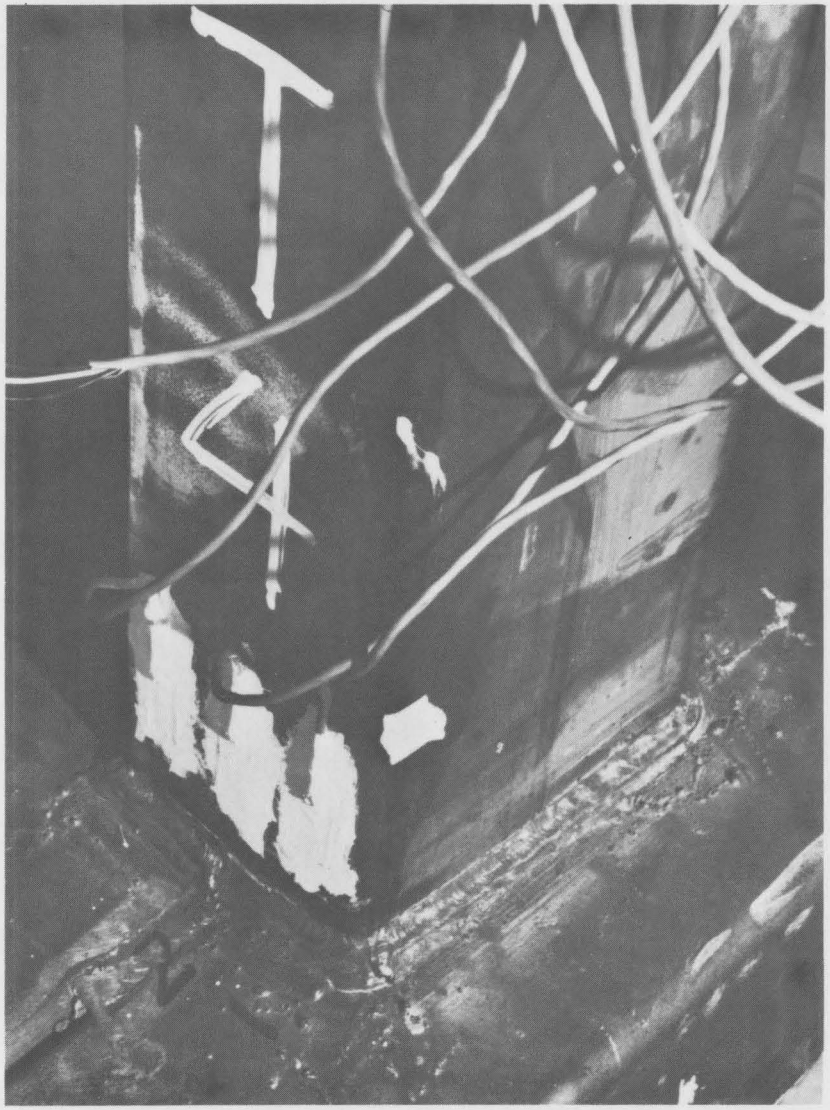

a) Tension side

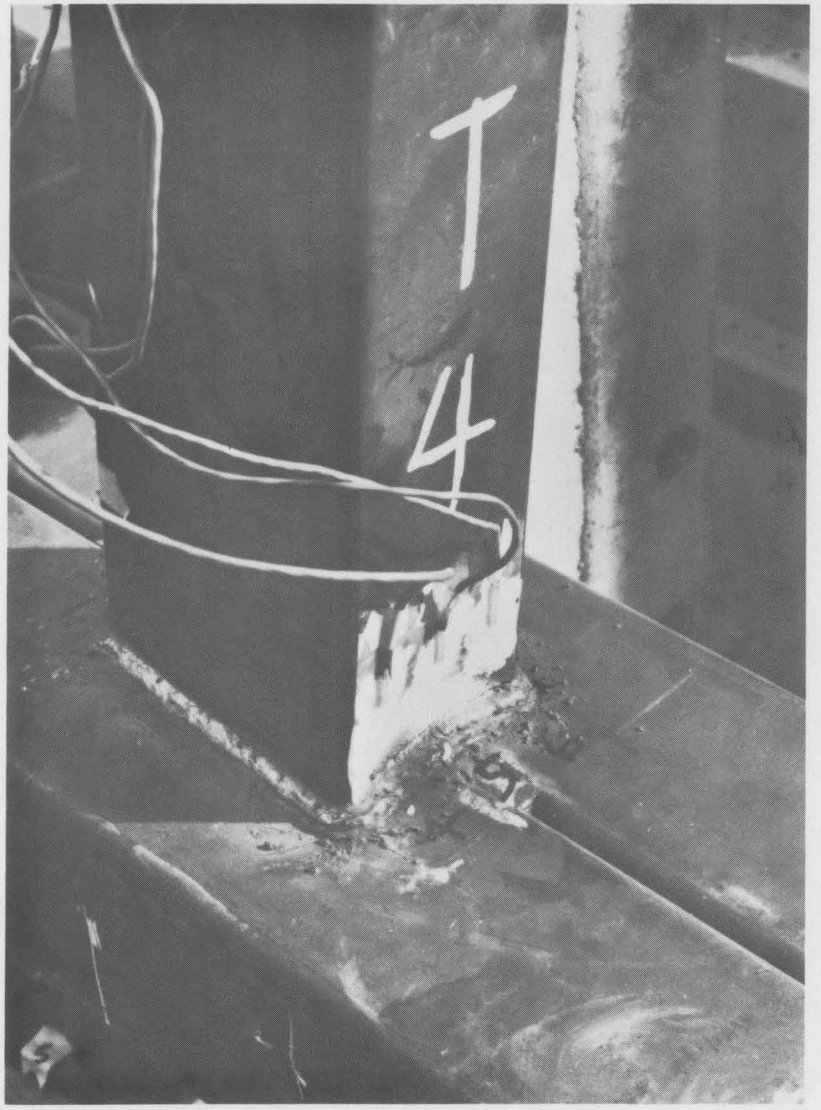

b) Compression side

FIGURE 6.7 — FAILURE MODE FOR SPECIMEN T4

and stiffness, are the thickness of the chord member and the ratio of the branch width-thickness ratio λ (= b/t_b). It appears that these parameters affected the intensity of stress transfer from the branch to the chord, and hence determined the failure mode observed and the strength capacity of the joints.

After a significant amount of yielding, two modes of failure were observed for the four specimens. Both T1 and T2 exhibited tearing of the parent metal of the chord inner web on the tension side of the branch member. Once the tearing occurred, cracks started to propagate in the chord member's top flanges along their intersection with the branch member, as is obvious in Figure 6.6(a) for specimen T2. Figure 6.6(b) shows that no localized buckling was observed on the compression side of the joint for T2. A similar observation was made for T1.

In contrast, T3 and T4 failed by local buckling of the branch flanges as indicated from Figure 6.7 for specimen T4. The smaller branch members required the development of smaller tensile forces in the adjoining webs of the double chord section, thus avoiding a tensile failure. In these two cases, the branch width-thickness ratio (b/t_b) was higher than that for T1 and T2, whereas the b/t_o value was lower. The numerical values for all specimens are listed in Table 6.1.

Although a brittle failure did not occur at ultimate load for either T1 and T2, designers may prefer connection details which result in a gradual localized buckling failure of the branch flange. Further tests are required to identify the critical width-thickness ratios both

for structurally efficient joints and for which the preferred failure modes are most probable.

6.5 Comparison with Single Chord T-Connections

For unreinforced T-joints, an interesting comparison can be made between a double chord connection and a single chord type. Joint T4 and a single chord specimen designated as A-3 in the work of Korol et al [39] are considered for this purpose. Reference is made to Table 6.3 for details. Both specimens were fabricated using fillet welds to connect the branch to its chord section. Also, the sectional properties for both branches were approximately equivalent. Thus the same moment transfer potential existed except that the single chord section was nominally superior to the composite chord both in stiffness and moment capacity. In addition, the width ratio λ and b/t_o value are both more favourable to the single chord case. By neglecting connection detailing, therefore, it might appear that A-3 would be superior to T4.

Figure 6.8 shows the load deflection curves for both specimens. It is obvious that the double chord section is superior both in stiffness and moment capacity despite the relatively poor sectional properties of the composite chord specimen.

Failure in the double chord specimen was caused by local buckling of the branch member's compression flange while the single chord specimen failed by local buckling of the chord's top flange. The latter case is potentially a more serious type of failure because a main member of the truss is affected. In a practical design, chord moments may be a

Member	Section Properties	Single Chord Joint	Double Chord Joint
Branch	Size (mm)	HSS 152 x 152 x 4.78	HSS 177 x 127 x 4.78
	Area (mm^2)	2760	2760
	Z_x (10^3 mm^3)	152	167
	DL Force (KN/m)	0.213	0.213
	M_{max} (KN.m)	50.4	56.7
	M_p (KN.m)	52.6	57.6
	M_{max}/M_p	0.96	0.98
	Failure	-	Local Buckling
Chord	Size (mm)	HSS 254 x 254 x 9.53	2 HSS 152 x 152 x 6.35
	Area (mm^2)	9090	7220
	Z_x (10^3 mm^3)	825	390
	DL Force (KN/m)	0.699	0.556
	λ*	0.6	0.417
	b/t_o	16	20
	Failure	Local Buckling	-

Table 6.3 Properties of T-Connections

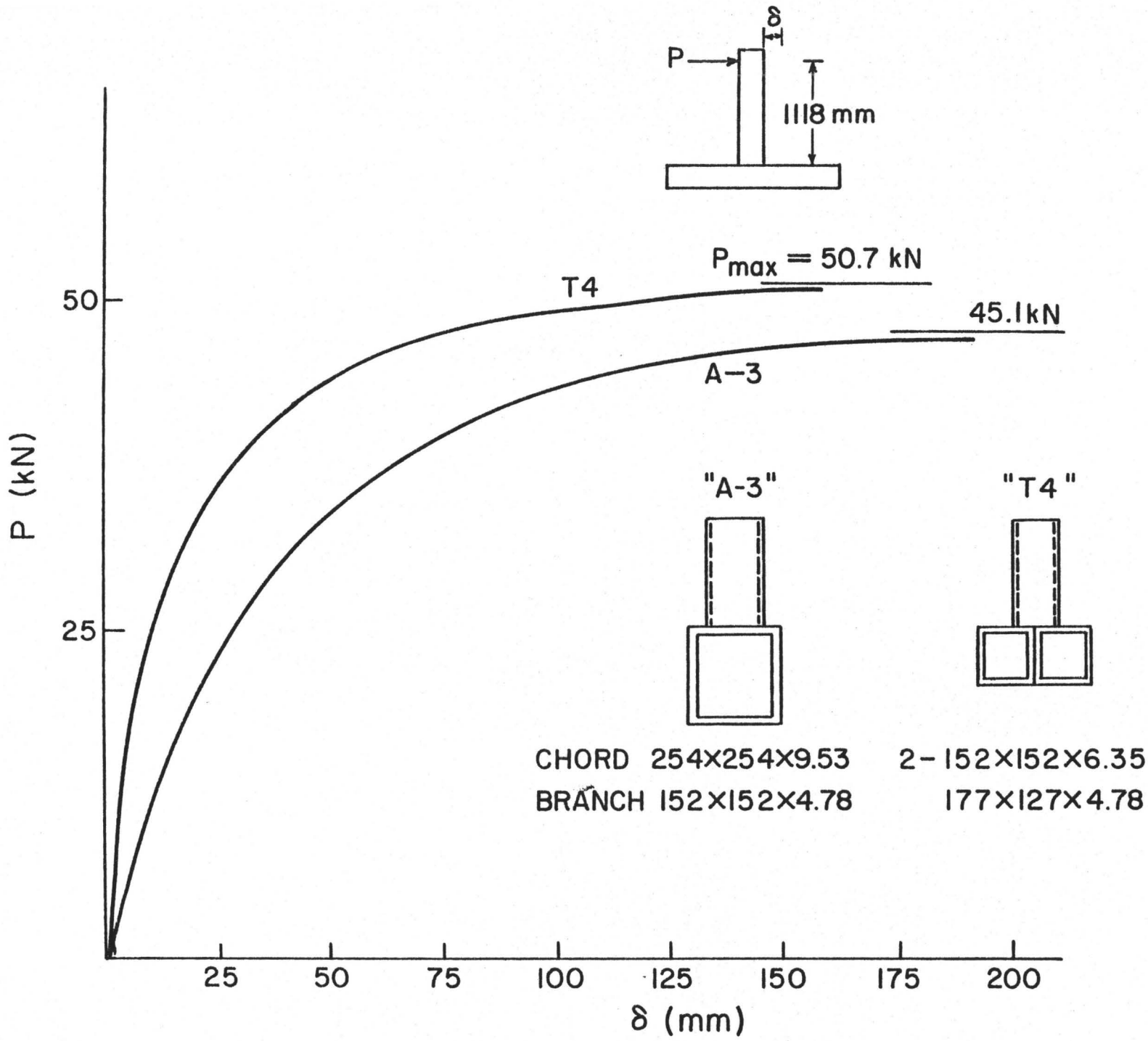

FIGURE 6.8 P_δ CURVES FOR SINGLE AND DOUBLE CHORD T-JOINT. CONNECTION.

magnitude or more greater than that of the connecting branch member. This situation will magnify the flange buckling problem existing in the single chord case.

To further demonstrate the potential for double chord T-joints consider specimens T2 and C-17 (Table I of Korol et al. [39]) as presented in Table 6.4. The latter specimen was provided with a 12.7 mm chord flange stiffening plate as well as having a more favourable width ratio λ^*. The b/t_o ratios were only marginally different. The results for maximum moment indicate that without any form of reinforcement, the double-chord connection performed at least as well as its plate-reinforced single-chord counterpart.

6.6 Discussion

As was the case for the K-joint specimens, the double chord T-type connection exhibits superior qualities than the equivalent unreinforced single chord connection in the following ways:

i) Greater joint stiffness is obtained.

ii) A higher moment capacity can be expected.

iii) Greater out-of-plane bending resistance is achieved.

iv) Redistribution of forces will occur in the event of a localized member failure, thus safeguarding the structure from complete collapse due to overloading.

v) Lighter HSS will be used for chord members, reducing the overall weight of the truss.

In general, the strength and stiffness of the joint is improved

Specimen Number	Branch Member HSS (mm)	Chord Member HSS (mm)	λ^*	b/t_c	Max. Moment as % of M_p	Strengthening Device
C-17	254 x 254 x 7.95	304 x 304 x 9.53	0.833	26.7	64	12.7 mm plate
T2	254 x 152 x 4.78	2 - 152 x 152 x 6.35	0.50	24	66	None

Table 6.4 Comparison with flange plate stiffener

when the individual chords are welded together near the joint to form a composite section.

CHAPTER 7

PREDICTIVE MODEL FOR THE STANDARD AND CHANNEL TYPE JOINTS

7.1 General Formulation

It was shown in Chapter 3 that the main failure for the standard joint was caused by shear distortion of the chord's webs. The joint was also subjected to bending moment, axial load and torsion. The torsional moment was primarily resisted by the flanges of the web members which tended to act as a rigid diaphragm. Hence for the S-type joint, the chord itself will be considered to be subject to shearing force, axial load and bending moment only. For the channel type, however, torsional moments will be included.

A method of calculating the ultimate load of a rectangular HSS subjected to moment, axial force and shear was developed by Brockenbrough [32] for beam column connections. The approach is to partition portions of the HSS to the various stress resultants. In Figure 7.1, the height, b_{va}, represents the width of the tube that has yielded under combined axial and shear stresses. Once b_{va} is known, the corresponding value for bending stresses that cause complete plastification of the remainder of the cross section is obtained from an interaction equation. The interaction equation for ultimate strength depends on whether the bending moment is dominant ($b_{va} \leq A/4t_o$) or the axial load is dominant ($b_{va} > A/4t_o$).

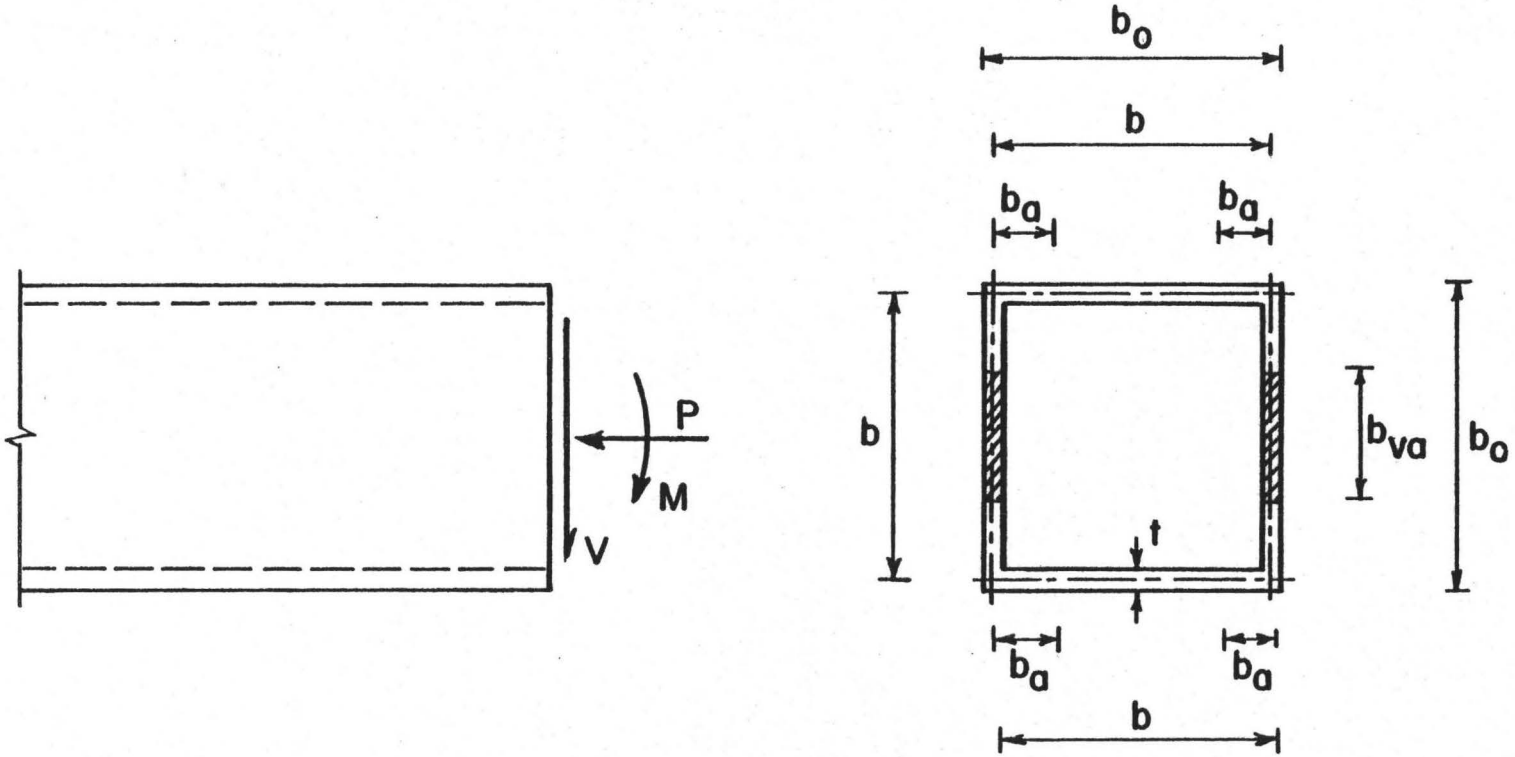

FIGURE 7.1 FORCES AND DIMENSIONS OF STANDARD TYPE DOUBLE CHORD WITH SINGLE H.S.S.

When the bending is dominant ($b_{va} \leq A/4t_o$), the shear stress, f_v, and axial stress, f_a, along the width b_{va}, for a section subjected to M, P and V and exhibiting elastic-plastic behaviour, are:

$$f_v = \frac{V}{2\, t_o\, b_{va}} \tag{7.1}$$

$$f_a = \frac{P}{2\, t_o\, b_{va}} \tag{7.2}$$

If Von Mises yield criterion is assumed, the plastic shear force, V_p, and the fully plastic axial load for the HSS are given by

$$V_p = \frac{A}{2} \cdot \frac{\sigma_y}{\sqrt{3}} \tag{7.3}$$

$$P_y = A \cdot \sigma_y \tag{7.4}$$

Substituting (7.3) and (7.4) into (7.1) and (7.2) yields

$$f_v = \frac{V}{V_p} \cdot \frac{A\, \sigma_y}{4\sqrt{3}\, t_o\, b_{va}} \tag{7.5}$$

$$f_a = \frac{P}{P_y} \cdot \frac{A\, \sigma_y}{2\, t_o\, b_{va}} \tag{7.6}$$

The yield condition under combined axial and shear stresses is

$$\sigma_y = \sqrt{(f_a^2 + 3f_v^2)} \tag{7.7}$$

Substituting (7.5) and (7.6) into (7.7) gives

$$b_{va}^2 = \frac{A^2}{16t_o^2} \left[\frac{4P^2}{P_y^2} + \frac{V^2}{V_p^2}\right]$$

therefore

$$b_{va} = \frac{A}{4t_o} \left[\left(\frac{2P}{P_y}\right)^2 + \left(\frac{V}{V_p}\right)^2 \right]^{1/2} \tag{7.8}$$

The bending moment is given by

$$M = \sigma_y \left(z - \frac{b_{va}^2 \, t_o}{2}\right) \tag{7.9}$$

where z = plastic section modulus of the section while the last term in equation (7.9) represents the plastic modulus of the yielded width b_{va} denoted as $z_{b_{va}}$.

It follows that

$$\frac{M}{M_p} = \frac{z - \frac{b_{va}^2 \, t_o}{2}}{z} \tag{7.10}$$

where M_p = plastic moment = $z \, \sigma_y$

Substituting (7.8) into (7.10) and replacing A by $4bt_o$ and z by $(3 \, b^2 \, t_o)/2$ gives equation (7.11)

$$\frac{M}{M_p} + \frac{4}{3}\left(\frac{P}{P_y}\right)^2 + \frac{1}{3}\left(\frac{V}{V_p}\right)^2 = 1 \tag{7.11}$$

for $$b_{va} \leq \frac{A}{4t_o}$$

If the value of b_{va}, calculated from equation (7.8) exceeds $A/4t_o$; the height, b, has completely yielded and a portion of the axial load must be assigned to a width b_a, shown in Figure 7.1. Now, replacing b_{va} by $A/4t_o$ in equation (7.8) and simplifying gives

$$1 = \left(\frac{2P}{P_y}\right)^2 + \left(\frac{V}{V_p}\right)^2$$

which can be expressed in the form

$$\left(\frac{P}{P_y}\right)^* = \frac{1}{2}\left[1 - \left(\frac{V}{V_p}\right)^2\right]^{1/2} \tag{7.12}$$

where $(P/P_y)^*$ is the maximum normalized axial load which may be taken by the height b. The remaining axial load should be taken by part of the flanges, b_a, so that

$$\left[\frac{P}{P_y} - \left(\frac{P}{P_y}\right)^*\right] = \frac{4\, b_a\, t_o}{A} \tag{7.13}$$

Substituting (7.12) into (7.13) leads to

$$b_a = \frac{A}{8t}\left[\frac{2P}{P_y} - \left[1 - \left(\frac{V}{V_p}\right)^2\right]^{1/2}\right] \tag{7.14}$$

Since the bending moment is

$$M = \sigma_y\left[z - \frac{b^2\, t_o}{2} - 2b\, b_a\, t_o\right], \tag{7.15}$$

Substitution from equation (7.14) into (7.15) and simplifying gives

$$\frac{3M}{2M_p} + \frac{2P}{P_y} - \left[1 - \left(\frac{V}{V_p}\right)^2\right]^{1/2} = 1 \tag{7.16}$$

for $$b_{va} > \frac{A}{4t_o}$$

Brockenbrough's approach will now be extended to account of the strain hardening effect, since it was found from the tests that a considerable amount of inelastic deformation occurred prior to failure. From the numerous tensile tests that were conducted, average physical

properties were as follows:

$$\left(\frac{\sigma_u}{\sigma_y}\right)_{AV} = 1.25$$

$$\left(\frac{E}{E_{st}}\right)_{AV} = 90.60 \qquad (7.17)$$

$$\left(\frac{\varepsilon_{st}}{\varepsilon_y}\right)_{AV} = 8.70$$

where σ_u = the ultimate strength of the material, and other quantities are defined in Figure 7.2.

The ultimate moment capacity, M_u, will now be computed. It will be assumed that the outside fibre stress reaches σ_u such that $\sigma_u = \sigma_y + \sigma_{ex}$ where σ_{ex} is the additional exterior fibre stress above and beyond σ_y. Therefore

$$\sigma_{ex} = 0.25\ \sigma_y \qquad (7.18)$$

$$E_{st} = \frac{\sigma_{ex}}{\varepsilon_u - \varepsilon_{st}}$$

$$\sigma_{ex} = (\varepsilon_u - \varepsilon_{st}) \cdot E_{st} \qquad (7.19)$$

Substituting (7.17) and (7.18) into equation (7.19)

$$0.25\ \sigma_y = (\varepsilon_u - 8.7\ \varepsilon_y) \cdot \frac{E}{90.6}$$

or

$$\varepsilon_u = 31.35\ \varepsilon_y \qquad (7.20)$$

Now, the inside fibre strain, assuming plane sections to remain plane, is given by:

$$\varepsilon_{in} = \left(\frac{b_o - 2t_o}{b_o}\right) \varepsilon_u \qquad (7.21)$$

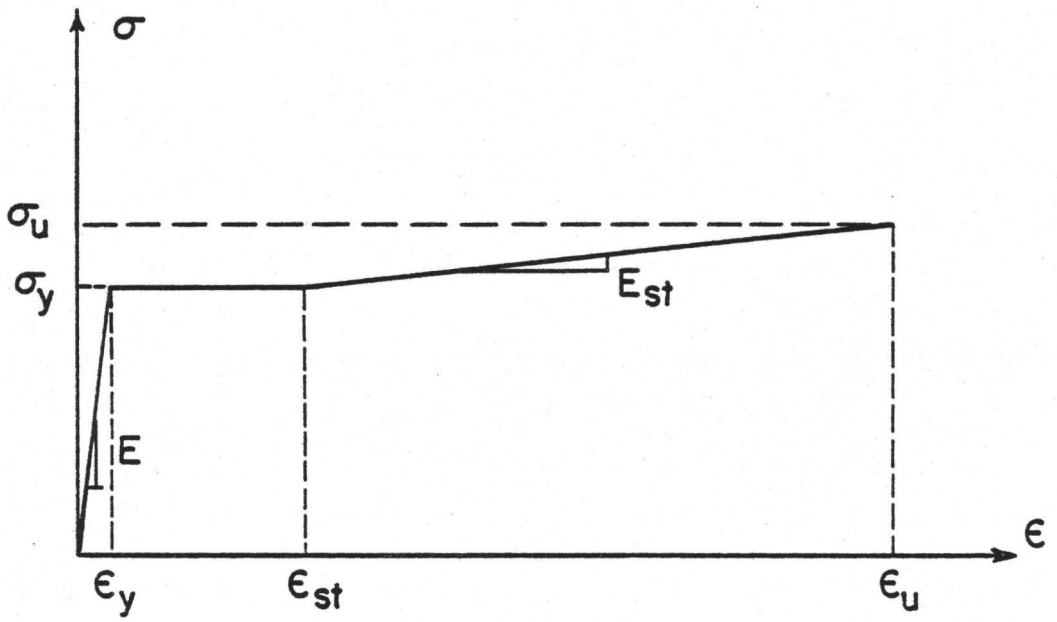

FIGURE 7.2 IDEALIZED STRESS-STRAIN RELATION FOR STEEL.

The additional stress above σ_y at the inside flange fibre is:

$$\sigma_{in} = (\varepsilon_{in} - \varepsilon_{st})\, E_{st} \tag{7.22}$$

The height above the neutral plane for which strain hardening affects the stresses is related to ε_{st} and ε_u given by equations (7.17) and (7.20), and is equal to $0.14\ b_o$ as is shown in Figure 7.3.

Hence,

$$\sigma_{in} = \left(\frac{0.36\ b_o - t_o}{0.36\ b_o}\right) \sigma_{ex}$$

$$= \left(1 - 2.78\ \frac{t_o}{b_o}\right) \sigma_{ex} \tag{7.23}$$

Now the ultimate moment is

$$M_u = \sigma_y\, z + M_{st} \tag{7.24}$$

where M_{st} is the strain hardening contribution and is equal to

$$M_{st} = \left(\frac{\sigma_{in} + \sigma_{ex}}{2}\right) b^2\, t_o + \left(\frac{\sigma_{in} + \sigma_{ex}}{2}\right) \frac{t_o}{2} \left(0.36\ b_o - \frac{t_o}{2}\right)$$

$$4\ \left(0.14\ b_o + \frac{2}{3}\left\{0.36\ b_o - \frac{t_o}{2}\right\}\right) \tag{7.25}$$

From (7.23), (7.25) and (7.18) equation (7.24) reduces to

$$M_u = \sigma_y\, z + \frac{\sigma_y}{4}\, b^2\, t_o \left(1 - 1.39\ \frac{t_o}{b_o}\right)$$

$$+ \frac{1}{2}\, \sigma_y \left(1 - 1.39\ \frac{t_o}{b_o}\right) \left(0.36\ b_o - \frac{t_o}{2}\right) \left(0.38\ b_o - \frac{t_o}{3}\right) t_o \tag{7.26}$$

Equation (7.26) represents the ultimate moment that could be carried by

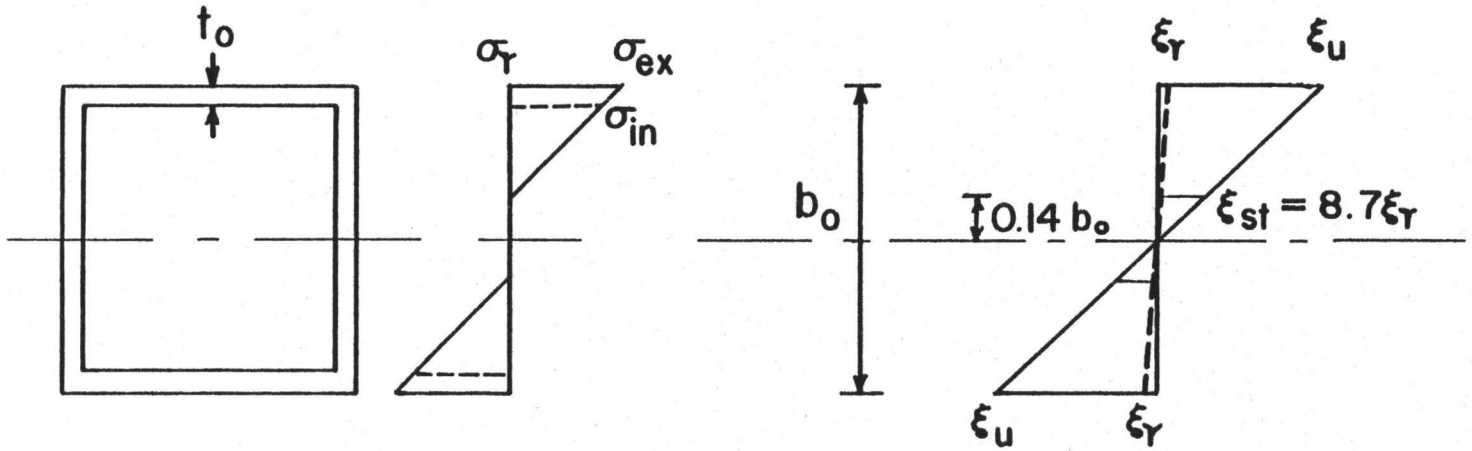

FIGURE 7.3 STRAIN HARDENING STRESS AND STRAIN DISTRIBUTIONS.

the section in the absence of other force systems, and ignores residual stresses. If one selects a 152 x 152 x 6.35 mm HSS

$$\frac{M_u}{M_p} = 1.21 \text{ or, in general}$$

$$\frac{M_u}{M_p} = K_t, \text{ a constant for any section with prescribed physical properties.}$$

A similar calculation can be done for the flanges and the webs to yield 1.236 and 1.127 for K_f and K_w respectively.

Hence, if the actual maximum moment M can only utilize part of the flanges and none of the web, then

$$M = K_t \sigma_y z - K_w \sigma_y z_w - K_f \sigma_y z_f \tag{7.27}$$

where z_w and z_f are the plastic section moduli for the webs and the b_a portions of the flanges.

For the strain hardening case, equation (7.8) becomes

$$b_{va} = \frac{A}{4t_o} \left[\left(\frac{2P}{P_u}\right)^2 + \left(\frac{V}{V_u}\right)^2 \right]^{1/2} \tag{7.28}$$

for $$b_{va} \leq \frac{A}{4t_o}$$

If $b_{va} > A/4t_o$, then b_a must be determined which will validate equation (7.27). The revised equation (7.14) for the strain hardening case then becomes

$$b_a = \frac{A}{8t_o} \left\{ 2 \frac{P}{P_u} - \left[1 - \left(\frac{V}{V_u}\right)^2 \right]^{1/2} \right\} \tag{7.29}$$

The interaction formula which now applies is found by utilizing equation

(7.27) so that

$$M = 1.21\ \sigma_y\ z - 1.127\ \sigma_y\ z_w - 1.236\ \sigma_y\ z_f$$

since

$$M_u = 1.21\ \sigma_y\ z$$

therefore

$$\frac{M}{M_u} = \frac{z - 0.93\ z_w - 1.02\ z_f}{z}$$

$$= 1 - 0.93\ \frac{b^2\ t_o}{2} \cdot \frac{2}{3\ b^2\ t_o} - 2.04\ b\ t_o\ b_a \cdot \frac{2}{3\ b^2\ t_o}$$

$$= 1 - 0.31 - 1.36\ \frac{b_a}{b}$$

$$\frac{M}{M_u} = 0.69 - 1.36\ \frac{b_a}{b} \qquad (7.30)$$

From (7.29), equation (7.30) becomes

$$1.45\ \frac{M}{M_u} + 1.97\ \frac{P}{P_u} - 0.985\ [1 - (\frac{V}{V_u})^2\ ]^{1/2} = 1 \qquad (7.31)$$

where

$$P_u = A\ \sigma_u \text{ and } V_u = \frac{A}{2}\ \frac{\sigma_u}{\sqrt{3}}$$

Figure 7.4 indicates the web and chord forces P_w and N, acting on a standard joint. It is clear that at the critical section,

$$M = \frac{P_w}{2}\ e\ \cos\theta$$

$$P = \frac{N}{2} + P_w\ \cos\theta$$

and

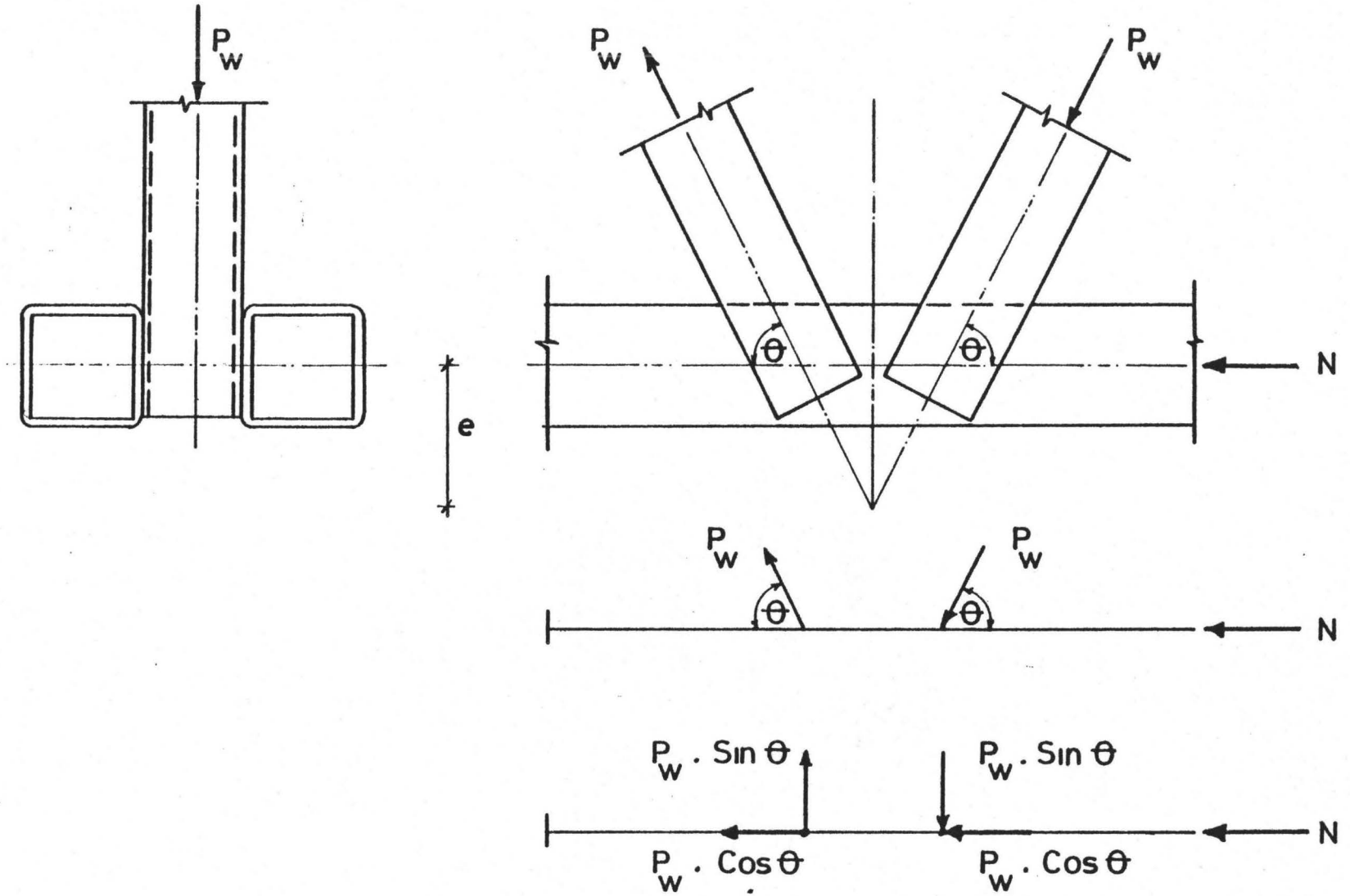

FIGURE 7.4 FORCE SYSTEM ON STANDARD JOINT.

$$V = \frac{P_w}{2} \sin \theta$$

These quantities are the stress resultants acting on one member of the chord.

7.2 Sample Calculation - Specimen S2P76C

For the testing program, all standard type specimens utilized 2 HSS 152 x 152 x 6.35 for chord members. The average yield and ultimate strengths for the 6 joints in group 1 will be used.

Test data are:

σ_y = 388 MPa

σ_u = 485 MPa

e = 178 mm

N = 590 KN

A = 3610 mm^2

z = 195000 mm^3

tan θ = 2

The moment M,

$$M = \frac{P_w}{2} e \cos \theta = \frac{1}{2} P_w \times 178 \times 0.4472 = 39.8 P_w \text{ (KN-mm)}$$

The chord axial force P,

$$P = \frac{N}{2} + P_w \cos \theta = 295 + 0.4472 P_w \text{ (KN)}$$

The shear force V,

$$V = \frac{P_w}{2} \sin \theta = 0.4472 P_w \text{ (KN)}$$

The ultimate stress resultants are given by:

$$M_u = k_t \sigma_y z = 1.21 \times .388 \times 195000 = 91549 \text{ KN.mm}$$

$$P_u = A \sigma_u = 3610 \times .485 = 1751 \text{ KN}$$

and

$$V_u = \frac{A}{2} \frac{\sigma_u}{\sqrt{3}} = \frac{3610}{2} \times \frac{.485}{\sqrt{3}} = 505 \text{ KN}$$

Substituting into equation (7.31) gives

$$\frac{1.45 \times 39.8 P_w}{91549} + \frac{1.97 [295 + 0.4472 P_w]}{1751}$$

$$- 0.985 \left[1 - \left(\frac{0.4472 P_w}{505}\right)^{2\ 1/2}\right] = 1$$

Solving for the web force gives the result that

$$P_w = 998 \text{ KN (v.s. 1010 KN by test).}$$

From equation (7.28), it is evident that $4 t_o b_{va} > 1$ which validates the use of equation (7.31).

7.3 Comparison Between Theory and Tests

For the standard type joints, predictions of web force capacity to cause failure were made using Brockenbrough's equation (7.16) and strain hardening equation (7.31).

The results are presented for each of groups 1, 2 and 3. Figure 7.5 shows experimental points for group 1 and theoretical curves in which average yield and ultimate chord member stresses were used in the Brockenbrough and strain hardening cases respectively. The upper curves, which take into account strain hardening and for which a sample calculation was presented earlier, give a reasonable indication of joint strength. The "C" curve is to be compared with the "C" group of

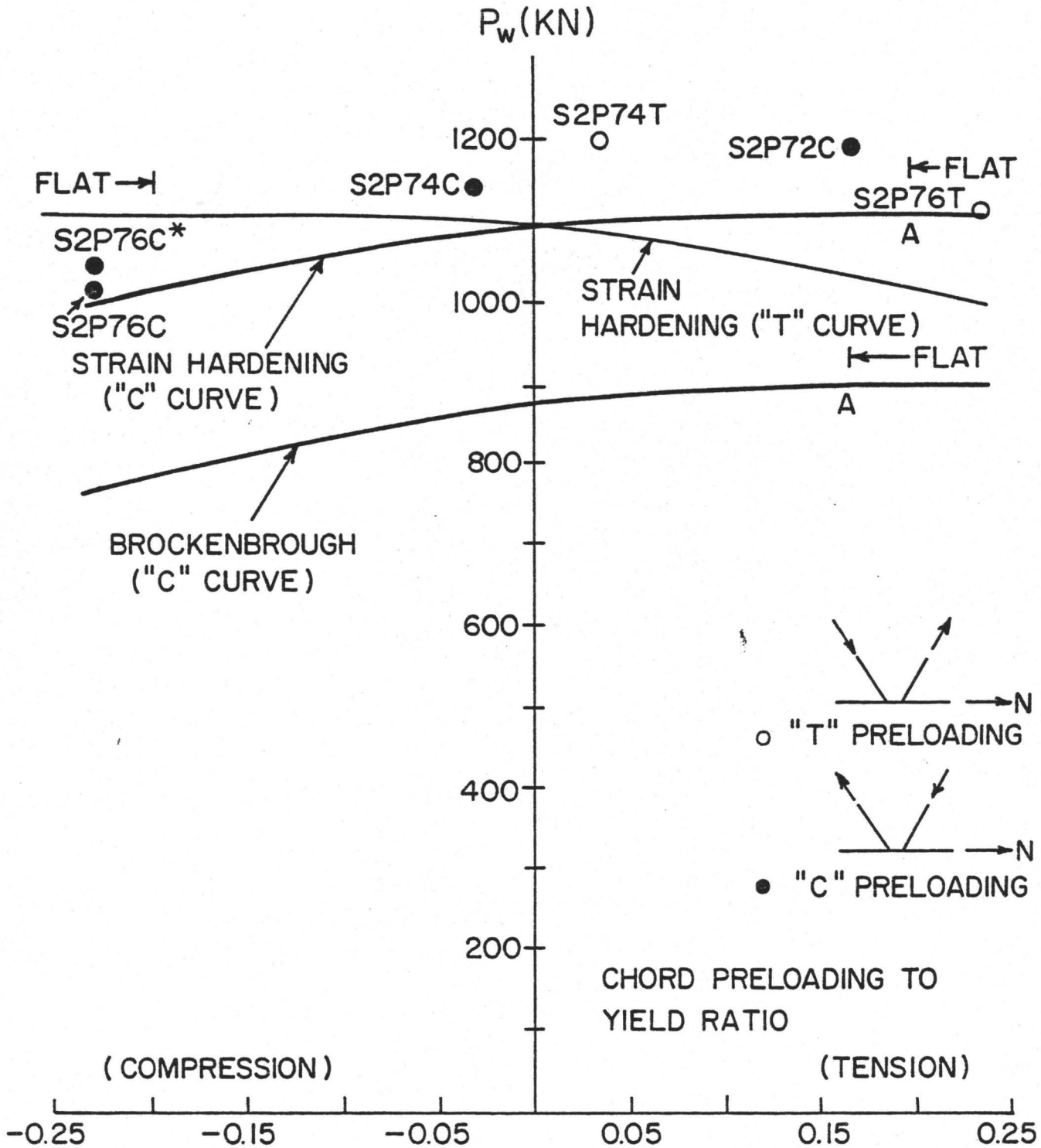

FIGURE 7.5 STRAIN HARDENING THEORY AND TEST RESULTS FOR GROUP I.

specimens i.e. S2P76C, S2P74C and S2P72C, while the "T" curve is applicable to S2P74T and S2P76T. Thus for a given preload, the axial force at the centerline of the joint will be different depending on the direction of the web forces. These are indicated in the inset of Fig. 7.5. The lower Brockenbrough elastic plastic prediction, (equation (7.16)), is seen to substantially underestimate capacity for the C specimens. To the left of points A, the chord webs resist a combination of axial and shear forces. To the right of A, the entire chord web area is devoted to providing shear resistance which limits the member force.

Table 7.1 shows the predicted values for the standard joints where the actual yield stresses were used in equation (7.37). The predicted values are within 8% range from the actual joint capacities obtained from the testing program , which is a very good prediction.

Figure 7.6 presents the results for group 2 series. The strain hardening curve again predicts the joint strength at values below the experimental points. The agreement is somewhat poorer than for the group 1 set. The reason is that both S2P44C and S2P46C had weld bridging which tended to reduce the load transferred through the chord. Consequently there was more capacity in the connection than would normally occur with minimum weldment. After the test was terminated for both specimens, a smooth cut was made on both through the bridging zone to calculate the bridging areas, 254 and 238 mm^2 respectively. It is obvious from Table 7.2 that without taking the weld bridging effect into account, the predicted capacities for the previous two specimens would be less than the experimental values by 15.5 and 14.6% respectively. By

Specimen Number	P_w (KN) Prediction	P_w (KN) Test	% of error
S2P76C	975	1010	3.5
S2P74C	1060	1144	7.3
S2P72C	1112	1188	6.4
S2P74T	1115	1206	7.5
S2P76T	1040	1117	6.9
S2P76C*	998	1050	5

Table 7.1 Predicted Values Using Actual Yield Stress

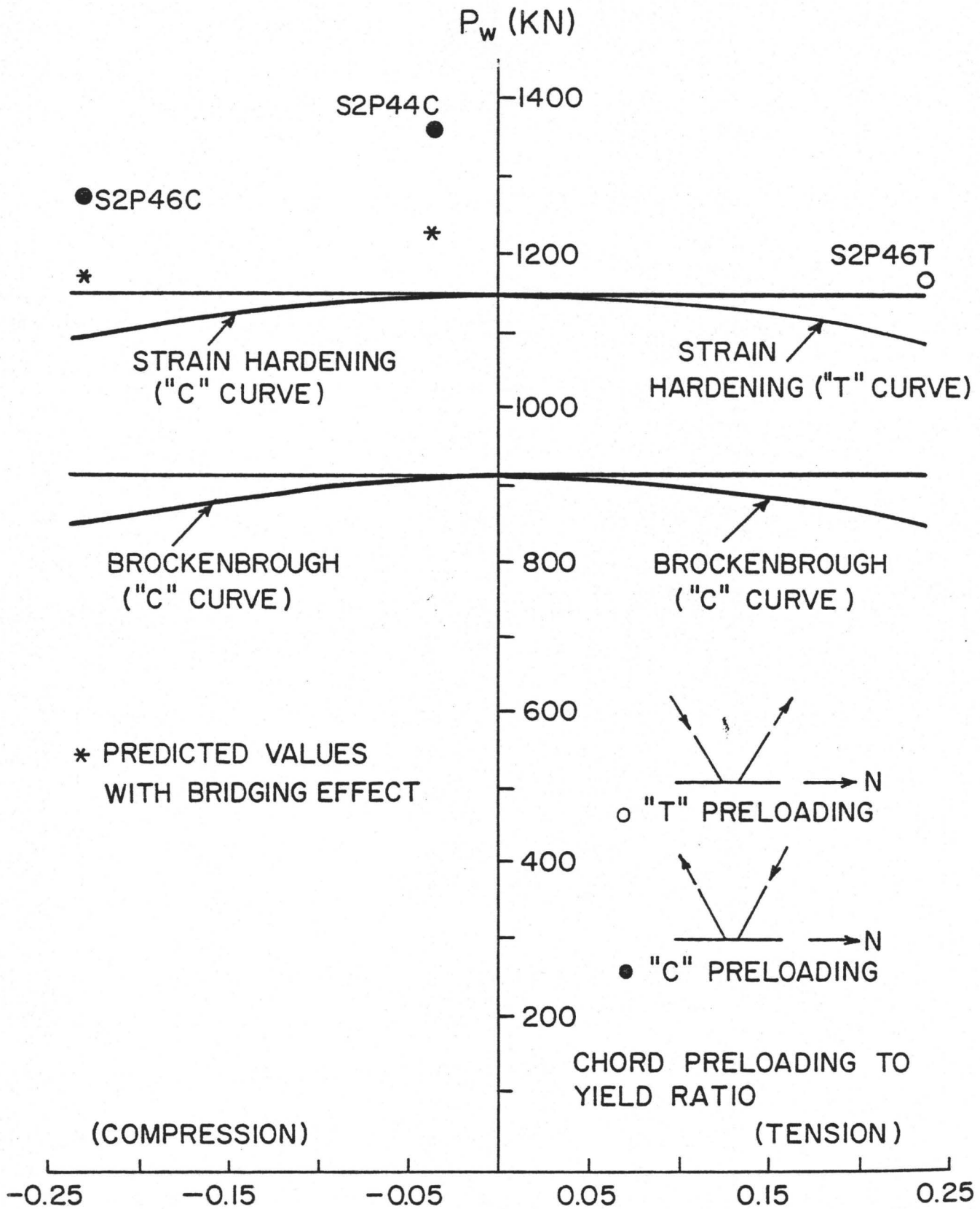

FIGURE 7.6 STRAIN HARDENING THEORY AND TEST RESULTS FOR GROUP 2 .

Specimen Number	P_{web} (KN)			Bridging Area (mm^2)
	Test	Predicted No bridging effect	Predicted With bridging effect	
S2P46C	1277	1090 (14.6%)	1165 (8.8%)	238
S2P44C	1352	1142 (15.5%)	1230 (9%)	254
S2P46T	1188	1090 (9.2%)		0

Table 7.2 Weld Bridging effect on joint capacity

introducing the bridging area as an extra cross sectional area the differences between the predicted and experimental capacities were reduced to 9 and 8.8% respectively. Specimen S2P46T, on the other hand, did not contain the unspecified weldment found for the other two and its predicted capacity was within 9% of the tested one. Note the slightly higher position of the computed curves of Figure 7.6 as compared to Figure 7.5. The difference is due to the reduced eccentricity of the group 2 specimens (108 mm v.s. 178 for group 1).

Figure 7.7 shows the results for the group 3 series. By decreasing the slope of the web members, the shearing component was reduced from 0.4472 P_w to 0.3536 P_w while the axial component was considerably increased from 0.447 P_w to 0.707 P_w. Agreement between the experimental and theoretical results was reasonable for the three specimens which failed by local buckling of the compression web member after shear distortion deformation was observed, and detection of a crack in the weld or in the inner web of the chord member. An indication of good performance of the joint is failure of the web or chord members; i.e. the members are fully used to resist the loads. The capacities of the three specimens exceeded the yield web load by 13, 15 and 16%. However, the predicted capacity for specimen S1P46T was higher than the one obtained from the test by 5.5%. The reason for this short fall in strength was apparently due to a very low yield stress value for the compression web member (340 MPa), as compared with yield stress of 399 and 385 for specimens S1P26C and S1P26C* respectively.

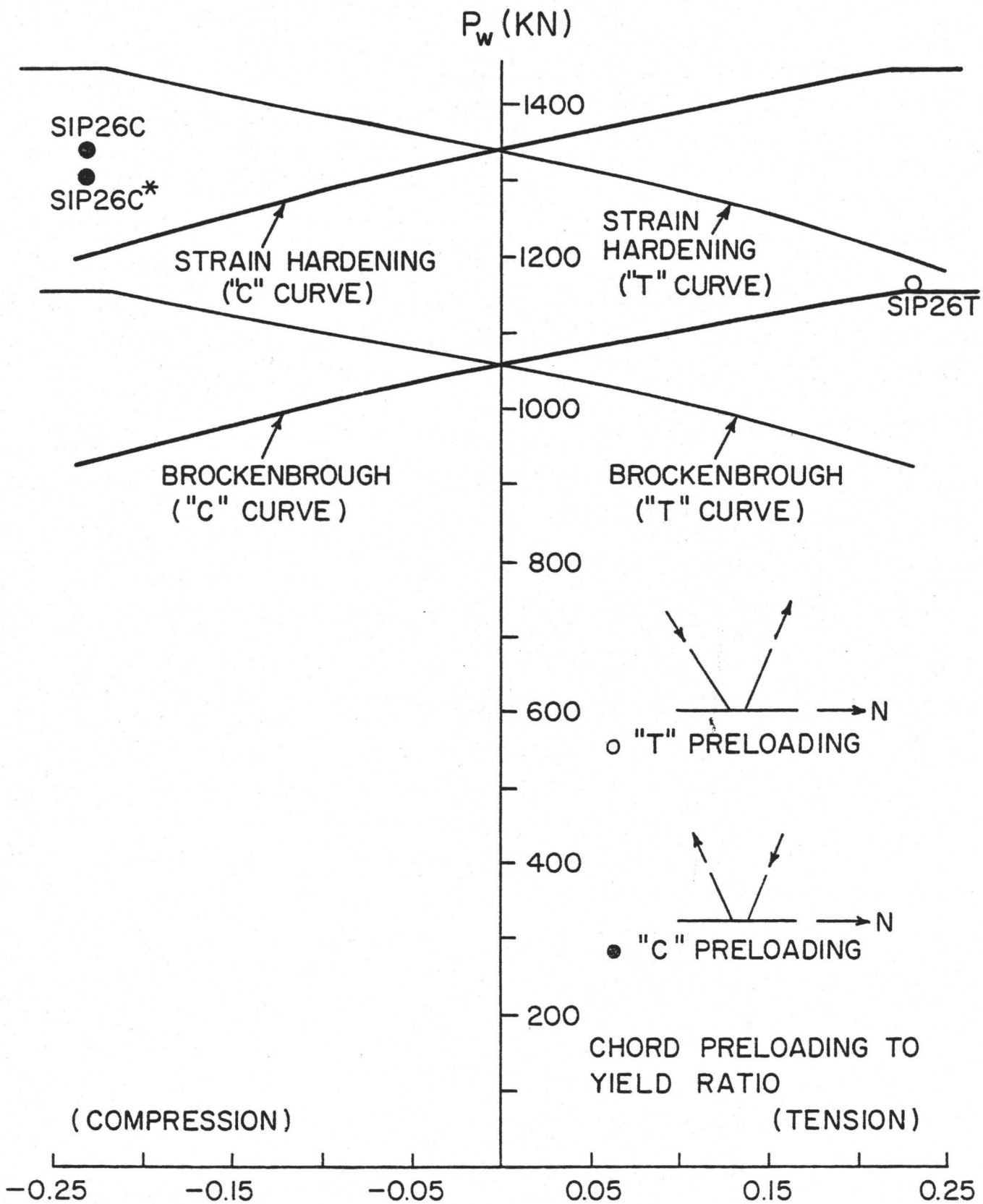

FIGURE 7.7 . STRAIN HARDENING THEORY AND TEST RESULTS FOR GROUP 3 .

7.4 Capacity of Channel Type Joints

The channel type joints may be subjected to axial and shearing forces, bending moment and torsional moments. Hence torsion is introduced to the previous procedure, used to derive (7.31) for the standard joints, to obtain a new equation for the channel type joints.

By using the same partitioning approach described earlier for the standard type, the height b_{va}, shown in Fig. 7.1, represents the width of the tube that has yielded under combined axial, shear and torsional stresses.

Shear and axial stresses were obtained earlier

$$f_v = \frac{V}{V_p} \cdot \frac{A\ \sigma_y}{4\sqrt{3}\ t_o\ b_{va}} \tag{7.5}$$

$$f_a = \frac{2P}{P_y} \cdot \frac{A\ \sigma_y}{4\ t_o\ b_{va}} \tag{7.6}$$

Assuming that half the torsional moment (T) is resisted by the webs and that the other half is resisted by the flanges, the following shear stress is obtained

$$f_{vt} = \frac{T}{2\ b_{va}\ t_o\ b} \tag{7.32}$$

Now

$$T_p = \frac{\sigma_y}{\sqrt{3}}\ z_t \tag{7.33}$$

where T_p is the plastic torsional moment and

$$z_t = \text{torsional modulus} = 2\ b^2 t \tag{7.34}$$

Substituting (7.33) and (7.34) into (7.32) yields

$$f_{vt} = \frac{T}{T_p} \cdot \frac{A\,\sigma_y}{4\sqrt{3}\,t_o\,b_{va}} \tag{7.35}$$

Total shear stress is $\Sigma f_v = f_v + f_{vt}$

$$\Sigma f_v = \frac{A}{4\sqrt{3}\,t_o\,b_{va}} \left[\frac{V}{V_p} + \frac{T}{T_p}\right] \sigma_y \tag{7.36}$$

The yield condition under combined axial and shear stresses is

$$\sigma_y^2 = f_a^2 + 3\,\Sigma f_v^2 \tag{7.37}$$

Substituting (7.6) and (7.36) into (7.37) gives

$$b_{va} = \frac{A}{4\,t_o} \left[\left(\frac{2P}{P_y}\right)^2 + \left(\frac{V}{V_p} + \frac{T}{T_p}\right)^2\right]^{1/2} \tag{7.38}$$

for

$$b_{va} \leq \frac{A}{4\,t_o}$$

If the value of b_{va} exceeds $A/4t_o$, the height, b, has completely yielded and a portion of the axial load must be assigned to a width b_a, shown in Fig. 7.1. Now, replacing b_{va} by $A/4t_o$ in (7.38) and simplifying gives

$$\left(\frac{P}{P_y}\right)^* = \frac{1}{2} \left[1 - \left(\frac{V}{V_p} + \frac{T}{T_p}\right)^2\right]^{1/2} \tag{7.39}$$

where $(P/P_y)^*$ is the maximum normalized axial load which may be taken by the height b. The remaining axial load should be taken by part of the flanges, b_a, so that

$$\left[\frac{P}{P_y} - \left(\frac{P}{P_y}\right)^*\right] = \frac{4\,b_a\,t_o}{A}$$

Substituting (7.39) into the above equation leads to

$$b_a = \frac{A}{8\ t_o}\left[\frac{2P}{P_y} - \left\{1 - \left(\frac{V}{V_p} + \frac{T}{T_p}\right)^2\right\}^{1/2}\right] \tag{7.40}$$

The remainder of the section will resist the bending moment and the other half of the torsional moment T.

The bending stresses are

$$f_b = \frac{M}{M_p} \cdot \frac{\sigma_y\ z}{(z - t_o\ b^2/2 - 2\ bb_a\ t\ )} \tag{7.41}$$

where

$$z = \frac{3\ b^2\ t_o}{2} \tag{7.42}$$

Substituting (7.42) into (7.41) yields

$$f_b = \frac{M}{M_p} \cdot \frac{\sigma_y}{(2/3 - 4b_a/3b} \tag{7.43}$$

Torsional stresses in the flanges are

$$f_{vt} = \frac{T}{2} \cdot \frac{1}{z\ - b\ t_o\ b - 2b_a\ b\ t_o} \tag{7.44}$$

But

$$T_p = z_t\ \frac{\sigma_y}{\sqrt{3}} \quad \text{and} \quad z_t = 2\ b^2\ t_o$$

Therefore (7.44) becomes

$$f_{vt} = \frac{1}{2\sqrt{3}} \cdot \frac{T}{T_p} \cdot \frac{\sigma_y}{[1/2 - b_a/b]} \tag{7.45}$$

Substituting (7.43) and (7.45) into (7.37) yields

$$\left(\frac{M}{M_p}\right)^2 \cdot \frac{1}{[2/3 - 4b_a/3b]} + \frac{1}{4}\left(\frac{T}{T_p}\right)^2 \cdot \frac{1}{[1/2 - b_a/b]^2} = 1 \tag{7.46}$$

For five of the six joints in group 4 the critical section at the joint was subjected to torsional moment and axial load only. Hence the capacity of the channel joint having zero eccentricity may be predicted from equation (7.46) by utilizing the simplified force system as shown in Fig. 7.8. Shear and bending moment both vanish in this case.

Figure 7.9 shows the predicted curves obtained from equation (7.46). The average yield stress was used for each chord thickness. There is good agreement between predicted and experimental values without taking into account strain hardening. The reason for the close prediction utilizing the simple elasto-plastic model is that all the rosette readings at the end of the tests were observed to be smaller than 8.7 ε_y. Hence failure occurred with principal stresses in the flat plateau region of Fig. 7.2. The lower curve predicts the capacity of the channel type joint for a chord composed of 2 HSS 152 x 152 x 6.35 mm while the upper curve is for the thicker HSS, i.e. 152 x 152 x 9.53 mm. Specimen C2P02C was actually comprised of two chords of different thicknesses, the nominal average being 7.94 mm. Its position seems reasonable, i.e. about midway between the two curves.

The capacity of specimen C2N36C is obtained from (7.46) as it is shown below:

σ_y = 392 MPa

e = 76 mm

N = 860 KN

A = 5210 mm^2

Z = 275000 mm^3

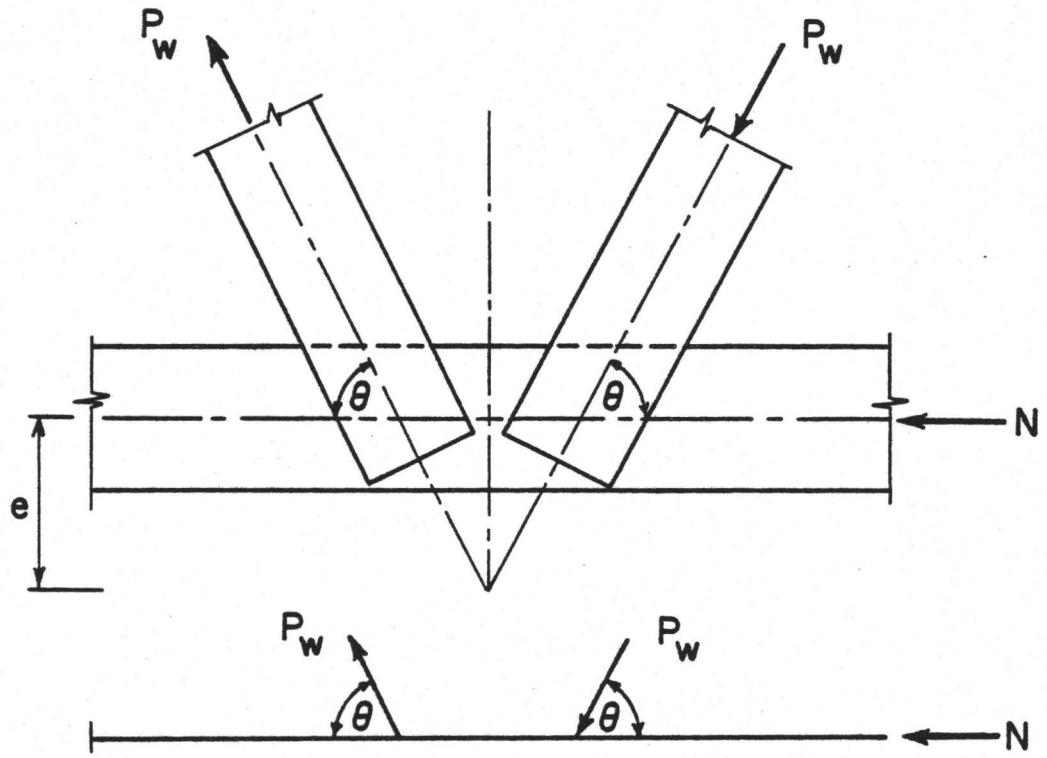

(a)

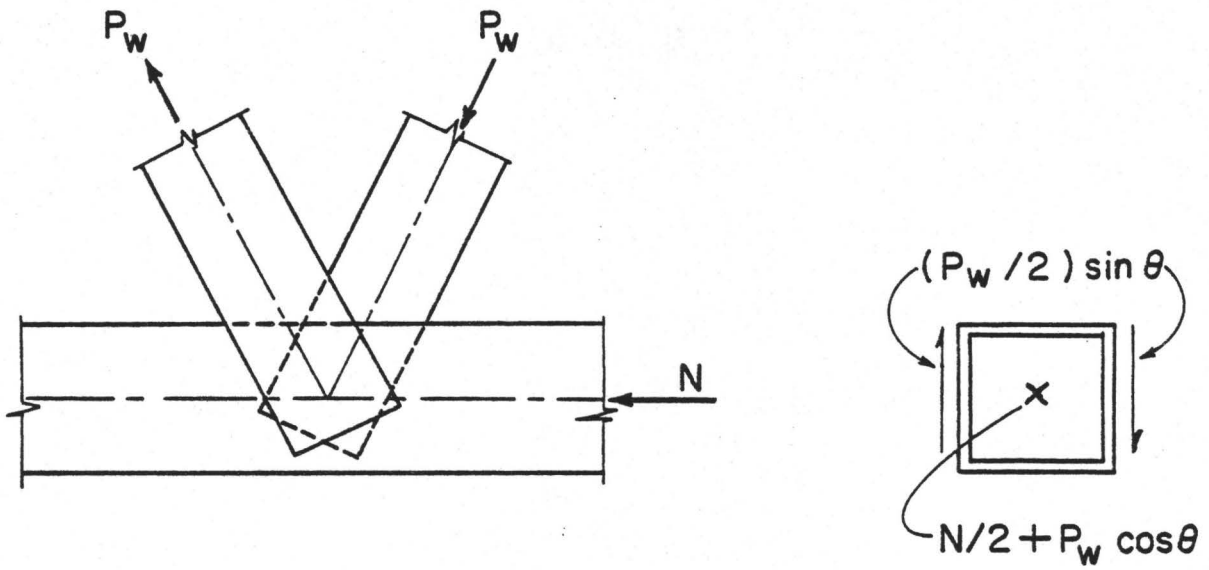

(b)

FIGURE 7.8 FORCE SYSTEM ON CHANNEL TYPE.

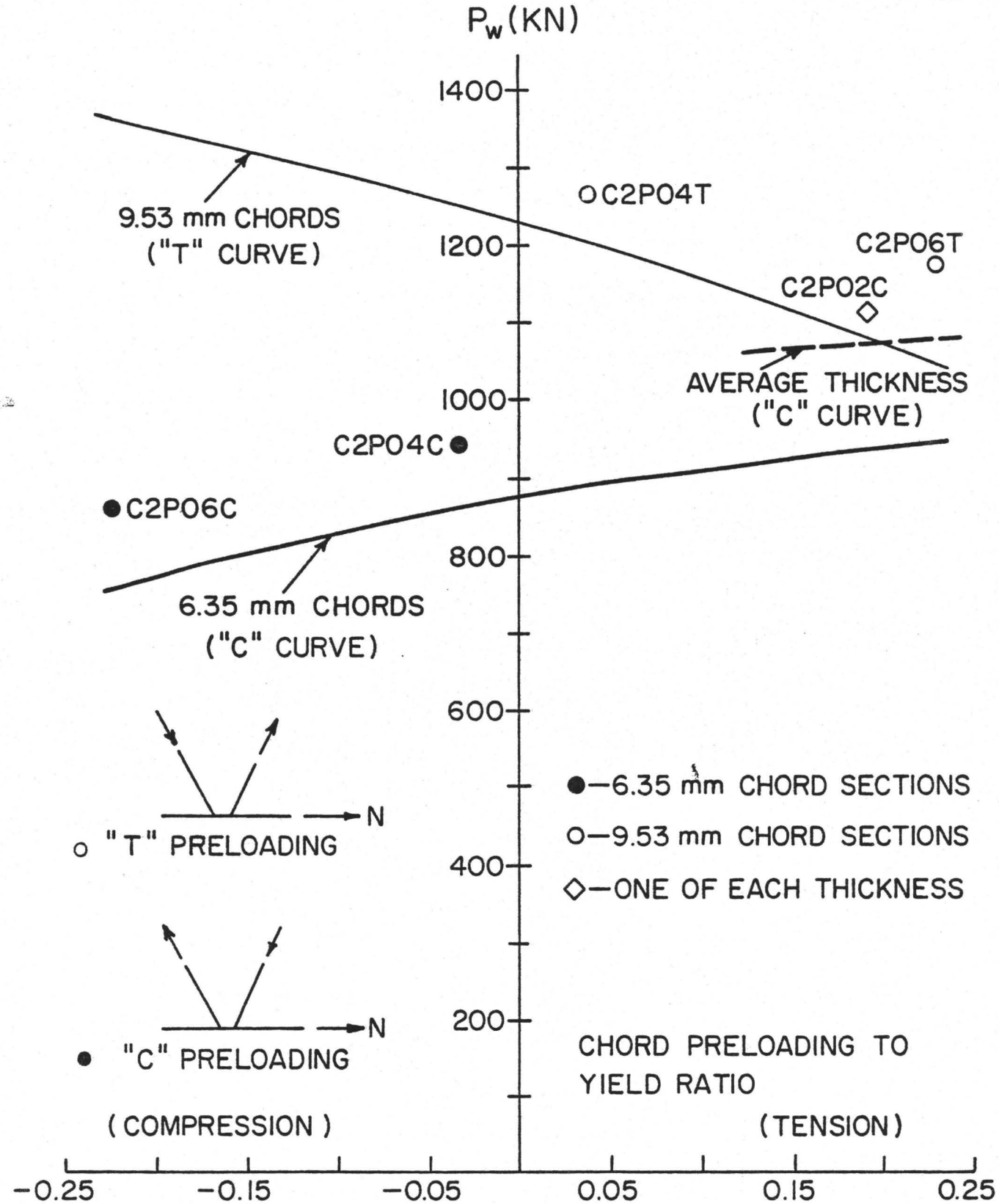

FIGURE 7.9 ELASTIC PLASTIC THEORY AND TEST RESULTS FOR THE CHANNEL TYPE.

$$\tan \theta = 2$$

The moment M,

$$M = \frac{P_w}{2} e \cos \theta = \frac{1}{2} P_w \times 76 \times 0.4472 = 17\ P_w \text{ (KN - mm)}$$

The chord axial load P,

$$P = \frac{N}{2} + P_w \cos \theta = 430 + 0.4472\ P_w \text{ (KN)}$$

The shear force, V,

$$V = 0$$

The plastic bending moment M_p,

$$M_p = \sigma_y \cdot z = 0.392 \times 275000 = 107800 \text{ (KN - mm)}$$

The yield force P_y,

$$P_y = A \cdot \sigma_y = 5210 \times .392 = 2042 \text{ (KN)}$$

The plastic torsional moment T_p,

$$T_p = 2b^2 t_o \cdot \frac{\sigma_y}{\sqrt{3}} = 2 \times (152.4 - 9.53)^2 \times 9.53 \times \frac{.392}{\sqrt{3}}$$

$$= 88048 \text{ (KN - mm)}$$

Substituting the above values into (7.46) gives

$$\left[\frac{17\ P_w}{107800}\right]^2 \times \frac{1}{\left[\frac{2}{3} - \frac{4}{3} \times \frac{1}{2} \left\{\frac{2(430+0.4472P_w)}{2042} - \left[1 - \left(\frac{63.89P_w}{88048}\right)^2\right]^{1/2}\right\}\right]}$$

$$+ \frac{1}{4}\left[\frac{63.89P_w}{88048}\right]^2 \times \frac{1}{\left[\frac{1}{2} - \frac{1}{2} \left\{\frac{2(430+0.4472P_w)}{2042} - \left[1 - \left(\frac{63.89P_w}{88048}\right)^2\right]^{1/2}\right\}^2\right]}$$

$$= 1$$

Solving for the web force gives the result that

$$P_w = 1040 \text{ KN (v.s. } 1090 \text{ KN by test).}$$

7.5 Application of Strain Hardening To Brockenbrough's Results

Brockenbrough concluded that his theoretical interaction diagram was reasonably conservative for compact tubes [32]. Moments much higher than those predicted by his theoretical interaction diagram were obtained in some instances as shown in Fig. 7.10(a).

Predictions from the strain hardening model will now be used to compare with Brockenbrough's experimental results that are shown in Fig. 7.10. Figure 7.10(a) shows the theoretical curve obtained by Brockenbrough [32], where strain hardening was not taken into consideration. The results of three specimens (6.7A, 6.7B and 6.7C) are also shown in the diagram. These three specimens were beam column connections. The column was composed of an HSS 152 x 152 x 4.78 mm with 1220 mm height. Two arms were connected to the column at its mid height and each arm was 610 mm long and comprised of an HSS 152 x 152 x 4.78 mm. Only one value for the yield stress was available for all the specimens viz. 326 MPa. Since no extra strength beyond the yield stress was taken into account by Brockenbrough, then $\sigma_{ex} = 0$ as in Fig. 7.10(a). The rays from the origin depict the loading path for each specimen, whereas the portion of the ray shown connects the test point to the appropriate theoretical interaction curve. It is clear that the predicted values are very conservative specially those for specimens 6.7B and 6.7C where the predicted values were less by 45% than those

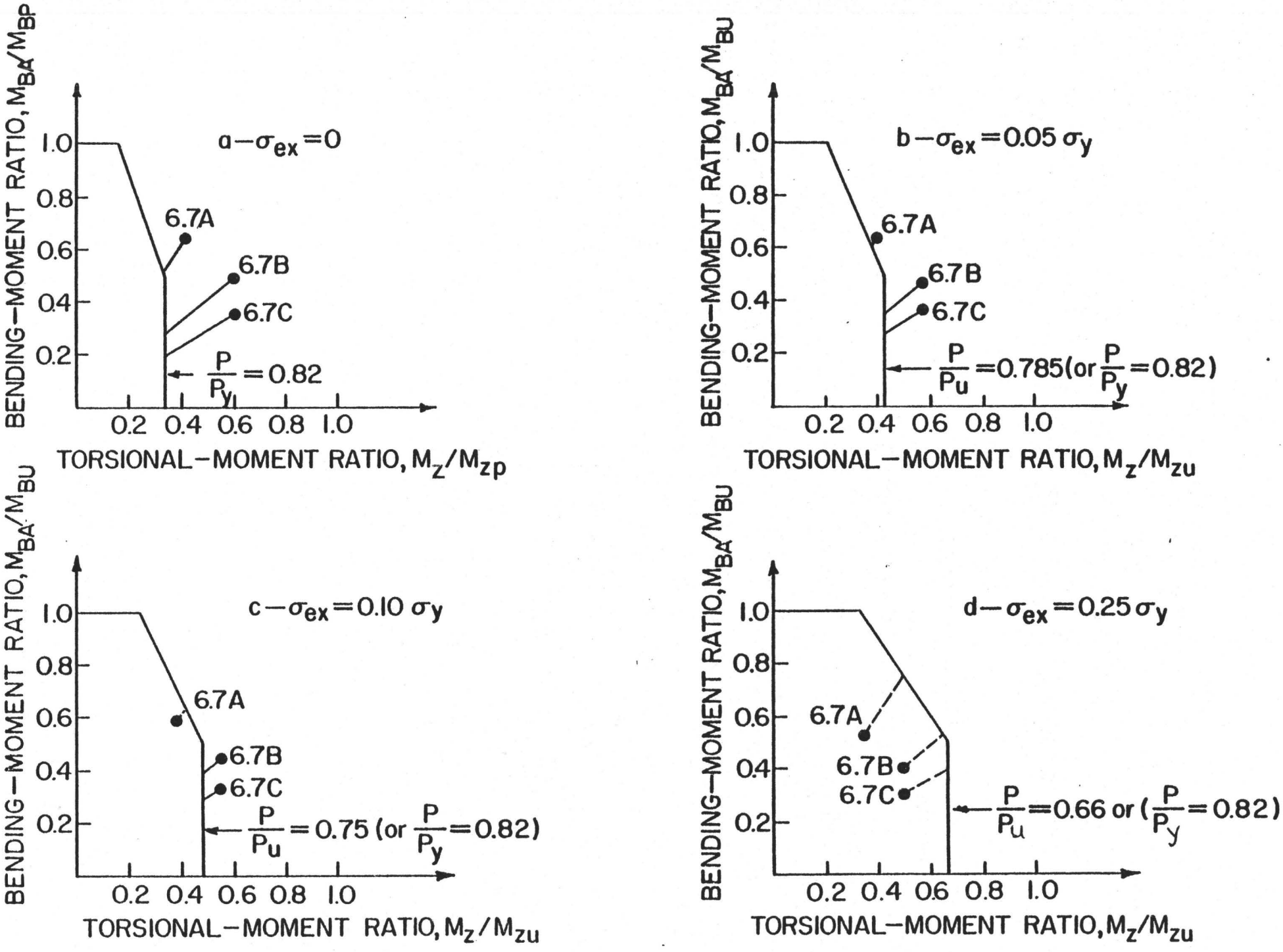

FIGURE 7.10 EFFECT OF STRAIN HARDENING ON BROCKENBROUGH RESULTS.

from the tests. Figure 7.10(d) shows the results for the same specimens when strain hardening was used in predicting the joint capacity. The theoretical curve was obtained for $\sigma_{ex} = 0.25\ \sigma_y$. It is clear from the figure that the predicted values were larger than the experimental ones. The reason for this is that the failure was caused by a localized column failure due to combined local buckling and crippling under axial load and bending. Hence failure occurred somewhere in the strain hardening zone but below its ultimate strength capacity. Figures 7.10(b) & (c) show the results for the same specimens, with intermediate values for σ_{ex}. It is clear from both figures that the best theoretical prediction may be obtained when the σ_{ex} value is close to 10% of σ_y. The results shown in Fig. 7.10 are a clear indication that expanding the Brockenbrough approach to take strain hardening into consideration, improves the theoretical prediction considerably.

CHAPTER 8

SUMMARY AND CONCLUSIONS

8.1 Summary

The purpose of this investigation is to introduce and study the use of the double chord HSS concept in trusses. To the author's knowledge this concept has not been used previously nor has it been proposed in the literature for Hollow Structural Sections.

An experimental investigation was initiated to study the performance of four different K-types of joints; the Standard, Channel, Bolted and Back-to-Back joints. A total of 29 specimens were tested. The different parameters which were investigated are the eccentricity, the slope angle and the preloading effects. A comparison in performance between single and double chord K-type joints as well as a cost comparison are herein reported.

Four tests were conducted on T-types joint to study the performance of the double chord HSS concept in Vierendeel connections. These results are reported and compared with those of the single chord which are described in the literature.

An interaction formula was developed, by extending Brockenbrough's approach to take into account strain hardening which permits a more accurate assessment of the capacity of the standard joint. Also a simple elasto-plastic model was developed to predict the capacity of the channel joint.

8.2 Conclusions

Comparing the behaviour and performance of the 29 double chord tested specimens with the available results on single chord specimens, it is evident that the double chord concept provides stronger joints with higher capacity and stiffness.

The performances of the double chord specimens were dependent on the joint type. It is evident from this investigation that the standard, bolted and back-to-back type joints have considerable promise in long span applications. The channel type requires a heavier chord to attain similar capacity and hence does not appear as viable an alternative in practice.

The ultimate load for some of the joints configurations for the standard, bolted and back-to-back connections exceeded the web yield load. However the cost of fabrication of the standard joints was approximately half the cost of the bolted and back-to-back joints, for little additional material indicating a potential for economies as well as high structural performance. The standard double chord joint was found (overall) to be less expensive than a full overlap single chord joint.

The mode of failure for the standard joint was mainly a shear distortion failure of the chord member. Hence the capacity of the joint was governed by the shearing area of the web of the chord members. Normal fillet welding of the webs to the double chord provided adequate strength and stiffness. Chord preloading was shown to have an effect on joint capacity. Increasing the chord preload, either in tension or

compression, has the effect of reducing the joint strength. In an actual truss, high web forces are likely to be nearer the truss ends, rather than mid span, and hence reduced joint strength due to preloading may not be of major concern.

If web end cuts are made for the standard joints, member positioning for fabrication is facilitated. This step also reduces the eccentricity on the joint and improves the joint strength. A reduction in eccentricity from 178 mm to 108 mm tended to increase joint strength by 10%. It was obvious during the investigation that bridging the webs with weldment at their nearest position tended to directly transfer stress from one web member to the other. A study of this transfer mechanism was not attempted in this program.

For the double chord, the advantage using a smaller slope angle is that smaller eccentricities are obtained. Since the eccentricity is reduced, a higher capacity can be obtained. In a practical situation the purpose of the double chord is to extend the span. As such, the depth will also increase. A 45° slope angle, therefore, will produce very large diagonal members. Thus, compression members may become susceptible to buckling since the increase in effective length will tend to reduce the capacity of the web member.

The mode of failure for the channel type joints was mainly a shear and torsion failure when the same nominal chord thickness as all other types was used. Large deformations were obtained as well as lower capacities and stiffnesses, when compared with the other three types. Normal fillet welding was sufficient to prevent premature weld failure

at the joint. Higher capacities and smaller deformations were obtained after increasing the chord thickness by 50%.

The bolted joints failed by local buckling of the compression web member. This type of connection holds considerable promise when transportation and erection of large trusses pose problems because of size. Although the chord thickness was 50% larger than specified, nonetheless, the observed behaviour suggests that the gusset plates will transfer much of the web force to its connecting diagonal, thus relieving the chord of some load. Chord deformations were minimal and high capacity and stiffness of the joints were obtained. The use of tie plates to connect the outside flanges of the chords improves the behaviour of the joint and increases its capacity and stiffness.

The back-to-back joints showed good strength and stiffness qualities provided that the webs are overlapped at the ends or an adequate stiffening plate is utilized under conditions of positive gap. The failure mode of the tested specimens was mainly that of a local buckling failure of the compression web member. For full overlapped joints, higher capacities were obtained when the compression branch member was welded to the tension member. A gap joint without a stiffening plate was shown to be very weak and is therefore not recommended in practice.

For Vierendeel connections, the double chord concept appears to have superior qualities than the equivalent unreinforced single chord connection, where greater joint stiffness, moment capacity and out-of-plane bending resistance are obtained. Also lighter HSS can be used

which reduces the overall weight of the truss.

An extension to Brockenbrough's theoretical work taking the strain hardening effect into account, provides reasonably good agreement with the tests of the standard type. The interaction formula that has been developed (7.31), is simple to apply to joints of this type and provide a good indication of connection strength being within 8% for this test series.

Bridging the web members, increases the capacity of the standard joint. By adding the exact amount of bridging area to the axial and shear areas in (7.31), for group 2 specimens, the predicted results will still remain within the 8% range. Only one experimental value was below that predicted and this was mainly due to a very low yield strength of the compression web member. Using equation (7.31) to predict the results obtained by Brockenbrough, improves the prediction over his original formula by an average of 20 per cent, as indicated earlier.

Predictions for the capacities of the channel joints were obtained from a simple elasto-plastic model (7.46) and were short from the experimental values by an average of 10 to 12% range.

8.3 Suggestions for Future Research

To complete this promising work, tests on full size trusses should be done. The author has already designed five trusses using only three types of joints. The standard joint was used for 2 trusses with two eccentricities 178 and 108 mm. The bolted joint was used for the third truss with tie plates. For the fourth truss, a full overlapped

back-to-back joint was used, while a gap joint with an adequate stiffening plate was used for the fifth truss. Each truss is 14.5 m long and 1.80 m deep. Better understanding for the behaviour of the double chord concept will be available once those trusses are tested.

For the bolted joints, some tests should be done on different gusset plate thicknesses to study the effect of this parameter.

A Ph.D. research program has already been started to study and predict the behaviour of the back-to-back type of joints for truss and Vierendeel connections.

REFERENCES

[1] Cran, J.A., Gibson, E.B. and Standnyckyj, S., "Hollow Structural Sections - Design Manual for Connection", The Steel Company of Canada, 1971.

[2] STELCO, "Hollow Structural Sections Welded Joint Research Summaries", The Steel Company of Canada, May 1974.

[3] Blockley, D.I., "Joints between structural hollow sections in plane frameworks", Ph.D. Thesis, University of Sheffield, England, June 1967.

[4] Shinouda, M.R., "Stiffened tubular joints", Ph.D. Thesis, University of Sheffield, England, June 1967.

[5] Babiker, D.B., "The fatigue behaviour of welded joints between structural hollow sections", Ph.D. Thesis, University of Sheffield, England, December 1967.

[6] Mee, B.L., "The structural behaviour of joints in rectangular hollow section", Ph.D. Thesis, Sheffield University, England, September 1969.

[7] Eastwood, W. and Wood, A.A., "Welded joints in tubular structures involving rectangular sections", Conference on Joints in Structures, Session A Paper 2, University of Sheffield, July 1970.

[8] Chidiac, M.A. and Korol, R.M., "Rectangular hollow section double-chord T-joints", Technical notes, Journal of the Structural Division, ASCE, Vol. 105, No. ST8, Proc. Paper 14730, August 1979, pp. 1717-1721.

[9] C.I.S.C., Canadian Institute of Steel Construction, "Limit states design steel manual", 1st Edition, Willowdale, Ontario, Canada, January 1977.

[10] Chandrakeerthy, S.R., "Structural behaviour related to stress analysis of joints in cold-formed square hollow sections", Ph.D. Thesis, University of Sheffield, 1972.

[11] Dasgupta, A., "The behaviour of joints in tubular trusses", Ph.D. Thesis, University of Nottingham, November 1970.

[12] Packer, J.A., "Theoretical Behaviour and Analysis of Welded Steel Joints with R.H.S. Chords", CIDECT Report 5U-78/11.

[13] Wardenier, J., "Results of Research E.C.S.C.: Welded girder joints in structural hollow sections", Acier-Stahl-Steel, Vol. 43, No. 1, 1978, pp. 29-33.

[14] BRITISH STEEL CORPORATION TUBES DIVISION, "Tests on complete girders", Draft Report CE73/95, Corby, 1977.

[15] BRITISH STEEL CORPORATION TUBES DIVISION, "Tests on isolated joints", Report CE73/96/D, Corby, August 1977.

[16] Haleem, A.S., "Some aspects of SHS welded joint behaviour", British Steel Corporation Tubes Division, Corby, January 1977.

[17] Coutie, M.G., Davies, G., Packer, J.A. et al., Draft recommendations for "CONSTRADO Design Guide on SHS Connections", CONSTRADO, London, 1979.

[18] Haleem, A.S., "Determination of Ultimate joint strength for statically loaded SHS welded lattice girder joints with RHS Chords", CIDECT Report 77/37, British Steel Corporation Tubes Division, October 1977.

[19] Mang, F., "Report on rectangular hollow sections (RHS) joint study programme - CIDECT Programme 5P", Mannesman Research Institute, Dusseldorf, West Germany, September 1973.

[20] Davie, J. and Giddings, T.W., "Research into the strength of welded lattice girder joints in structural hollow sections", British Steel Corporation Tubes Division, Corby, CIDECT Report CE 70/3, 1970.

[21] Hohl, "Failure load tests on large size RHS Warren joints", Mannesman Research Institute Report No. 93/74 and CIDECT Report No. 74/15/5M(E), Dusseldorf, West Germany, June 1974.

[22] Mang, F., "Test on Warren joints in large size RHS", CIDECT Programme 5M Interim Report, Mannessman Research Institute, Dusseldorf, West Germany, 1976.

[23] Jubb, J.E.M. and Redwood, R.G., "Design of joints to box sections", Industrial Building and the Structural Engineer Institution of Structural Engineers Conference, May 1966, U.K.

[24] Patel, N.M., "Experimental and analytical investigation of punching shear characteristics of rectangular tubular welded joints", Ph.D. Thesis, University of Houston, U.S.A., December 1972.

[25] Wardenier, J. and De Koning, C.H.M., "Investigation into the static strength of welded lattice girder joints in structural hollow sections, Part 1: Rectangular Hollow Sections", CIDECT Report 76/12/5Q, Delft University of Technology, June 1976.

[26] Davies, G. and Roper, C.G., "Gap joints with tubular members - A yield line approach", Building Science, Vol. 10, 1975, pp. 199-205.

[27] Davies, G. and Roper, C.G., "Gap joints with tubes - A yield line modified by shear approach", Building and Environment, Vol. 12, 1977, pp. 31-38.

[28] Roper, C.G., "An analytical study of the strength and flexibility of tubular joints", M. Phil. Thesis, University of Nottingham, May 1974.

[29] Mouty, J., "Calcul des charges ultimes des assemblages soudes de profils creux carres et rectangulaires", Construction metallique, No. 2, Paris, June 1976.

[30] Mouty, J., "Behaviour of welded joints of square and rectangular structures - A theoretical approach based on the method of yield lines", International Institute of Welding Annual Assembly, Document XV-426-78, Dublin, 1978.

[31] Packer, J.A., "Theoretical Behaviour and analysis of welded steel joints with RHS chords", CIDECT, Report 5U-78/19, October 1978.

[32] Brockenbrough, R.L., "Strength of square-tube connections under combined loads", Journal of the Structural Division, ASCE, Vol. 97, No. ST12, Proc. Paper 9425, Dec. 1972, pp. 2753-2768.

[33] ASTM, Annual Standards 1972, Part 31, Section E8, "Standard Methods of Tensile Testing Metallic Materials".

[34] Lazar, B.E. and Fang, P.J., "T-type moment connections between rectangular tubular sections", Res. Rep., Sir George Williams University, Faculty of Engineering, Montreal, P.Q., 1971.

[35] Duff, G., "Joint behaviour of a welded beam-column connection in rectangular hollow sections", Ph.D. Thesis, The College of Aeronautics, Cranfield, U.K., 1963.

[36] Cute, D., Camo, S., Rumpf, J.L., "Welded Connections for square and rectangular structural steel tubing", Res. Rep. No. 292-10, Drexel Institute of Technology, Philadelphia, P.A., 1968.

[37] Brady, F.J., "An Experimental Investigation of Unequal Width HSS Moment Connections for Vierendeel Trusses", Project Report in partial fulfillment of the requirements for the Degree Master of Engineering, McMaster University, Hamilton, Ontario, Canada, 1974.

[38] El-Zanaty, M., "Vierendeel Trusses with Hollow Structural Sections", M.Eng. Thesis, McMaster University, Hamilton, Ontario, Canada, 1976.

[39] Korol, R.M., El-Zanaty, M., and Brady, F.J., "Unequal Width Connections of Square Hollow Sections in Vierendeel Trusses", Canadian Journal of Civil Engineering, Volume 4, Number 2, 1977, pp. 190-201.

[40] Private Communication, Mr. Tim Gillies, CANRON, 100 Disco, Rexdale, Toronto, November 28, 1979.